MASTER IN BIOCHEMISTRY AND MOLECULAR AND CELL BIOLOGY RESEARCH FOCUS

Study of the impact of UVB-induced senescent keratinocytes on skin cancer cells

Bouriez, Inès

Award date:
2022

Awarding institution:
University of Namur

Faculté des Sciences

STUDY OF THE IMPACT OF UVB-INDUCED SENESCENT KERATINOCYTES ON SKIN CANCER CELLS

Mémoire présenté pour l'obtention

du grade académique de master 120 en biochimie et biologie moléculaire et cellulaire

Inès Bouriez

Janvier 2022

Université de Namur
FACULTE DES SCIENCES
Secrétariat du Département de Biologie
Rue de Bruxelles 61 - 5000 NAMUR
Téléphone: + 32(0)81.72.44.18 - Téléfax: + 32(0)81.72.44.20
E-mail: joelle.jonet@unamur.be - http://www.unamur.be

Study of the impact of UVB-induced senescent keratinocytes on skin cancer cells

BOURIEZ Inès

Résumé

Le vieillissement est associé avec l'accumulation de cellules sénescentes dans les tissus mais également avec un risque accru de développer certains cancers. Le sécrétome des cellules sénescentes est connu pour être impliqué dans le développement de certains cancers. Pour étudier le vieillissement et l'apparition de cancers, la peau est un tissu de choix puisqu'elle est très exposée aux stress environnementaux comme les rayons solaires, qui favorisent à la fois le développement de cancers de la peau et le vieillissement accéléré de la peau. Dans ce mémoire, l'effet du sécrétome des kératinocytes sénescents sur la migration de cancers cutanés a été investigué. Pour ce faire, des expositions répétées aux UVB ont permis d'induire la sénescence prématurée de kératinocytes cultivés en monocouche. L'induction de la sénescence a été confirmée par l'analyse de plusieurs biomarqueurs. Ensuite, le milieu conditionné des kératinocytes sénescents a été utilisé pour tester son effet sur la migration de cellules issues de mélanomes et de carcinome et a montré un léger effet pro-migratoire dans certaines conditions. L'analyse de la composition du sécrétome des kératinocytes sénescents a permis de mettre en évidence la présence de protéines ayant un effet pro-migratoire. En parallèle, un modèle d'épiderme reconstruit intégrant des cellules de mélanomes exprimant la GFP (green fluorescent protein) a été développé pour étudier l'impact croisé des kératinocytes sénescents et des cellules de mélanomes dans un modèle plus proche des conditions *in vivo*. Pour induire la sénescence des kératinocytes dans des épidermes reconstruits, ces derniers ont été exposés aux UVB ou incubés avec du milieu conditionné provenant de kératinocytes sénescents.

Mémoire de master 120 en biochimie et biologie moléculaire et cellulaire

Janvier 2022
Promoteur: F. Debacq-Chainiaux
Co-Promoteurs: Y. Poumay, J.P. Gillet

Université de Namur
FACULTE DES SCIENCES
Secrétariat du Département de Biologie
Rue de Bruxelles 61 - 5000 NAMUR
Téléphone: + 32(0)81.72.44.18 - Téléfax: + 32(0)81.72.44.20
E-mail: joelle.jonet@unamur.be - http://www.unamur.be

Study of the impact of UVB-induced senescent keratinocytes on skin cancer cells

BOURIEZ Inès

Summary

Aging is associated with the accumulation of senescent cells in tissues but also with an increased risk of developing certain cancers. The senescent cell secretome is known to be involved in the development of certain cancers. To study aging and cancer development, skin is a tissue of choice since it is highly exposed to environmental stresses such as solar radiation, which promotes both the development of skin cancers and accelerated skin aging. In this master thesis, the effect of the senescent keratinocyte secretome on the migration of skin cancers was investigated. For this purpose, repeated exposures to UVB were used to induce premature senescence of keratinocytes cultured in monolayer. The induction of senescence was confirmed by the analysis of several biomarkers. Next, the conditioned medium of senescent keratinocytes was used to test its effect on the migration of melanoma and carcinoma cells and showed a slight pro-migratory effect under certain conditions. Analysis of the composition of the secretome of senescent keratinocytes revealed the presence of proteins with a pro-migratory effect. In parallel, a reconstructed epidermis model integrating melanoma cells expressing GFP (green fluorescent protein) was developed to study the interconnection of senescent keratinocytes and melanoma cells in a model closer to *in vivo* conditions. To induce keratinocyte senescence in reconstructed epidermis, the latter were exposed to UVB or incubated with conditioned medium from senescent keratinocytes.

Mémoire de master 120 en biochimie et biologie moléculaire et cellulaire

Janvier 2022
Promoteur: F. Debacq-Chainiaux
Co-Promoteurs: Y. Poumay, J.P. Gillet

Acknowledgments

Je tiens à adresser mes remerciements aux personnes qui m'ont aidé au cours des 10 derniers mois et qui ont contribué au développement de ce mémoire. Je voudrais d'abord remercier l'ensemble des membres de l'URBC et du LabCeTi pour leur accueil chaleureux pendant ces 10 mois.

Merci aux membres de mon jury de prendre le temps de lire ce mémoire, j'espère que la lecture sera agréable.

Un tout grand merci à ma promotrice, Florence Debacq-Chainiaux pour m'avoir patiemment guidée et encadrée tout au long de ces 10 mois. Vos conseils, votre bienveillance et vos encouragements ont grandement aidé à la réalisation de ce mémoire. Merci également pour ces dernières semaines de corrections effrénées.

Ensuite, je tiens à remercier Yves Poumay, mon co-promoteur qui m'a aiguillée et conseillée tout au long de ce mémoire.

Je souhaite adresser un remerciement particulier aux techniciens qui m'ont aidés tout au long de mon mémoire. Merci Valérie pour ta grande aide, tes conseils et pour tout le temps que tu m'a accordé pour mes expériences sur les épidermes. Merci à Catherine pour tout le temps passé au confocal à faire des images de mes (trop) nombreuses lames. Merci Marc pour ton aide pour toute la partie analyse protéomique mais surtout pour ta patience pour régler mes multiples soucis informatiques. Merci Antoine d'avoir volé à ma rescousse dès que j'avais un problème. Merci également au reste de l'équipe technique de l'URBC, Sophie et Dorian pour votre travail indispensable au bon fonctionnement du labo.

Merci à Joëlle de m'avoir pris sous ton aile les premières semaines et de nous avoir soutenues, aidées et conseillées avec Coline pendant ces 10 mois. Merci aux doctorants et post-doctorants de l'URBC pour leurs nombreux conseils et leur bonne humeur.

Enfin merci aux mémorants de l'URBC pour cette année riche en émotions, pour leur soutien et pour tous les bons moments partagés. Merci Louise, Amandine, Youri, Lisa, Thomas et Manon pour tous ces souvenirs, ces soirées, ces pizzas, ces larmes et ces fou rires… Je ne suis pas prête d'oublier cette année à vos côtés. Je remercie particulièrement Coline, ma co-mémorante et jumelle de labo pour son soutien mental et pratique tout au long de ce mémoire.

Pour terminer, merci à ma famille pour leur soutien tout au long de mon parcours, et pour s'être donné du mal à essayer de comprendre ce que je faisais.

Table of contents :

ABBREVIATIONS

2D : Two-Dimension

3D : Three-Dimension

53BP1 : p53-Binding Protein-1

ARF : ADP-ribosylation factor

ATM : Activating transcription factor

BAK : BCL-2 antagonist killer 1

BAX : BCL-2-associated X protein

BCC : Basal Cell Carcinoma

BCL 2 : B cell lymphoma 2

BH3 : Bcl-2 homology domain 3

BrDU : 5-Bromo-2´-Deoxyuridine

BSA : Bovine Serum Albumin

C/EBPβ : CCAAT/enhancer-binding protein-β

CCL-2, -5,-17 : Chemokine (C-C motif) ligand- 2, -5,-17

CCRL2 : C-C chemokine receptor-like 2

CDC25 : Cell-Division Cycle 25

CDK : cyclin dependant kinase

CDKI : cyclin-dependent kinase inhibitor

CDKN2A : Cyclin-Dependent Kinase-Inhibitor 2A

cGAS : GMP–AMP synthase

CHK1, 2 : Checkpoint kinase 1, 2

CM : Conditioned Medium

CM CTL : Conditioned Medium from control

CM UVB : Conditioned Medium from UVB-exposed cells

cSCC : cutaneous Squamous Cell Carcinoma

CTL : Control

CXCL1,-6, -8, -10 : C-X-C chemokine ligand -1,-6, -8, -10

CXCR1,-2 : C-X-C chemokine receptor 1,-2

D : dispase incubation during 15 min

D+T-1h : dispase incubation for 15 min followed by trypsin incubation at 37°C during 1h

D+T-20' : dispase incubation for 15 min followed by trypsin incubation at 37°C during 20 min

D+T-40' : dispase incubation for 15 min followed by trypsin incubation at 37°C during 40 min

DAPI : 4',6-diamidino-2-phénylindole

DDR : DNA damage response

DHG : DMEM High Glucose

DPX : Dibutylphthalate Polystyrene Xylene

DSB : Double Strand Break

EDTA : Éthylènediaminetétraacétique

EdU : 5-Ethynyl-2′-deoxyuridine

EGF : Epidermal Growth Factor

ELISA : Enzyme-linked immunosorbent assay

EMT : Epithelial to Mesenchymal Transition

ER : Endoplasmic Reticulum

ERK : Extracellular signal-Regulated Kinase

FBS : Fetal Bovine Serum

FGF : Fibroblast Growth Factor

GATA4 : GATA binding protein 4

GFP: Green Fluorescent Protein

GROα, β : Growth-Regulated Oncogene α, β

HEKa 1 : Human Epidermal Keratinocytes 1

IL-1α/β-6, -8 : Interleukin -1α/β,-6,-8

IκBα : inhibitor-kB

KSFM : Keratinocyte Serum-Free Medium

LDH : lactate deshydrogenase

MAPK : Mitogen-Activated Protein Kinase

MAPKAPK2 : mitogen-activated protein kinase-activated protein kinase 2

MCD1 : Mediator of DNA damage Checkpoint-1

MCP-2 : Monocyte chemoattractant protein-2

MDC1 : Mediator of DNA damage checkpoint protein 1

MIP-1α : Macrophage Inflammatory Proteins 1α

MMP-9 : Matrix Metallo Proteinase 9

MRE11 : Meiotic Recombination 11

MRN : MRE11–RAD50–NBS1

mRNA : messenger RNA

mTOR : Mechanistic Target Of Rapamycin

NBS1 : Nijmegen breakage syndrome protein 1

NF-κB : Nuclear factor-kappa B

NHEKs : Normal Human Epithelial Keratinocytes

NT : Non treated

OCT : Optimal Cutting Temperature compound

OIS : oncogene-induced senescence

PBS : Phosphate Buffer Saline

PFA : Paraformaldehyde

pRB : retinoblastoma protein

PTEN : Phosphatase and Tensin homologue

RAD50 : ATP-binding cassette–ATPase

RAD9–RAD1–HUS1

RHE : Reconstructed Human Epidermis

RIN : RNA integrity number

ROCK1,-2 : rho-associated, coiled-coil-containing protein kinase 1, -2

RS : Replicative-like Senescence

RT : Reverse Transcription

RT-qPCR : Quantitative Reverse Transcription polymerase chain reaction

SA-βgal: Senescence-associated β-galactosidase

SAHF : Senescence-Associated Heterochromatin Foci

SASP : Senescence-Associated Secretory Phenotype

SIPS : Stress-Induced Premature Senescence

SMAC : Second Mitochondria-derived Activator of Caspase

STING : stimulator of interferon genes

TF-0°C-ON : trypsin incubated at 0°C overnight followed by cell disaggregation by flushing

TF-37°C-1h : trypsin incubated at 37°C for 1h followed by cell disaggregation by flushing

TF-4°C-1h : trypsin incubated at, 4°C for 1h followed by cell disaggregation by flushing

TF-4°C-ON : trypsin incubated at, 4°C overnight followed by cell disaggregation by flushing

TGFβ: transforming growth factor β

TP53 : Tumor-Protein p53

TT-37°C-1h : trypsin incubated 1h at 37°C followed by cell disaggregation by trituration

TT-4°C-ON : trypsin incubated 1h at 4°C overnight followed by cell disaggregation by trituration

UPR : Unfolded Protein Response

UV : UltraViolet rays

UVB-SIPS : UltraViolet – Stress Induced Premature Senescence

VEGF : Vascular Endothelial Growth Facto

INTRODUCTION

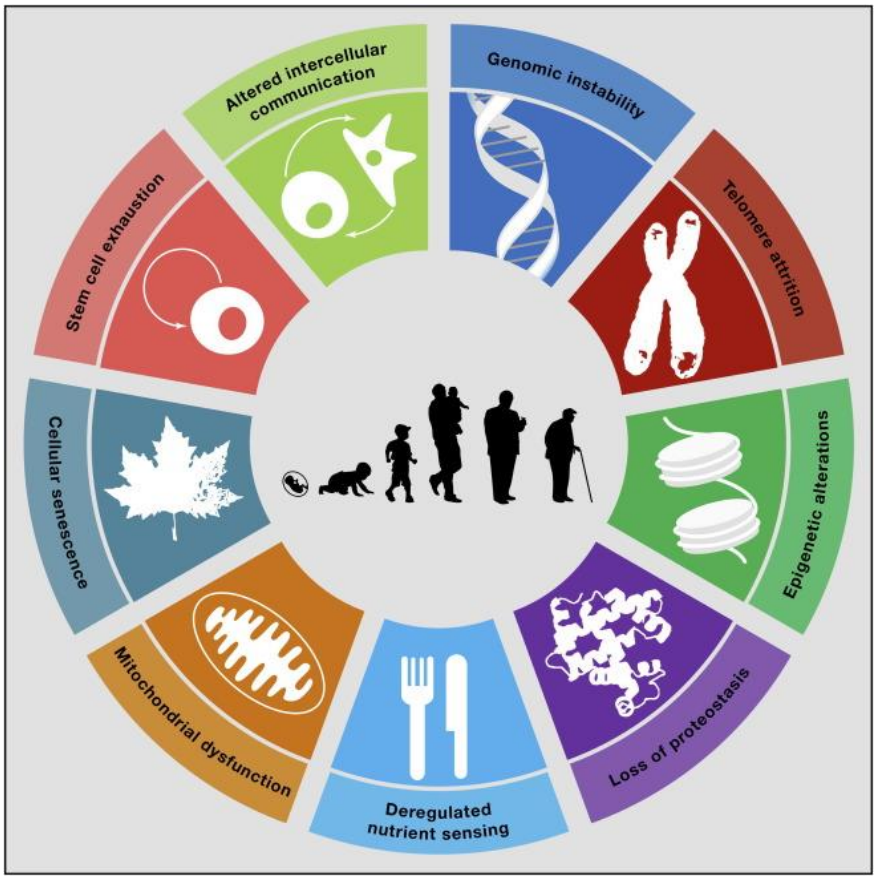

Figure 1 : Hallmarks of aging. Schematic representation of cellular and molecular hallmarks that contribute to aging (López-Otín et al., 2013)

The world's population is aging: in the last 70 years, the proportion of elderly people (>60 years) has increased from 8% to 14%. Moreover, it is predicted that the elderly people will represent more than 21% of the population in 2050 (WHO, 2021). Aging is often associated with a weakening of the organism and the onset of age-related diseases, representing a global burden for the population. At cellular and molecular levels, aging can be characterized by several hallmarks such as cellular senescence, telomere attrition, genomic instability, epigenetic alterations or alterations of intercellular communication (**Figure 1**) (López-Otín et al., 2013). Interestingly, the clearance of senescent cells delays the apparition of the aging phenotype in mice, suggesting that senescence has an impact on the global aging of the organism (Baker et al., 2011). Senescent cells were first discovered in *in vitro* cultures of human fibroblasts and described as cells that have reached their proliferation limit (Hayflick and Moorhead, 1961). Despite their permanent cell cycle arrest, these cells remain metabolically active and can interact with their cellular environment, contributing to the aging of the tissues (Childs et al., 2017). Moreover, cellular senescence could be perceived as a stress response. This stress can be of several natures, the most common are telomere shortening, genomic damage, and oncogene activation (Campisi, 2013).

1. Senescence induction

1.1. Replicative senescence

The cellular senescence discovered at first on fibroblasts by L. Hayflick was defined as "replicative senescence" (Hayflick and Moorhead, 1961). This type of senescence is mostly occurring because of telomere erosion. Indeed, DNA polymerase is not able to replicate the extremity of the DNA 5' end on the lagging strand, leading to the loss of 50 to 200 base pairs of DNA in telomeres at each replication (Campisi and d'Adda di Fagagna, 2007). When telomeres are too short, they lose their physiological structure (which is ending by a loop) and they are therefore recognized as DNA strand breaks, inducing DNA damage response (DDR) pathway (Di Micco et al., 2021). The activation of DDR pathway by shortened telomeres could lead to senescence (Campisi and d'Adda di Fagagna, 2007). To support this idea, in fibroblasts in replicative senescence, the length of telomeres is highly reduced and this replicative senescence could be counteracted by the expression of the catalytic subunit of the telomerase, allowing the DNA replication at 5' end on the lagging strand (Bodnar et al., 1998).

1.2. SIPS

Afterwards it was shown that senescence could also be induced *in vitro* prematurely, i.e. before the exhaustion of the proliferative potential by external factors, inducing oxidative stress and/or DNA damage leading to stress-induced premature senescence (SIPS) (Toussaint et al., 2000). This stress-induced senescence occurs independently from telomere shortening and is induced by persistent cellular damage (Burton and Krizhanovsky, 2014).
Several factors could induce SIPS such as genotoxic stress induced by X-ray or UV-rays inducing direct DNA damage, leading to the activation of the DDR pathway that could lead to

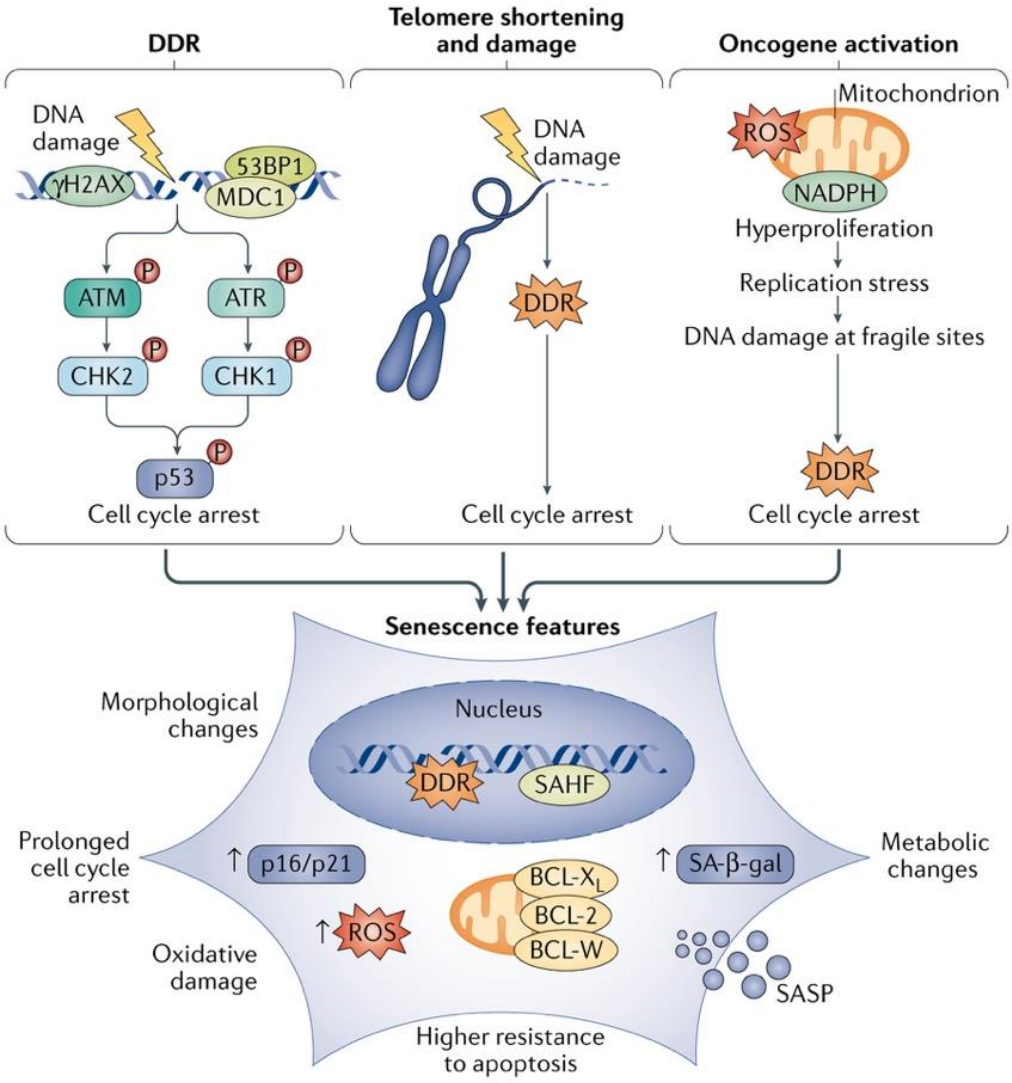

Figure 2 : Senescence inducers and biomarkers

External factors, as well as telomere shortening or oncogene activation can induce DNA damage. These DNA damage are recognized by actors of the DDR (see **Figure 3**), inducing the cell cycle arrect via ATM/ATR-p53 pathway. Senescent cells present various biomarkers, as morphological changes, SA-Bgal activity, a prolonged DDR activation, an arrest of the cell cycle induced by p16 or p53/p21 pathway as well as an overexpression of the BCL2-family proteins (Di Micco et al., 2021).

cell senescence (described in paragraph 2.3). In addition, oxidative stress, due to senescence-associated mitochondrial dysfunction or induced by external stressors, could also induce premature telomere attrition and DNA damage (Hewitt et al., 2012)

1.3. OIS

Senescence can also be induced following the activation of oncogenes, such as *RAS* or *BRAF*, or the inactivation of tumor suppressor genes, such as *PTEN*, and is therefore named oncogene-induced senescence (OIS) (Burton and Krizhanovsky, 2014). These oncogenic activations lead to cell hyperproliferation and could be associated with an alteration of DNA replication, inducing senescence (Di Micco et al., 2021). Indeed, the constitutive expression of RasV12 in fibroblasts is associated with increased DNA damage response such as γH2AX and 53BP1 foci (see paragraph 2.3) due to DNA replication stress (Maya-Mendoza et al., 2015). OIS is therefore presented as a tumor suppressor mechanism, inhibiting the proliferation of premalignant cells (Burton and Krizhanovsky, 2014).

2. Senescence biomarkers

Senescent cells are characterized by several biomarkers **(Figure 2).** As these biomarkers are not specific to senescent cells when taken individually, it is necessary to use several of them to detect senescent cells (González-Gualda et al., 2021).

2.1. Cell morphology

First of all, senescent cells are known to present a flattened and enlarged morphology *in vitro* but also *in vivo* (Herranz and Gil, 2018). These morphological changes are linked with an increase of caveolin-1 in senescent cells, inducing the increase of their focal adhesion (Cho et al., 2004). Furthermore, induction of senescence is often linked to the UPR-mediated endoplasmic reticulum (ER) stress. This ER stress leads to an increase in ER volume, correlated with the increase in size of senescent cells. Moreover, when UPR is blocked by an ATF6α inhibitor, senescent fibroblasts regain their fusiform shape, indicating that ER stress is also contributing to the enlargement of senescent cells (Druelle et al., 2016).

2.1.1. SA β–galactosidase activity

In proliferating and quiescent cells, the lysosomal β-galactosidase (β-gal) enzyme is active around pH 4 - 4.5. In senescence, an increase in lysosomal mass as well as an increased expression of the β-galactosidase gene (*GLB1*) lead to an increased abundance of the protein allowing to detect its enzymatic activity at a suboptimal pH (around pH 6.0) and is therefore identified as the senescence-associated β-galactosidase (SA-βgal) (Kurz et al., 2000; Lee et al., 2006). This senescence biomarker can be studied *in vitro* and *ex vivo* by using x-gal, a chromogenic substrate that turns blue when cleaved by β-galactosidase (Dimri et al., 1995).

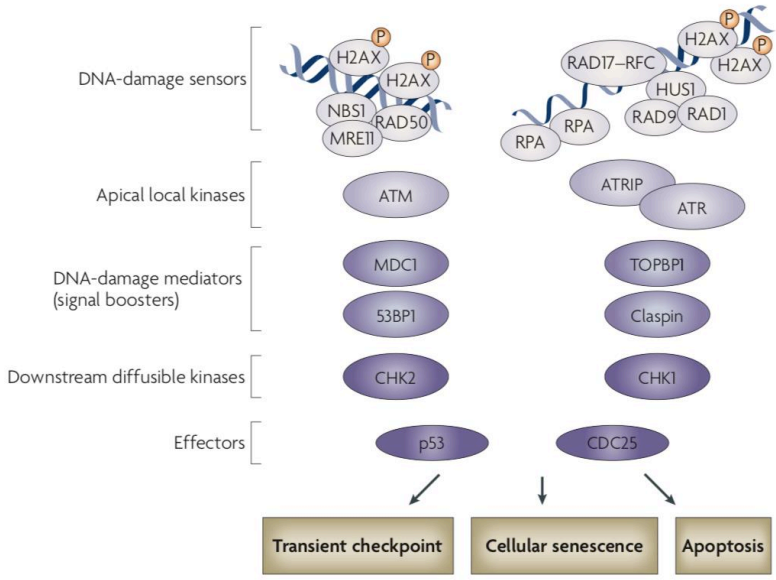

Figure 3 : The DDR (DNA Damage Response) pathway

DNA double strand breaks are recognized by MRE11, RAD50 and NBS complex, which activate ATM leading to the phosphorylation of H2AX histones (γH2AX). ATM activation also activates MDC1 and then 53BP1. This ATM activation ends with the phosphorylation of CHK2, which activates p53 (see **Figure 4**). DNA single strand are covered by RPA and recognized by the RAD9–RAD1–HUS1 complex, recruiting ATR and its DNA-binding subunit ATRIP, also leading to γH2AX and to the activation of Claspin and TopBP1. ATR signaling results in the inhibitory phosphorylation of CDC25, resulting in the cell cycle inhibition. *53BP1: p53-binding protein 1; ATM: ataxia-telangiectasia mutated; ATR: ataxia telangiectasia and Rad3-related; ATRIP: ATR-interacting protein; CDK: cyclin-dependent kinase; MDC1: mediator of DNA-damage checkpoint 1; MRE11: meiotic recombination 11; NBS1: Nijmegen breakage syndrome 1; RPA: replication protein A; RFC: replication factor C; TOPBP1: DNA topoisomerase-II-binding protein 1* (d'Adda di Fagagna, 2008).

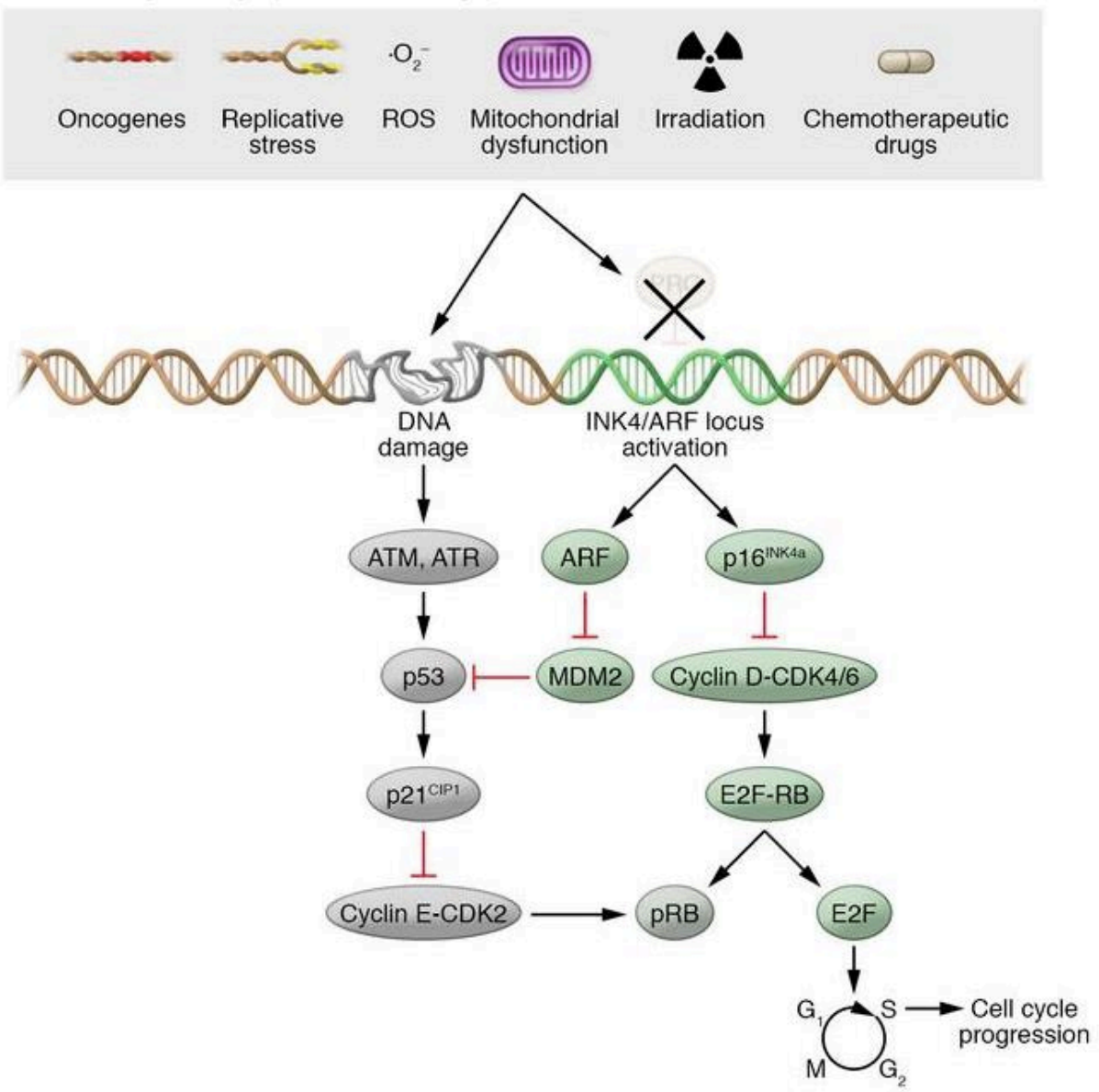

Figure 4 : Major pathways for cell cycle arrest

Senescence-inducing stress signals activate either the p53 signaling pathway, the p16-pRB signaling pathway, or both. DDR results in the p53 stabilization, resulting in the expression of p21 (a CDKI). P21 can impairs pRB hyperphosphorylation by inhibiting Cyclin E/CDK2 and thus pRB still sequesters the E2F transcription factors.
In addition, the INK4/ARF locus, which is expressed in senescent cells, encodes for several CDKI : p16, p14 (ARF) and p15. ARF prevents p53 degradation by inhibiting MDM2. Like p21, p16 can also indirectly maintain pRB hypophosphorylation by inhibiting CDK4/6. *MDM2= E3 ubiquitin ligase; ARF= alternate reading-frame protein; pRB = protein retinoblastoma; CDKs=cyclin-dependent kinases* (Herranz and Gil, 2018).

SA-βgal biomarker is one of the most used to detect senescence. However, SA-βgal activity can also be detected in overconfluent cells as well as in starved cells, so it is not a very specific marker of senescence (Di Micco et al., 2021).

2.2. DNA damage and DDR

Whether senescence is induced by intrinsic (telomere attrition, oxidative damage) or extrinsic factors (UV, X-rays), senescent cells exhibit DNA damage inducing persistent DDR **(Figure 3**) (Di Micco et al., 2021; Herranz and Gil, 2018). DNA double strand breaks are recognized by the MRN complex, composed of MRE11, RAD50 and NBS1. This MRN complex recruits ATM (d'Adda di Fagagna, 2008). DNA simple strand breaks are recognized by the 9-1-1 complex (RAD9–RAD1–HUS1) which activate ATR. ATR and ATM induce the phosphorylation of H2AX histones (γH2AX), allowing the recruitment of DNA damage mediators such as 53BP1 (p53-Binding Protein-1), MCD1 (Mediator of DNA damage Checkpoint-1) or Claspin (d'Adda di Fagagna, 2008). Mediators, like 53BP1 can be detected in DNA damage foci in the nuclei of senescent cells (Fumagalli et al., 2012). In addition, the activation of ATR and ATM induces CHK1 and CHK2 downstream kinases phosphorylation, leading to the phosphorylation of p53 and CDC25 (Cell-Division Cycle 25). When phosphorylated, p53 is activated and can lead to cell cycle arrest (see paragraph 2.4). On the other hand, CDC25 is a cyclin-activating phosphatase that is necessary for cell cycle progression as CDC25 activates cyclin-dependent kinases. Phosphorylation of CDC25 by the DDR leads to its inactivation and thus to cell cycle arrest (d'Adda di Fagagna, 2008).

2.3. Cell cycle arrest

Senescent cells are characterized by an irreversible cell cycle arrest in G1/S phase mainly driven by p16 and/or p53-p21 pathways resulting in the maintenance of the hypo-phosphorylation of the retinoblastoma protein (pRB), leading to the sequestration and inhibition of E_2F, a transcription factors family implicated in the expression of genes coding for proteins that are required for the cell cycle progression such as CDC25 (**Figure 4**) (Bracken et al., 2004; Campisi and d'Adda di Fagagna, 2007). As explained before (paragraph 2.3), p53 is a transcription factor activated by the DDR and it promotes the expression of the cyclin-dependent kinase inhibitor (CDKI) p21, inducing cell cycle arrest (d'Adda di Fagagna, 2008).
In addition, INK4/ARF locus is expressed in senescent cells but is silenced in normal cell. This INK4/ARF locus is composed of the *CDKN2A* gene, encoding for p16 and p14 (ARF) and by *CDKN2B* gene, coding for p15. ARF inhibits p53 degradation, promoting p53/p21 mediated cycle arrest. Moreover, p16 is also a CDKI that inhibits CDK4/6, also resulting in cell cycle arrest by the sequestration of E_2F by hypo-phosphorylated pRB (Herranz and Gil, 2018).
Since p16 and p21 are transcriptionally regulated in senescence, the study of their gene expression is a good indicator of their protein expression. In addition, cell cycle arrest results in a decrease of proliferation which can be demonstrated with a decreased Ki67 immunostaining or EdU/BrdU incorporation (Di Micco et al., 2021).

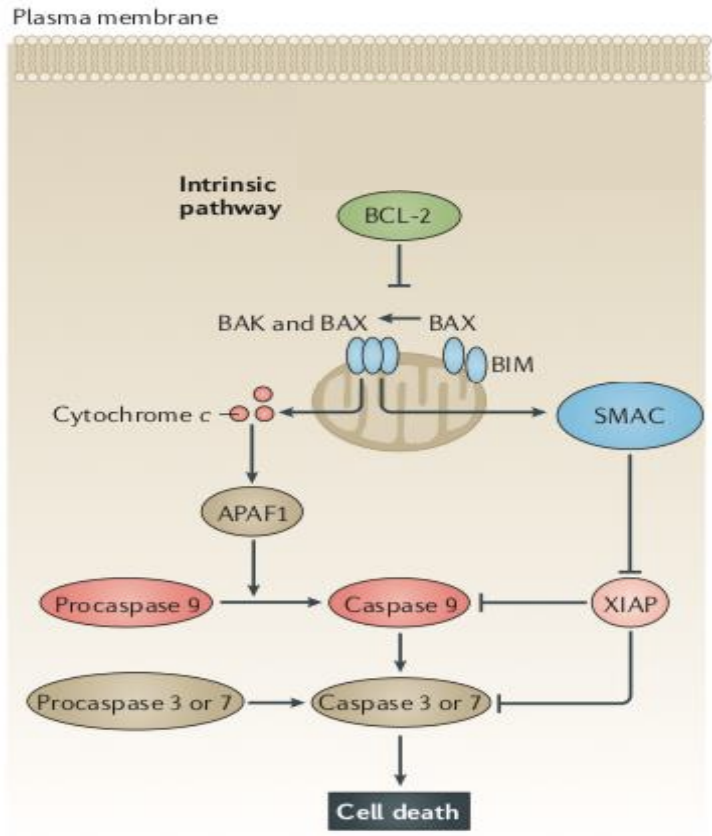

Figure 5 : The intrinsic apoptosis pathway. The oligomerization of the pro-apoptotic proteins BAK and BAX induces the mitochondrial outer membrane permeabilization (MOMP), resulting in the release of cytochrome c from the mitochondria. Cytochrome c forms a complex with procaspase 9 and APAF1, inducing caspase 9 activation. Caspase 9 then activates procaspase 3 and procaspase 7, resulting in cell apoptosis. In addition, MOMP allows the release of SMAC in the cytosol, inhibiting XIAP. Anti-apoptotic BCL-2 proteins inhibit the MOMP by sequestering BAK and BAX through their BH3 domain. *APAF1: apoptosis protease-activating factor 1; BAX: BCL-2-associated X protein; BAK: BCL-2 antagonist killer 1; SMAC: second mitochondria-derived activator of caspase; XIAP: X-linked inhibitor of apoptosis.* (Ashkenazi et al., 2017).

2.4. Apoptosis resistance

Senescent cells are more resistant to apoptosis. This is associated with their overexpression at the mRNA and protein levels of several members of the anti-apoptotic BCL 2 (B cell lymphoma 2) protein family, such as BCL-2, BCL-W and BCL-XL (Yosef et al., 2016). BCL-2 proteins are preventing apoptosis by binding to the BH3 motifs of pro-apoptotic proteins BAX (BCL-2-associated X protein) and BAK (BCL-2 antagonist killer 1), thus preventing their oligomerization. When oligomerized, BAX and BAK induce mitochondrial outer membrane permeabilization and the release of cytochrome c and SMAC (second mitochondria-derived activator of caspase) in the cytosol, leading to the apoptosis of the cell (**Figure 5**) (Ashkenazi et al., 2017).
The inhibition of BCL-2 and BCL-XL by ABT-737 or ABT-263 (Navitoclax) results in the death of senescent cells, confirming that the overexpression of BCL-2 family proteins are involved in the apoptosis resistance of senescent cells (Yosef et al., 2016).

2.5. Chromatin changes

Senescent cells also show changes in their chromatin organization. When stained with DAPI, the nucleus of senescent cells can present senescence-associated heterochromatin foci (SAHF), which are enriched in silencing markers like histone H3K9 methylation (Di Micco et al., 2021). SAHF have a role in the cell cycle arrest as some proliferation-promoting genes (for example E_2F target genes, like cyclin A) are silenced in this heterochromatin structure (Aird and Zhang, 2013).
Moreover, senescent cells present a loss of lamin B1 which is an important structural protein of the *nuclear lamina* that borders the inner surface of the nuclear envelope. *LMNB1*, which encodes for lamin B1, is an E_2F target gene. As the activation of p53/p21 or p16 pathways in senescent cells results in E_2F inactivation, this leads to a decreased expression of *LMNB1* and to lamin B1 loss (Shimi et al., 2011). Decreased expression of lamin B1 at the mRNA and protein level can therefore be used as a senescence biomarker (Freund et al., 2012).

2.6. SASP

SASP composition

Senescent cells display a senescence-associated secretory phenotype (SASP) composed of pro-inflammatory cytokines (IL-1α/β, IL-6, IL-8), chemokines (CXCL1/GROα, CCL-2/MCP-1, CCL-5/RANTES, MCP-2, MIP-1α), proteases (MMP) and growth factors (VEGF, EGF, FGF) (Basisty et al., 2020; Salminen et al., 2012). Although the expression of some SASP factors seem to be common to the majority of senescent cells, as IL-6, IL-8 or CXCL1, the SASP composition is changing over time and is depending on several factors such as the cell type and the senescence inducer (Basisty et al., 2020; Coppé et al., 2008; Faget et al., 2019).

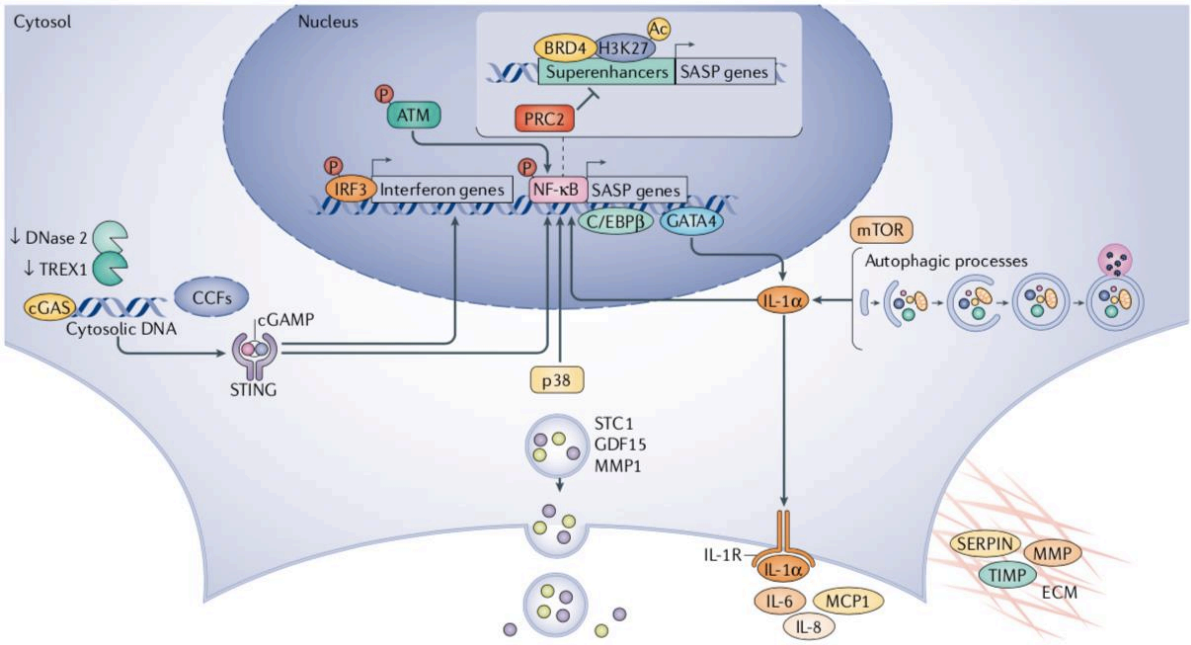

Figure 6: SASP regulation

SASP is predominantly regulated by NF-κB and its cofactor C/EBPβ. NF-κB could be activated by several pathways activated in senescent cells, like $p38^{MAPK}$, mTOR, IL1α signaling and it is also suggested that cGAS–STING pathway could induce SASP genes transcription through NF-κB activation (Di Micco et al., 2021).

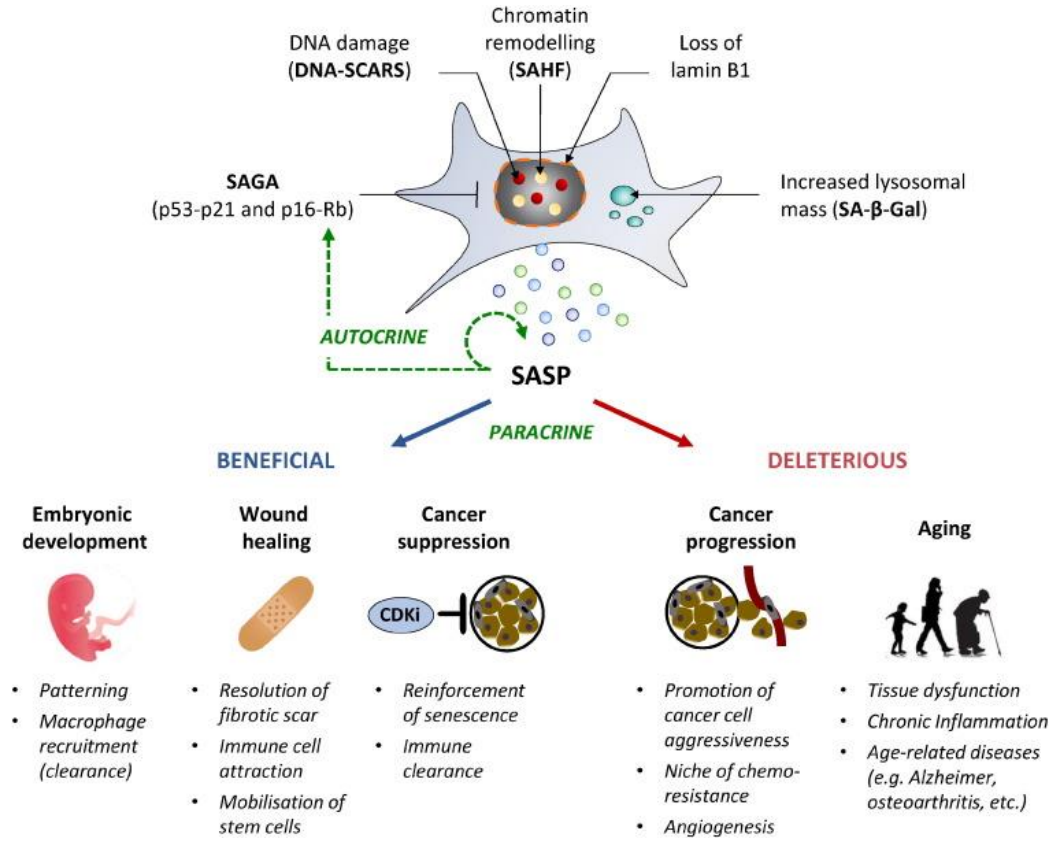

Figure 7 : Beneficial and detrimental SASP effects

Senescent cells interact with their environment via their SASP. Although SASP could have some beneficial effects (as it is important for embryonic development and favors wound healing), it could also have detrimental effects. Indeed, SASP from senescent cells is implicated in the development of various age-related diseases and tissue dysfunctions. In addition, some SASP components are also known to be pro-tumorigenic (Malaquin et al., 2016).

SASP induction

The DDR activation, but not p53 and pRB, is required to induce SASP factors (as IL-6) secretion in senescent cells (Rodier et al., 2009). Moreover, most of the SASP factors are regulated at the transcriptional level by the transcription factor NF-κB (Salminen et al., 2012). NF-κB is sequestered in the cytosol by its inhibitor, IκBα. When phosphorylated, IκBα is degraded and NF-κB is released, allowing its translocation to the nucleus and the activation of downstream genes. NF-κB pathway can be activated by several factors **(Figure 6)** (Salminen et al., 2012). First, $p38^{MAPK}$, which is activated by several stress such as DNA damage and oxidative stress and is known to be activated in senescent cells, can lead to NF-κB activation and therefore to SASP genes transcription (Salminen et al., 2012). Moreover, IL1α, which is a SASP component, also reinforces senescence by activating NF-κB-dependent SASP genes transcription (Salminen et al., 2012). mTOR activation, leading to the induction of MAPKAPK2 (mitogen-activated protein kinase-activated protein kinase 2) pathway is also shown to be required to induce SASP genes transcription in fibroblasts (Herranz et al., 2015).
The transcription factor GATA4, which is a NF-κB activator and is activated by the DDR pathway, also plays a role in SASP genes expression (Kang et al., 2015).
Finally, senescent cells present cytosolic DNA fragments, due to the downregulation of DNases (DNase2 and TREX1) which are degrading cytosolic DNA fragments in non-senescent cells. Theses cytosolic DNA fragments activate cyclic GMP–AMP synthase (cGAS)–stimulator of interferon genes (STING) pathway. The activation of cGAS–STING pathway then promotes SASP gene expression notably via NF-κB activation (Faget et al., 2019).

SASP effect on cellular environment

Senescent cells can impact their cellular environment through their SASP. A recent study showed that the SASP from senescent keratinocytes induces major proteomic changes in immortalized keratinocytes (Valerio et al., 2021).
The SASP could be both beneficial or detrimental for the neighboring tissue (**Figure 7**). Indeed, SASP is for example involved in wound healing repair and senescent cells clearance delays wound closure (Demaria et al., 2014). However, in the context of aging, senescent cells accumulate in the tissues instead of being cleared by the immune system (Ovadya et al., 2018). When accumulated in tissues, senescent cells could have deleterious effect and lead to chronic inflammation, fibrosis and the onset of several age-related diseases through their SASP (Malaquin et al., 2016). Indeed, in the past few years, senescent cells have been shown to play a role in several age-related diseases such as osteoarthritis, idiopathic pulmonary fibrosis or cancers (Childs et al., 2017). Indeed, SASP from X-radiation induced premature senescent fibroblasts showed a propensity to promote EMT and invasiveness of breast cancer cell lines, caused in part by the secretion of IL-6 and IL-8 from senescent fibroblasts (Coppé et al., 2008). Moreover, studies have shown that senescent cells clearance in mice reduces age-related issues like muscle and adipose tissue loss and improved the physical function of aged mice (Baker et al., 2011; Cai et al., 2020). In addition, the accumulation of senescent cells in aged dermis or epidermis lead to epidermal atrophy and therefore to skin aging (Victorelli et al., 2019;

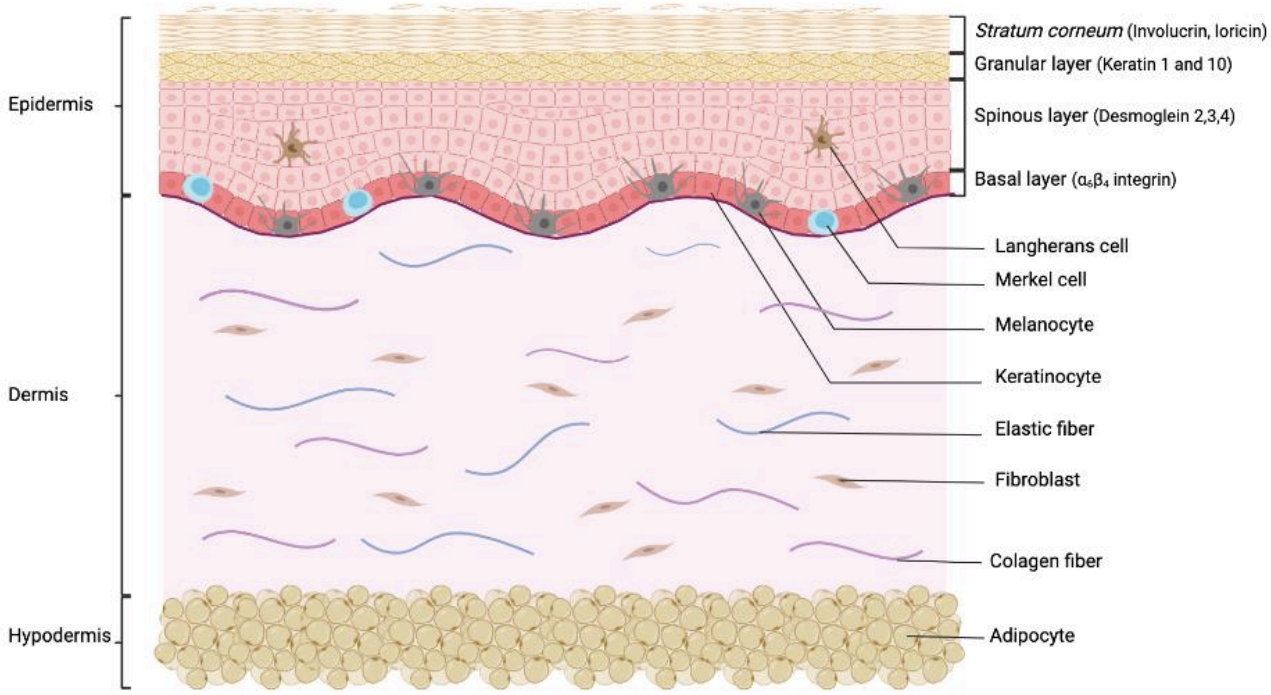

Figure 8 : Skin structure and composition

The skin is divided in 3 parts : the upper part, called epidermis is composed at 90% by keratinocytes which are going through a differentiation process, forming 4 different layers : the basal layer, where keratinocytes are proliferating, the spinous layer where keratinocytes begin their differentiation, the granular layer containing keratinocytes that are releasing keratohyalin granules and the *stratum corneum*, containing anucleated keratinocytes aggregated with lipids and filaggrin and involucrin to form a tight barrier. Some proteins are expressed in particular epidermis layer during skin differentiation and can be used as markers such as $\alpha 6\beta 4$ integrin for the basal layer, desmogelin 2, 3 and 4 for the spinous layer, keratin 1 and 10 for the granular layer and involucrin and loricrin for the *stratum corneum*. The dermis is made by fibroblasts secreting an extracellular matrix composed of collagen and elastic fibers. Finally, adipocyte are composing the dermis. This illustration does not include hairs and blood vessels (made with Biorender).

Weinmüllner et al., 2020). Senescent cells can therefore promote aging phenotype in multiple organs.

3. Aging of the skin

The skin is an interesting model to study aging, senescence and cancer. Indeed, as the skin is highly exposed to environmental aggressions, it is subject to extrinsic aging, in addition to chronological aging (Wang and Dreesen, 2018; Zhang and Duan, 2018). The environmental aggressions, such as ultraviolet radiations (UV) can promote premature senescence as well as the onset of skin cancers (Liu-Smith et al., 2017; Toutfaire et al., 2017).

3.1. Skin structure

Skin constitutes the main barrier between our organism and the external environment and therefore protects against pathogens infections, dehydration, pollution and ultraviolet radiations (UV) (Graham et al., 2019). This protective tissue is divided in three layers: the epidermis, the dermis and the hypodermis **(Figure 8**). The epidermis is the skin upper layer and consists in a stratified epithelium mainly composed of keratinocytes that undergo a differentiation process. The epidermis basal cell layer is composed of proliferative keratinocytes that are attached to the *basal lamina* by hemidesmosomes containing $\alpha_6ß_4$ integrins (Candi et al., 2005). Keratinocytes differentiate during their migration through the upper layers of the epidermis to form a protective barrier. The spinous layer is composed of polyhedral keratinocytes interconnected with desmosomes and producing keratin filaments. In the granular layer, keratinocytes are producing keratin 1 and 10 and release their keratohyalin granules (containing profilaggrin allowing keratin filaments aggregation). The "barrier" layer, the *stratum corneum* is composed of anucleated keratinocytes, structural proteins such as involucrin and loricrin and lipids creating a tight barrier (Candi et al., 2005; Zaidi and Lanigan, 2010). The epidermis also contains three other cell types: first, the melanocytes which are producing melanin to protect the epidermis against UV radiation. In addition, the epidermis contains immune cells called the Langerhans cells and Merkel cells, which are mechanoreceptors (Zaidi and Lanigan, 2010).
The dermis contains fibroblasts that are secreting an extracellular matrix composed of collagen and elastic fibers. Nerves, blood and lymphatics vessels are also present in the dermis (Graham et al., 2019).
Finally, the hypodermis is mainly composed of adipocytes, allowing thermoregulation, insulation and protection of the deeper tissues (Graham et al., 2019).

3.2. Photoaging of the skin

The skin, as the whole organism is subject to chronological aging, also called intrinsic aging. Intrinsic aging of the skin is observed in photo-protected area like the inner upper arm. This intrinsic aging results in thinning of the epidermis and dermis, caused by decreased proliferation of keratinocytes and fibroblasts, notably through cellular senescence. Moreover, a loss of

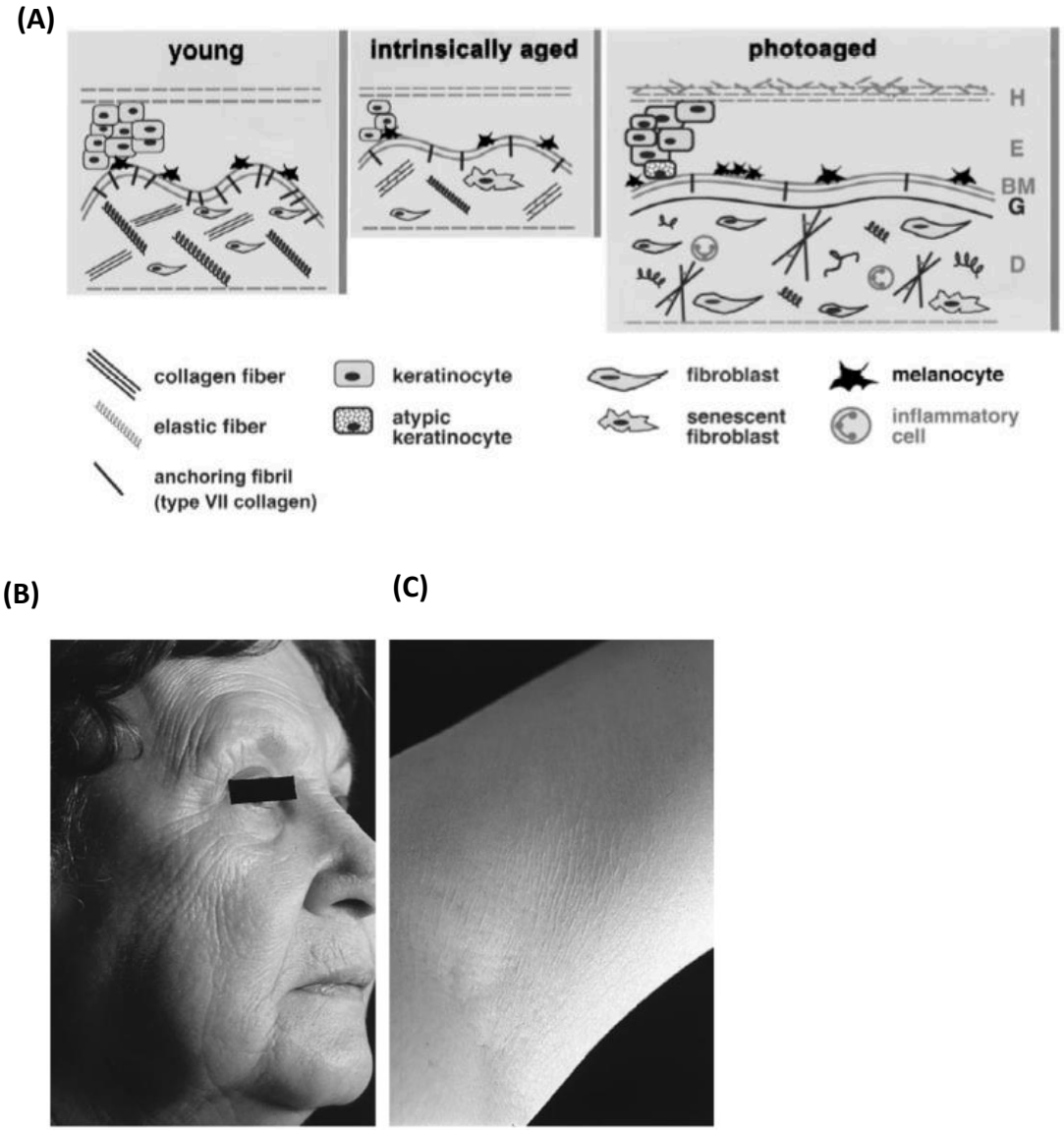

Figure 9: Comparison between photoaging and intrinsic skin aging. (A) Illustration of characteristic features in young, intrinsically aged and photoaged skin. Intrinsic aging of the skin results in a thinning of the epidermis and dermis. The components of the extracellular matrix, such as collagen and elastin are reduced. Fibroblasts are less numerous than in young skin and may show a senescent phenotype. Photo-aged skin often shows thickening of the stratum corneum, epidermis and dermis. The epidermis also shows hyperkeratosis. The distribution of melanocytes becomes heterogeneous, resulting in pigmentary changes. The anchoring fibrils that connect the epidermis to the dermis are reduced in number, and the collagen is reduced and damaged. *H: horny layer; E: epidermis; BM: basement membrane; D: dermis* **(B)** Photoaged skin presenting deep wrinkles. **(C)** Aging of a photo-protected skin (inner upper arm) with thinning of the skin and fine wrinkles (Scharffetter–Kochanek et al., 2000; Wlaschek et al., 2001).

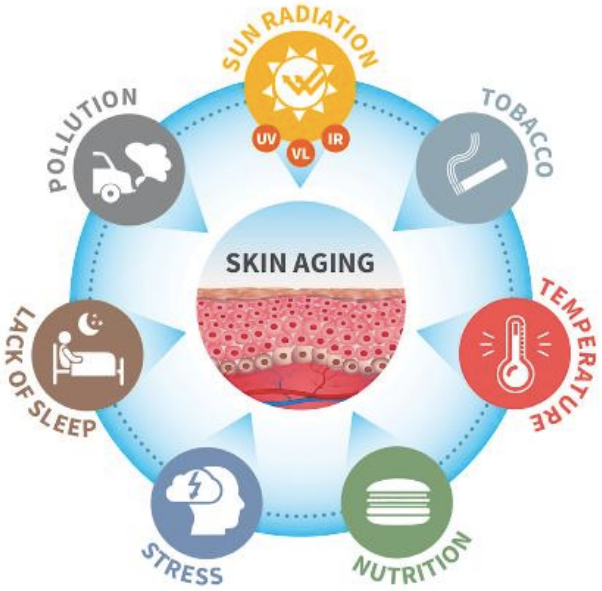

Figure 10 : Skin exposome. Exposure to sun, pollution and tobacco are known to damage the skin structure, impacting skin aging. In addition, other factors, such as stress, nutrition or lack of sleep can potentiate the skin aging (Krutmann et al., 2017).

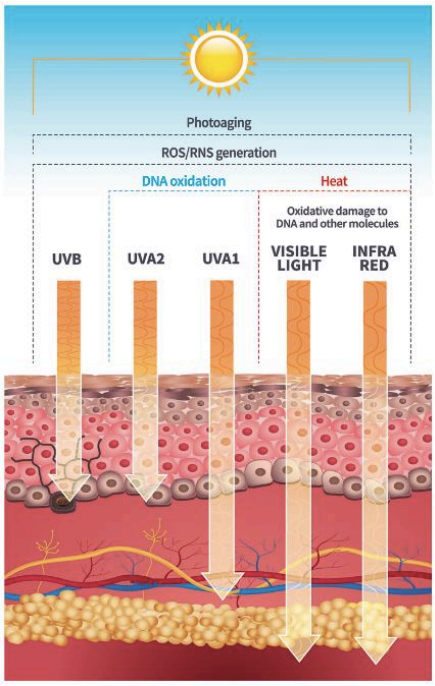

Figure 11 : Sun radiations penetrate into the skin (Krutmann et al., 2017).

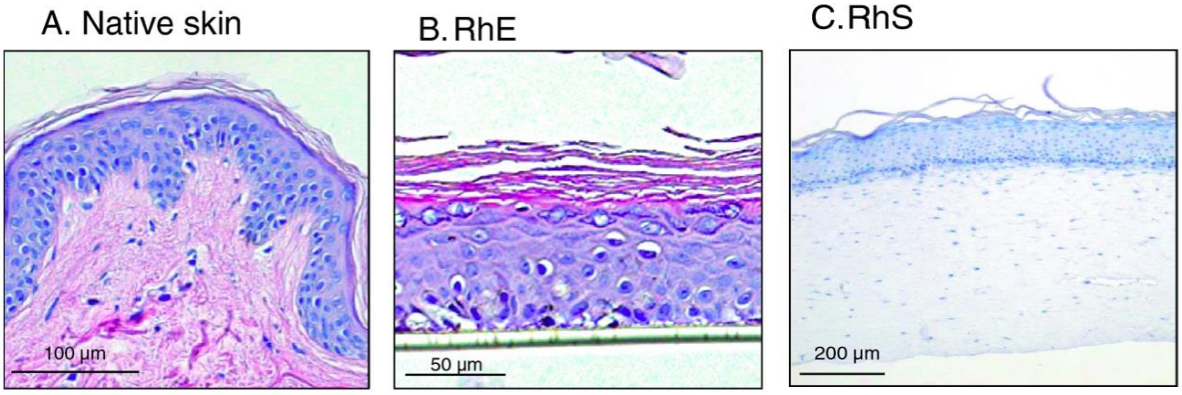

Figure 12 : Biopsy from human skin (A) compared to Reconstructed human Epidermis (RhE) (B) and to Reconstructed human skin (RhS). Hematoxylin/eosin staining (Rodrigues Neves and Gibbs, 2021).

elasticity is observed in skin undergoing intrinsic aging, due to the degeneration of the collagen and elastin fibers composing the extracellular matrix of the dermis (**Figure 9**) (Zhang and Duan, 2018). However, skin is also exposed to extrinsic aging, caused by environmental aggressions. The extrinsic aging results in a thickening and stiffening of the epidermis, as well as altered pigmentation (**Figure 9**) (Orioli and Dellambra, 2018). The skin "exposome" regroups the main factors contributing to skin aging and includes environmental factors such as air pollution, solar radiation or tobacco (**Figure 10)** (Krutmann et al., 2017).
Sun exposure is one of the major factors causing skin extrinsic aging and is specifically called "photoaging" (Blume-Peytavi et al., 2016; Toutfaire et al., 2017). UV rays are the most energetic solar rays and are involved in skin photoaging (Gilchrest and Krutmann, 2006). UV rays are classified in three categories depending on their wavelength: UVA (320-400 nm), UVB (290-320 nm) and UVC (100-290 nm). As UVC are stopped by the ozone layer, only UVA and UVB can reach the skin (**Figure 11**) (Gonzaga, 2009). UVA represent 95% of UV on Earth's surface and are able to penetrate in the deeper dermis, inducing oxidative damage, leading to indirect DNA damage. In addition, UVB are known to induce direct DNA damage because they can be absorbed by DNA and directly induce DNA damage such as pyrimidine dimers (Schuch et al., 2013). These UV-induced DNA damage could induce both skin cancers and premature senescence (Liu-Smith et al., 2017; Toutfaire et al., 2017).

UV-induced senescence of skin cells could be studied in classical cell culture. However, in a monolayer culture, keratinocytes are in a proliferative state which is far from the stratified layers of differentiated keratinocytes composing the epidermis that is observed *in vivo.*
To study epidermis aging *in vitro*, 3D models such as the reconstructed human epidermis (RHE), composed of keratinocytes, are available (**Figure 12**). These reconstructed epidermis are able to mimic the epidermis stratification as well as the barrier function of the epidermis (Hennies and Poumay, 2021). A recent study showed that UVB exposure could induce a significant decrease of *lamin B1* expression in monolayer keratinocytes while the same exposition to UVB did not affect *lamin B1* expression in RHE (Tan et al., 2021). This demonstrates that keratinocyte response to UVB could be different in monolayer culture and in a reconstructed skin model, underlining the importance of working with epidermal models to better approximate *in vivo* conditions. However, keratinocytes are not the only cell type of the skin and to reproduce the interaction between keratinocytes and fibroblast, reconstructed human skin can be used (**Figure 12**). It consists of an epidermis equivalent on a dermal matrix containing fibroblasts (Hennies and Poumay, 2021). Moreover, reconstructed epidermis can also be complexified by the adding of melanocytes to study the impact of senescent melanocyte in the epidermis (Victorelli et al., 2019).
Reconstructed epidermis models can also be used to study skin pathologies ; depending on the pathology, the reconstructed epidermis can be complexified by adding for example immune cells (Hennies and Poumay, 2021).

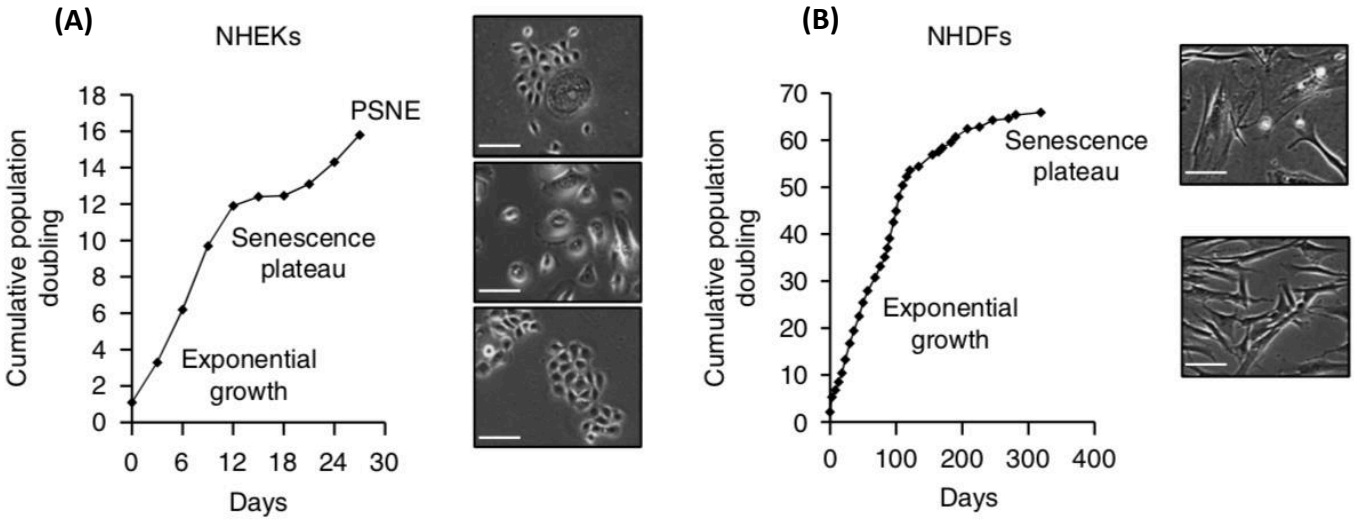

Figure 13 : Growth curve of keratinocytes (A) and dermal fibroblasts (B), associated with cell morphology micrography. *NHEKs: normal human epidermal keratinocyte; NHDF: normal human dermal fibroblast ; PSNE: post-senescence neoplastic evasion* (Nassour et al., 2016).

3.3. Senescent cells and skin aging

Fibroblasts

Almost all studies on *in vitro* senescence are performed on fibroblasts, as it is historically the first cell type in which senescence was discovered (Hayflick and Moorhead, 1961). Replicative senescence of fibroblasts occurs after 30 to 70 passages in culture and is associated with telomere shortening and DDR activation (Nassour et al., 2016). However, fibroblasts are rarely proliferating in the dermis and it is unlikely that replicative senescence occurs *in vivo*. However, senescent fibroblasts are detected in the skin and could result from premature senescence *in vivo* (Tigges et al., 2014).
Interestingly, H_2O_2-induced premature senescent fibroblasts induce hallmarks of skin aging like epidermis thickening and impairment of the epidermal barrier function while incorporated in the dermis of 3D organotypic culture, suggesting that senescent fibroblasts could play a role in the epidermis aging even if they are localized in the dermis (Weinmüllner et al., 2020).

Moreover, subcytotoxic exposition to UVB is known to induce fibroblasts' premature senescence. Indeed, ten exposures to 250 mJ/cm^2 of UVB during five days induce a premature senescent phenotype in dermal fibroblasts (increased SA-βGal activity, increased p53, p21 and p16 protein levels) (Debacq-Chainiaux et al., 2005). In addition, dermal fibroblasts exposed to 10 J/cm^2 of UVA per day for 3 days also present an increased SA-βGal activity, increased p53, p21 and p16 mRNA and proteins levels (Yi et al., 2018). These data suggest that photo-exposure can drive UV-induced premature senescence of dermal fibroblasts.

Keratinocytes

As for the fibroblasts, replicative senescence does not seem to occur in keratinocytes *in vivo* as their telomere length is not reduced in aged donors (Krunic et al., 2009). In addition, even in *in vitro* culture, keratinocytes are presenting a proliferation arrest at early passages (10-15) which is independent of telomere shortening and that is therefore referred as the "replicative-like" senescence. These keratinocytes in "replicative-like" senescence display several biomarkers of senescence such as increased SA-βgal activity, enlarged morphology and cell cycle arrest (Nassour et al., 2016). However, unlike in fibroblasts, the keratinocytes in "replicative-like" senescence could be transitory as some senescence keratinocytes are able to spontaneously bud into small clones that are able to proliferate again (**Figure 13**) (Gosselin et al., 2009). Moreover, unlike senescent fibroblast, this "replicative-like" keratinocyte senescence is not associated with the DDR activation and p53 pathway. Indeed, Nassour and his team showed that "replicative-like" senescence in keratinocytes is induced by oxidative stress inducing DNA single-strand breaks and the activation of the single-strand breaks repair pathway, leading to a p16-mediated senescence (Nassour et al., 2016).

However, keratinocytes in aged skins are showing a decrease of proliferation and lamin B1 *in vivo* (Dreesen et al., 2013). Moreover, p16 positive cells are increased in the epidermis of aged

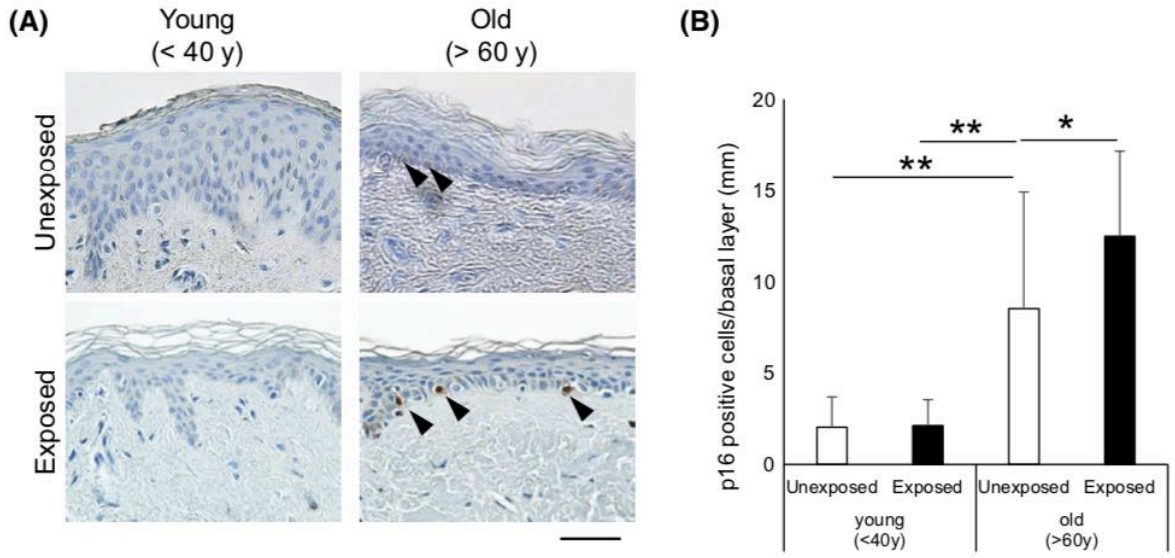

Figure 14 : Accumulation of p16 positive cells with age. (A) DAB (3,3'-Diaminobenzidine) staining of p16-positive cells in the epidermis of unexposed and exposed areas from young (30 and 34 years of age, respectively) and old (73 and 67 years, respectively) donors**. (B)** Quantification of p16-positive cells in the epidermal basal layer (n = 12 excepted for young exposed areas n= 9) (Yoshioka et al., 2021).

donors (**Figure 14**), suggesting that senescent keratinocytes accumulate in aged epidermis (Yoshioka et al., 2021).

A single dose of 6 J/cm^2 of UVA induces major proteomic changes associated with senescence and an increased SA-βGal activity *in vitro* in keratinocytes (Valerio et al., 2021). Additionally, repeated doses of UVB (3 doses at 675 mJ/cm^2 in a single day) also drive keratinocytes premature senescence in *in vitro* monolayer culture (Bauwens et al., *in revision*). Additionally, keratinocytes in RHE exposed to a single UVB dose of 100 mJ/cm^2 present a decreased *lamin B1* gene expression and an increase of IL-6 and IL-8 secretion that could be linked with senescence (Tan et al., 2021).

Melanocytes

The melanocyte senescence is poorly studied. The replicative growth arrest is depending on the donor age and skin type. Indeed, the proliferation arrest occurs after 60 to 90 population doublings in neonatal melanocytes while it appears under 40 population doublings in adult melanocytes. This proliferation arrest is associated with an increase of SA-βGal activity and a p16 activation (but no p53/p21 activation) (Bennett and Medrano, 2002).
Senescent melanocytes were shown to accumulate in the epidermis with age *in vivo* as p16 labeling in the basal epidermal layer is often colocalized with melanocytes markers. In addition, in aged epidermis, melanocyte telomeres are presenting γH2AX foci but telomeres length is not reduced, suggesting the activation of DDR at the telomeres independently from telomere length (Victorelli et al., 2019). In addition, reconstructed epidermises containing senescent melanocytes are thinner than the ones containing young melanocytes and senescent melanocytes are able to induce paracrine telomere damage in the neighboring cells (Victorelli et al., 2019).

Melanocytes daily irradiation with 400 mJ/ cm^2 of UVA and UVB for 5 consecutive days *in vitro* leads to senescence, characterized by a reduced proliferation, an increased SA-βGal activity and an increased p16 expression (Victorelli et al., 2019). Interestingly, when these UV-induce premature senescent melanocytes are seeded with keratinocytes to make a RHE containing melanocytes (called a melanoderm), keratinocytes proliferate less. In addition, keratinocytes in melanoderms containing senescent melanocytes are presenting a higher level of *p16* mRNA level than keratinocytes from melanoderms containing young melanocytes. In addition, the incorporation of UV-induced premature senescent melanocytes in melanoderms are associated with thinner epidermis, as it could be observed in aged skins (Victorelli et al., 2019).

Therefore, the main cellular types composing the skin can undergo senescence through UV-exposure and their accumulation *in vivo* is linked with skin aging. However, UV exposure are also well known to promote skin cancers (Pfeifer, 2020).. Moreover, the incidence of skin cancers increases significantly with age, as the average age of detection of skin carcinoma is over 65 years and the median age at melanoma diagnosis is 59 years (Matthews et al., 2017; Muzic et al., 2017). Aged and sun-exposed skin is therefore predisposed to accumulate

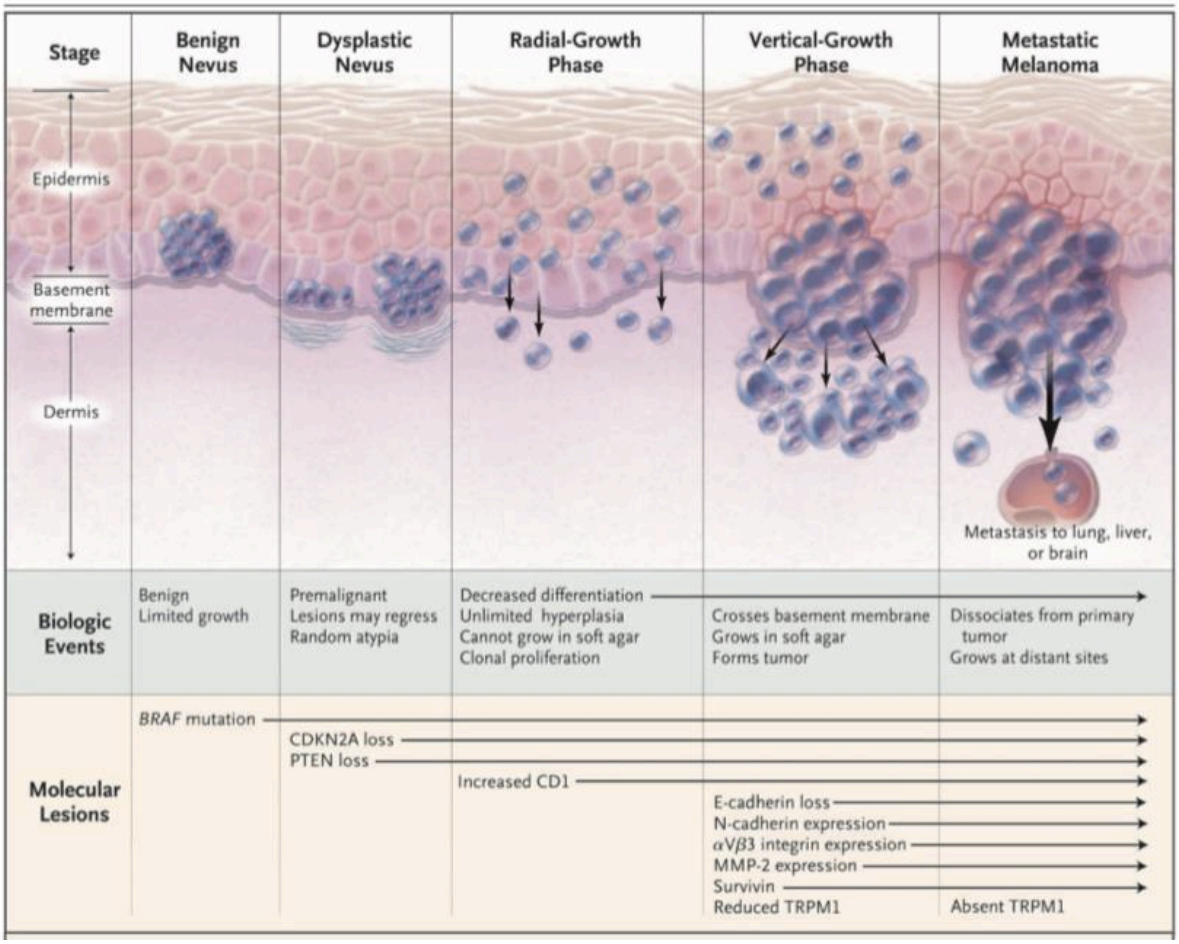

Figure 15: **Melanoma initiation progression.** Schematic representation of molecular events leading a melanocyte to a metastatic melanoma. It is important to know that only 25% of melanoma begin with a benign nevus, they also can emerge directly from a transformed melanocyte (Miller and Mihm, 2006).

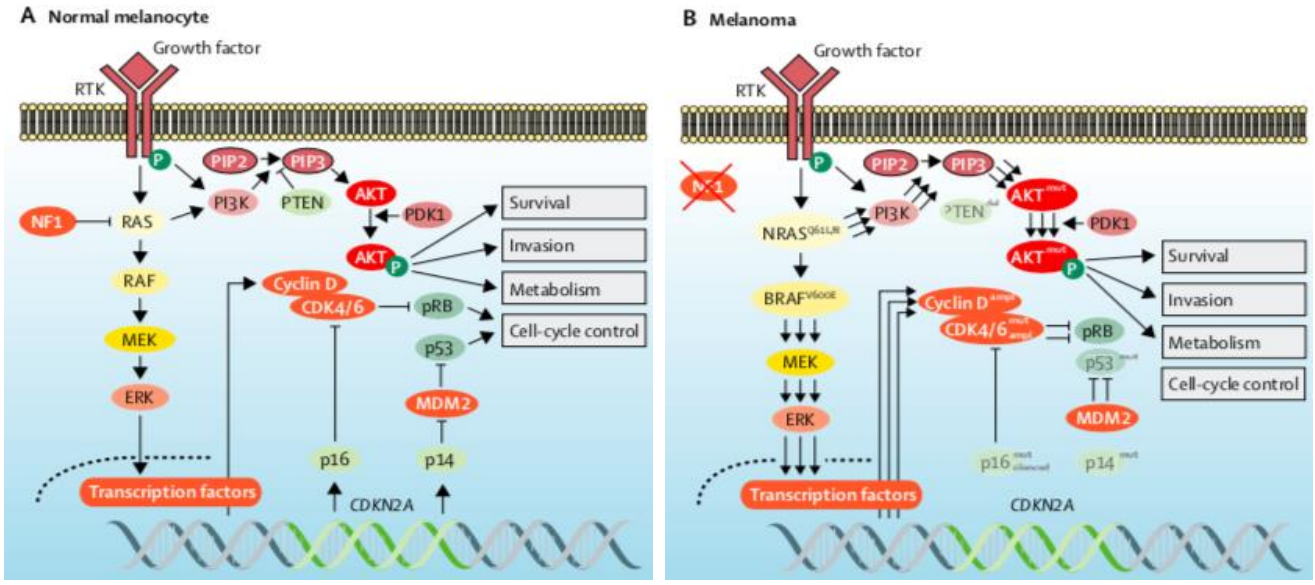

Figure 16 : Key signaling pathways in melanoma. (A) In melanocytes**,** balanced control of MAPK, PI3K-AKT signaling and cell-cycle regulation allows normal cell proliferation. **(B)** In melanoma, genetic alterations lead to constitutive pathway activation inducing high proliferative signals and the loss of cellular homeostasis**.** (Schadendorf et al., 2018)

senescent cells and to develop skin cancer. It is thus important to study the interactions between the skin senescent cells and skin cancer cells to better understand the development of skin cancers.

4. Skin cancers

Skin cancers are the most common cancer in Caucasian population (Apalla et al., 2017). They are divided in two main groups: melanomas, originating from melanocytes, and non-melanoma skin cancers, originating from keratinocytes and divided in cutaneous squamous cell carcinomas (cSCC) and basal cell carcinomas (BCC) (Pfeifer, 2020).
Non-melanoma skin cancers are very common, representing more than one third of all cancers in the US. However, non-melanoma skin cancers have a low mortality rate because their capacity to form metastasis is low (Leiter et al., 2014).
On the other hand, melanoma only represent 1,7% of the diagnosed cancers but have a higher mortality rate than carcinoma as they are responsible of 72% of death from skin cancers (Schadendorf et al., 2018).

As epidermis is the upper layer of the skin, it is particularly exposed to external stressors such as UV (Todorova and Mandinova, 2020). As described previously, UV can induce senescence in skin cells but they are also known to induce genetic mutation linked to the development of skin cancers (Singh et al., 2019). Indeed, when theses mutations lead to the inactivation of tumor-suppressor gene like p53 or to the overactivation of proto-oncogenes like Ras, it could induce cancer (Singh et al., 2019). 90% of cSCC and more than 50% of BCC are presenting UV-induced mutations of p53 (Gilchrest and Krutmann, 2006). Moreover, most of the melanoma cells are presenting UV-induced mutations which confirms that UV exposure is a major risk factor for developing skin cancers (Tang et al., 2020).
A malignant melanoma acquired several mutations: the first frequent mutation is a *BRAF* mutation, leading to the formation of a benign naevus. Melanoma formation requires additional inhibitory mutations in tumor-suppressor genes controlling the cell-cycle like *CDKN2A* (cyclin-dependent kinase-inhibitor 2A), *PTEN* (phosphatase and tensin homologue) or *TP53* (tumor-protein p53) (**Figure 15**) (Schadendorf et al., 2018). These mutations lead to the overstimulation of pro-proliferative pathways like the MAPK and AKT pathways, inducing uncontrolled cell division (**Figure 16**) (Schadendorf et al., 2018). Moreover, to cross the basement membrane and to migrate through the bloodstream and form metastases in other tissues, melanoma cells need to realize an epithelial to mesenchymal transition (EMT) resulting in the disruption of cell to cell junctions, the degradation of the basement membrane as well as the reorganization of the extracellular matrix (Dongre and Weinberg, 2019; Miller and Mihm, 2006).

The SASP from senescent cells could promote EMT and the disaggregation of the extracellular matrix by matrix metalloproteinases. In addition, as presented in paragraph 2.7.1, senescent cells also secrete VEGF that is known to promotes angiogenesis, leading to the vascularization of the tumor, therefore facilitating the migration of melanoma cells (Faget et al., 2019).

In addition, some fibroblast SASP components are known to promote carcinomas and melanomas such as CXCL1 and IL-8 that can bind to the CXCR2 receptor which is known to be overexpressed in melanoma cells (Coppé et al., 2010). CXCR2 receptor activation promotes angiogenesis and melanoma invasion (Gabellini et al., 2009). Farsam and colleagues also showed that fibroblasts in replicative senescence could promote cSCC migration through the secretion of chemerin in their SASP. Chemerin receptor is overexpressed in cSCC cells and its activation by chemerin activates the MAPK pathway that mediates the chemerin-induced cSCC migration (Farsam et al., 2016). In addition, the secretion of sFRP2 (secreted frizzled-related protein 2) by senescent fibroblasts promotes the invasion of melanoma by inhibiting β-catenin in melanoma cells (Kaur et al., 2016).
Moreover, senescent keratinocytes can also promote skin cancer cell migration. Indeed, the SASP from keratinocytes undergoing drug-induced premature senescence was shown to promote cSCC tumor growth and the malignant conversion (Alimirah et al., 2020). In addition, the SASP of UVB-induced premature senescent keratinocytes harvested 7 days after exposure promotes cSCC migration (Bauwens et al., *in revision*).

It thus seems that the accumulation of senescent cells with age impacts tumorigenesis. Since the incidence of cancer is also increased in the elderly, it is interesting to study the impact of senescent cells on cancer within the same tissue to better understand their interconnections. In this work, we will study the impact of senescent keratinocytes on the migration of skin cancer cells.

Objectives

The objective of this master thesis is to study the impact of senescent normal human epidermal keratinocytes (NHEKs) secretome on melanoma cells.
Previous experiments in our team showed that secreted proteins from UVB-exposed senescent NHEKs promotes cSCC migration in Boyden chambers and scratch assays (Bauwens et al., *in preparation*). As melanoma are more prone to metastasis, we decided to extend this study to melanoma.
We will first induce premature senescence of NHEKs following repeated UVB exposures (UVB-SIPS) and check the induction of several senescence biomarkers as morphological changes, SA-βgal activity, cell cycle arrest, lamin B1 loss and some SASP factors expression. When the senescence induction will be confirmed, we will then test the effect of the secretome of UVB-induced senescent NHEKs on skin cancer cell migration. To do so, Boyden chamber assays and scratch assays will be performed on primary and metastatic melanoma cell lines as well as on one cSCC cell line incubated with CM harvested from UVB-exposed and unexposed NHEKs.
Then, the composition of the secretome of NHEKs exposed to UVB will be analyzed by mass spectrometry to find proteins that may have a pro-tumorigenic effect.
Finally, reconstructed human epidermis (RHE) models including melanoma cells expressing GFP will be developed to study the relationship between senescent keratinocytes and melanoma cells in a more physiological model. In addition, to induce keratinocyte senescence in RHE, several protocols of UVB exposure and incubation with CM from senescent NHEKs will be tested.

MATERIALS AND METHODS

Cell culture

A375, A375-GFP, SKMEL-2, SKMEL-28 and A431 cells were grown in Dulbecco's Modified Eagle Medium High Glucose (DHG, Gibco, 41966029) + 10% FBS with penicillin and streptomycin. When cells reached around 90% confluence, they were subcultured. Cells were washed twice with PBS and then detached using trypsin + EDTA 0,05 % (Thermo Fisher, 25300054). Trypsin is inhibited by adding DHG + 10% FBS and cells are then centrifuged 4 min at 200 g. Cell pellet is resuspended in DHG + 10% FBS and then distributed in new T75 flasks and incubated at 37°C and 5% CO_2.

Normal Human Epidermal Keratinocytes (NHEKs) were isolated from foreskin's biopsies from young donors (St Luc Hospital, Bouge, Belgium) as described (Gilchrest, 1983). The procedure was approved by the ethical committee of the Clinique Saint Luc (Bouge). NHEKs were cultured in Keratinocyte Serum-Free Medium (KSFM) (Gibco, 107005075) supplemented with bovine pituitary extract (BPE, Gibco, 13028-014) and human epidermal growth factor (EGF, Gibco, 10450013) in a Greiner T75 flask. NHEKs were subcultured when they reached 80 % of confluence. First the medium is removed and the cells are incubated at 37°C with trypsin + EDTA 0,05 % (Thermo Fisher, 25300054). Cells are then resuspended in Phosphate Buffer Saline (PBS, 150 µM pH 7,4) + 10% Fetal Bovine Serum (FBS,10270-106, Gibco). Cells are then centrifuged 5 min at 200 g and the cell pellet is then resuspended in fresh KSFM. The cell suspension is then distributed in two new T75 flasks that are incubated at 37°C and 5% CO_2.

Human Epidermal Keratinocytes 1 (HEKa 1) were isolated from adult abdominal skin (St Luc Hospital, Bouge, Belgium). HEKa1 were thawed in cold Keratinocyte growth medium 2 (KGM-2, Lonza CC-3107) supplemented with KGM Supplements and Growth Factors: 50 µg/ml BPE (Bovine Pituitary Extracts) ; 10 ng/ml EGF; 5.10^{-7}M Hydrocortisone; 5 µg/ml Insulin; 5 µg/ml Transferrin; 0,15 mM Ca^{2+} (Lonza, CC-4152) except gentamycin replaced by penicillin (50 U/ml) and streptomycin (50 U/ml). After 6 h, KGM-2 is removed and substituted by EpiLife (Gibco, MEPI500CA) supplemented with HKGS (Gibco, 2340468) and penicillin + streptomycin. The medium is changed every 2 days. When cells reached 70–80 % of confluence they are seeded on polycarbonate filter (Millipore, PIHP01250) and Reconstructed Human Epidermis (RHE) are produced following the protocol described by De Vuyst et al. (De Vuyst et al., 2014). When HEKa 1 reached 70–80 % of confluence, the culture medium is removed and replaced by trypsin 0.025% +EDTA 0.01%. When cells are detached, trypsin is inhibited with cold *A Solution* (composition:10 mM Glucose, 3 mM KCl, 130 mM NaCl, 1 M $Na_2HPO_4.7H_2O$, 0.0033 mM Phenol Red, 30 mM Hepes) +2% FBS, and the cell suspension is transferred into a 50 ml tube. Cells are then centrifuged at 335 g at 4°C for 5 min. The supernatant is then removed, the pellet is resuspended in 1 ml of cold Epilife with 1,44 mM Ca^{2+}. 200,000 cells (HEKa1 ± A375-GFP) are seeded on polycarbonate filters (Millipore, PIHP01250) in 6-well plate and 2.5 ml Epilife with 1,44 mM $Ca^{2+}$are added at the bottom of the wells. After 24 h, cells are exposed to the air–liquid interface by removing the culture medium in the upper compartment of the insert. The medium from the well under the polycarbonate filter is replaced by 1.5 ml of Epilife with 10 ng/mL KGF, 1,44 mM Ca^{2+} and

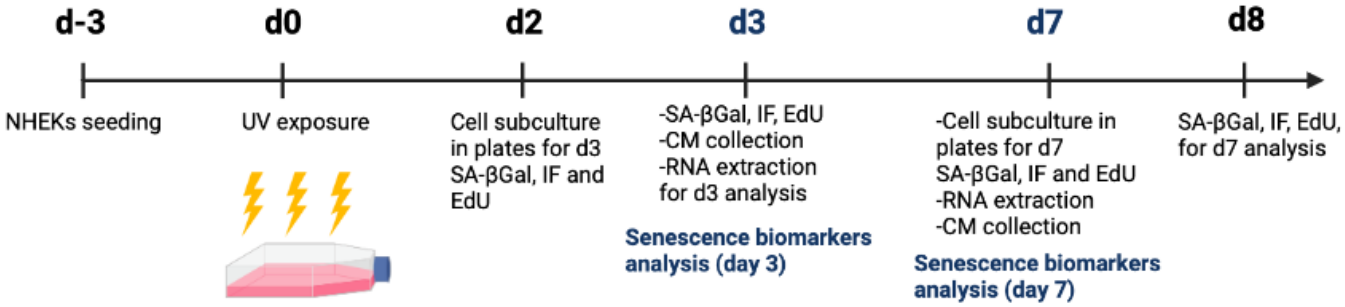

Figure 17 : UVB-SIPS protocol
Timeline of the UVB-SIPS protocol with UVB exposure at day 0 (D0) and study of the biomarkers of senescence at day 3 (D3) and day 7 (D7) (IF, EdU, SA-βGal and RNA extraction, conditioned medium (CM) collection). NHEKs are serum deprived 48h before CM collection.

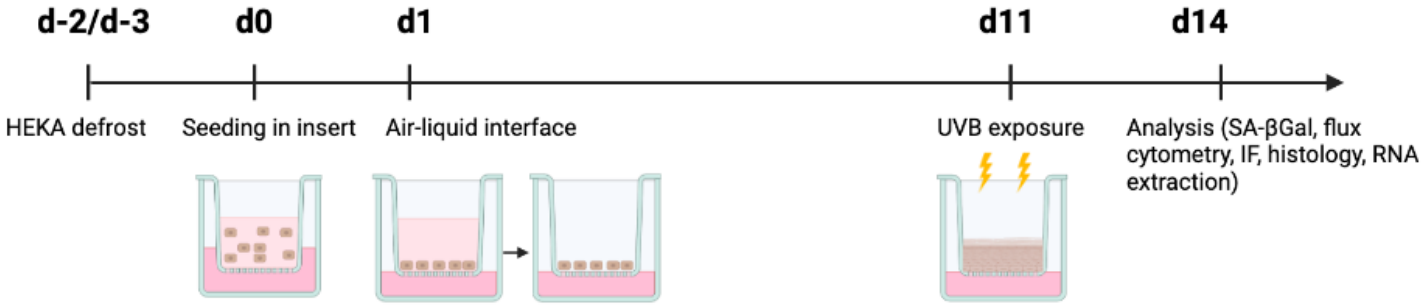

Figure 18 : RHE UVB exposure timeline
RHE are exposed to UVB once or twice at 11 days (d11) after seeding. Medium was collected at 8h and 3 days after UVB exposure for LDH activity assay. At 3 days after UVB exposure, RHE are fixed in formol or OCT to be used for histology, SA-βgal or immunofluorescence analysis or are disaggregated for flux cytometry analysis. In addition, some RHE are also used for RNA extraction.

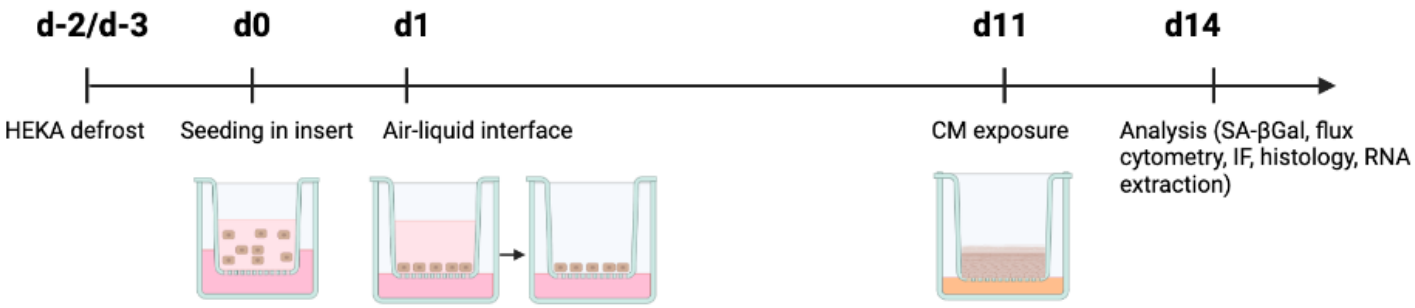

Figure 19: RHE CM exposure timeline
RHE are exposed to CM (form UVB-exposed or unexposed NHEKs) 11 days (d11) after seeding. RHE are incubated 3 days with CM and then are fixed in formol or OCT to be used for histology, SA βgal or immunofluorescence analysis or are disaggregated for flux cytometry analysis. In addition, some RHE are also used for RNA extraction.

50µg/L Na-VitC . The medium is renewed every 2 days until day 11 (post air-liquid interface). At day 11, RHE are used for disaggregation, immunofluorescence or are exposed to UVB.

UVB-Stress Induced Premature Senescence (UVB-SIPS)

NHEKs

NHEKs at early passage (P6-P7) are seeded at low confluence (7,000 cells/cm^2 for unexposed (control) condition and 12,000 cells/cm^2 for UVB condition) in KSFM. At 72 h after seeding, NHEKs were exposed to 675 mJ/cm^2 of UVB (Philips, TL20W/01 lamps) in a thin layer of PBS (3 mL/T75) 3 times a day, separated by 3 h. After UVB exposure, PBS is replaced by KSFM. Control flasks are not exposed to UVB. The UVB-SIPS protocol is presented in **Figure 17**.

RHE

10 days after air-liquid interface, RHE medium is replaced by PBS and RHE are exposed once or twice (with 4h between the 2 exposures) to different UVB doses (250, 500, 1000 or 2000 mJ/cm^2 of UVB) (Philips, TL20W/01 lamps). After UVB exposure, PBS is replaced by Epilife with 10ng/mL, 1,44 mM Ca^{2+} and 50 µg/L Na-VitC. The RHE UVB exposure protocol is presented in **Figure 18**.

Incubation of RHE with CM from senescent NHEKs

At 10 days after air-liquid interface, RHE medium is replaced by CM collected from UVB-exposed or unexposed NHEKs, adjusted with Epilife with 10ng/mL KGF, 1,44 mM Ca^{2+} and 50 µg/L Na-VitC. RHE are incubated with this CM for 3 days before being used for analysis. The protocol timeline is presented in **Figure 19.**

Senescence-Associated β-galactosidase assay (SA-βgal)

NHEKs in 2D culture

First, cells are seeded at 20,000 cells/well in 6-well plates. The next day, the medium is removed and cells are fixed with PBS + 0.2% glutaraldehyde + 2% formaldehyde (1.5 mL/well). Fixed cells are washed twice with PBS and incubated overnight at 37°C without CO_2 with staining solution as described by Dimri *et al*. (Dimri et al., 1995).

The next day, the staining solution is removed and cells are washed twice with PBS and once with methanol. The proportion of SA-βgal positive cells is determined by counting at least 400 cells per well.

RHE

RHE were frozen in OCT (Optical cutting temperature compound, Leica, 14020108926) and cut into 10 µm thick slices and put on Superfrost+ slides (VWR, 631). The protocol for SA-βgal staining is the same as for 2D cultured NHEKs. After the staining, RHE are mounted with DPX mounting medium and observed with Olympus BX63 microscope.

Table 1 : Antibodies summary

Primary antibody	**Secondary antibody** (dilution 1:1000)
Anti-lamin B1 (Abcam, ab16048, dilution 1:200)	Alexa fluor 488 goat anti rabbit IgG conjugates (Invitrogen, A11001)
Anti-53BP1 (Novus, N100-305, dilution 1:2000)	Alexa 568nm goat anti rabbit IgG conjugates (Invitrogen, A11011)
Anti- cleaved Caspase 3 (Cell Signaling, 9661, dilution 1: 400)	Alexa fluor 488 goat anti rabbit IgG conjugates (Invitrogen, A11001)
Anti-Ki67 (Cell Signaling, 9449S, dilution 1 :800)	Alexa 568nm goat anti-mouse IgG conjugates (Invitrogen, A11004)
Anti-K10 (DAKO, M7002, dilution 1 :100)	Alexa 568nm goat anti-mouse IgG conjugates (Invitrogen, A11004)

EdU (5-Ethynyl-2′-deoxyuridine) assay

Cells are seeded at a density of 40,000 cells/glass coverslip in 24-well plate. The next day, cells are incubated with 10 µM EdU (Baseclick, BCK-EdU488) at 37°C + 5% CO_2 overnight. Cells are then fixed in PBS with 4% paraformaldehyde during 10 min. The staining is made following manufacturer's instructions. Nuclei staining was performed by using TO-PRO-3 (Invitrogen, T3605). Coverslips are then mounted with mowiol (Aldrich, 32459-0). Staining is observed with Broadband Confocal TCS SP5 (Leica).

Immunofluorescence

NHEKs in 2D culture

Cells are seeded at a density of 40,000 cells/glass coverslip in 24-well plate. The next day, cells are fixed in PBS with paraformaldehyde 4% during 10 min. Fixed cells are washed three times with PBS and permeabilized with PBS + Triton X-100 0.5% ($C_{33}H_{60}O_{10}$, Sigma-Aldrich, 10789704001) during 5 min. Permeabilized cells are washed three times with PBS and then three times with PBS+BSA 3% (Carl Roth, T844.3). Coverslips are incubated overnight at 4°C with diluted primary antibodies (listed in **Table 1).** Then, coverslips are washed three times with PBS+BSA 3% and incubated 1 h with the secondary antibody. Coverslips are washed three times with PBS+BSA 3% and once with PBS. For nuclei labelling, coverslips are incubated 35 min with TO-PRO-3 (dilution 1:80 in RNAse 2 mg/ml, Invitrogen, T3605) and washed three times in PBS. Coverslips are then mounted with mowiol (Aldrich, 32459-0). Staining is observed with Broadband Confocal TCS SP5 (Leica).

RHE

RHE were frozen in OCT (Leica, 14020108926) and cut into 10 µm thick slices and put on Superfrost+ slides (VWR, 631). RHE are then fixed for 15 min in PBS with paraformaldehyde 4%. Then, RHE are washed 3 times with PBS and incubated 5 min with PBS-glycine 0,1 M. After one additional PBS wash, RHE are incubated with PBS +1% BSA + 0,3% Triton for 30 min. Primary antibodies diluted in PBS +1% BSA + 0,3% Triton are incubated overnight at 4°C. The next day, the slides are washed three times with PBS +1% BSA + 0,3% Triton X-100 before being incubated with the secondary antibody + 0,02% DAPI (Sigma-Aldrich, D9542) for 1h. RHE are then washed 3 times with PBS before being mounted with mowiol. Staining is observed with Broadband Confocal TCS SP5 (Leica) or with Olympus BX63 microscope.

Migration assays

Boyden chambers

Cancer cells were serum deprived overnight. The next day, cancer cells are seeded in a Boyden chamber (Cell culture insert with 8 µM pore size, Falcon, 353097) at a density of 15,000 cells/insert in DHG. Conditioned medium (CM), harvested from NHEKs and adjusted with KSFM (without complements) to normalize the number of secreting NHEKs/mL of CM, is added at the bottom of the well as chemoattractant following the published protocol (Malaquin et al., 2019). DHG+2% FBS is added to CM + KSFM in the same proportion. 500 µL (migration) of CM+KSFM+DHG+1%FBS is filled in each well. Boyden chambers are

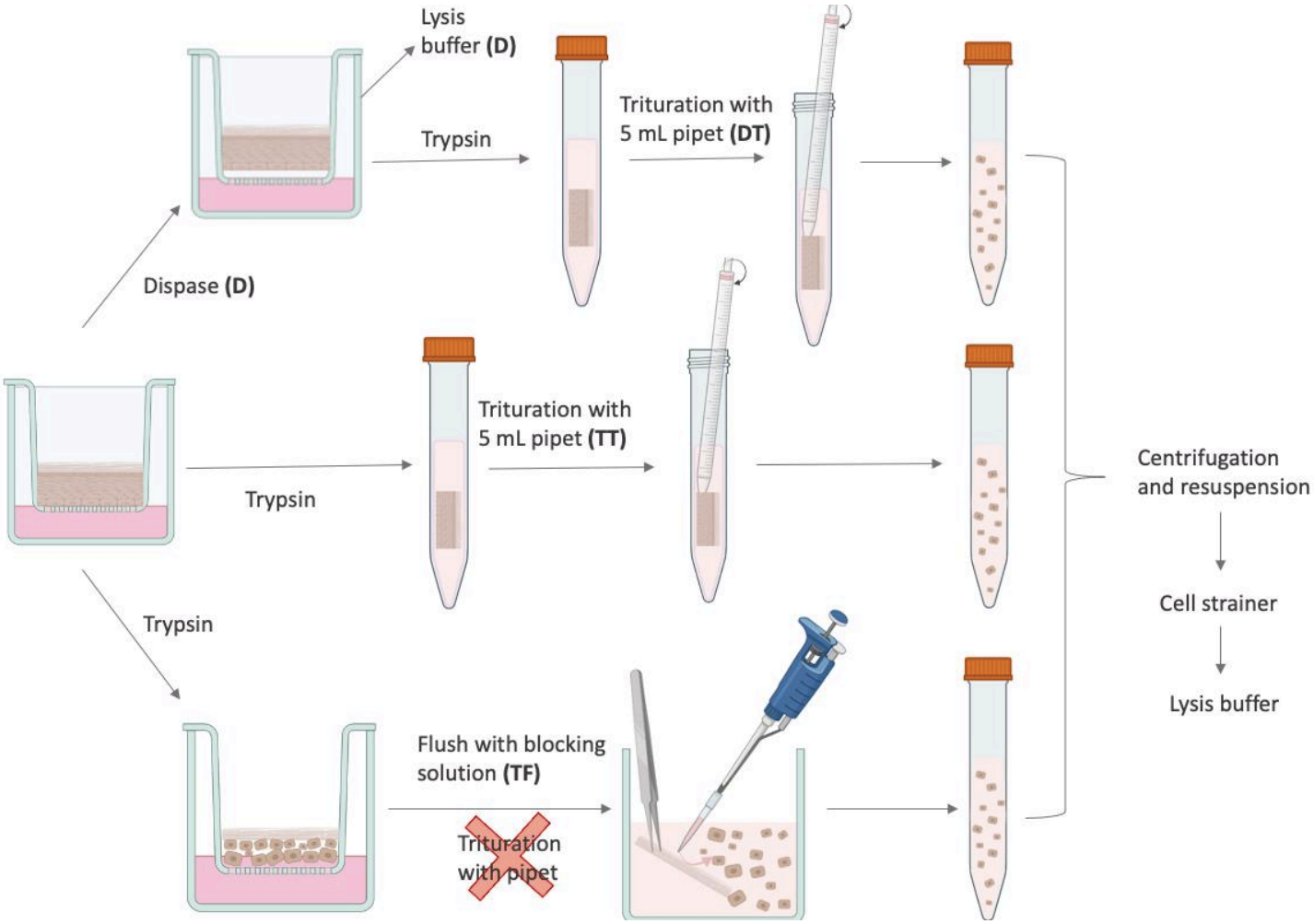

Figure 20 : RHE disaggregation protocols

D correspond to RHE treated with dispase during 15' and directly put into buffer lysis.

DT correspond to RHE treated with dispase 15' and trypsin (incubated for 1h, 40' or 20' at 37°C) which are triturated with a 5 mL pipet to collect cells.

TT correspond to RHE treated with trypsin (incubated 1h at 37°C or overnight at 4°C) and triturated with a 5 mL pipet to collect cells.

TF correspond to RHE treated with trypsin (incubated 1h at 37°C or 4°C / overnight at 4°C or 0°C) and gently flushed with a P-1000 pipet to collect cells.

For DT, TT and TF conditions, cell suspension is then centrifugated, the cell pellet is resuspended and passed through a 70µm cell strainer. 10µL of the cell suspension were diluted in trypan blue to count live cells and the remaining cell suspension is re-centrifugated and cell pellet is resuspended in lysis buffer.

NT (non-treated) RHE are directly incubated into the lysis buffer without any treatment.

Table 2 : RHE disaggregation protocols (see Appendix 1 for a more visual explanation)

Dispase + Trypsin **(1 h, 40 min or 20 min)**	**Trypsin - 37°C-1h / 4°C ON - Triturated**	**Trypsin - 37°C-1h / 4°C-ON / 0°C-ON - Flushed**
150 µl of 10X Dispase II (25mg/mL) is added into the medium in the well and incubated at 37°C for 15 min. The RHE is taken with forceps and submerged in 500 µL of 0.25% trypsin/0.01% EDTA (in a 15 mL tube). The tubes are incubated in a 37°C water bath for 1 h, 40 min or 20 min. After, tubes are placed on ice and 2,5 mL of cold *A Solution* + 10% FBS is added. Then, the cell suspension is gently triturate with a 5 mL serological pipet.	The polycarbonate filter is cut using a scalpel and submerged in 500 µL of 0.25% trypsin/0.01% EDTA (in 15mL tube). The tubes are incubated at 37°C for 1 h or at 4°C O/N. Then, tubes are placed on ice and 2,5 mL of cold *A Solution* + 10% FBS is added. Then, the cell suspension is gently triturate with a 5 mL serological pipet.	The medium of the well is removed and replaced by 1,5 ml of 0.25% trypsin/ 0.01% EDTA. The plate is incubated at 37°C for 1 h/ at 4°C or 0°C overnight and then, 7,5 mL of cold *A Solution* + 10% FBS is used to detach the RHE from the polycarbonate filter. The stratum corneum is held in place with forceps and washed using a P-1000. After being washed, the stratum corneum is removed and the cell suspension is transferred from the well to a 15 mL tube.

incubated with CM for 24 hr. Then, the nonmigrating cells were gently removed by a cotton swab, and the migrated cells were dyed with 0.2% cristal violet in 2% aqueous ethanol (Merck Millipore). Staining cells were counted using ImageJ cell counter.

Scratch assays

Cancer cells were seeded without FBS in 8 cm^2 plates (Corning 430165,) to be confluent 24h later (SKMel 2: 1 300 0000 cells, SKMel28 : 1 300 0000 cells, A375: 950 000 cells). Next day, when cancer cells reach 100% confluence, they are incubated for 1h with 10 µg/mL mitomycin C (Sigma, M4287). Then, a scratch is made with a 200 µL pipette tips and the plates are washed 3 times with PBS. Plates are filled with 2 mL of CM prepared as described for Boyden chambers assays. The scratch closure is monitored by taking one picture every hour during 24 h with CYTONOTE 1W (Iprasens) and analyzed with ImageJ.

LDH assay

Medium from UVB-exposed or unexposed RHE was collected at 8h and 3 days after the first UVB stress to quantify LDH release. LDH activity is quantified with the Cytotoxicity Detection Kit (Roche-applied-science, 11 644 793 001), following the manufacturers' instructions. Cytotoxicity was determined with the following equation (Epilife is used as the low control and RHE exposed to 1% Triton X-100 (diluted in Epilife) for 8h is used for the high control).

$$\textbf{Cytotoxicity (\%)} = \frac{\text{exp. value - low control}}{\text{high control - low control}} \times 100$$

RHE disaggregation

Different disaggregation protocols are tested to find out which one is the most appropriate for collecting live cells and good quality RNA (**Figure 20**).The different protocols are listed in **Table 2.** After the steps listed in **Table 2**, the cell suspension is centrifuged at 335 g at 4°C for 5 min and then, the supernatant is aspirated and the pellet is resuspended in 500 µL of cold *A Solution* (composition:10 mM Glucose, 3 mM KCl, 130 mM NaCl, 1 M $Na_2HPO_4.7H_2O$, 0.0033 mM Phenol Red, 30 mM Hepes) + 10% FBS. Cell suspension is passed through a 70 µm strainer into a clean 15 mL tube. Additional 500 µL of cold *A Solution* + 10% FBS are used to wash the strainer and recover remaining cells. Cells diluted in trypan blue (1:1) are counted using Corning cell counter (Corning, 6749) with Cytosmart software. Cell suspension is transferred into an Eppendorf tube and centrifugated at 350 g during 5 min. The supernatant is removed and the pellet is resuspended in 500 µL of lysis buffer + thioglycerol (ReliaPrep, Promega, Z6111) for RNA isolation.

Another treatment with Dispase only consists of adding 150 µl of 10X Dispase II (25mg/mL) into the medium in the well and incubating at 37°C for 15 min. Then, the RHE is taken with forceps and submerged in 500 µL of lysis buffer + thioglycerol.

To compare samples with RHE without any treatment, polycarbonate filters are cut with a scalpel and submerged in 500 µL of lysis buffer + thioglycerol.

Table 3 : q-PCR preparation

	RHE	NHEKs
cDNA dilution	25x	100x
cDNA/well	5 µL	4 µL
SYBR green	Takyon Rox SYBR MasterMix dTTP Blue (Eurogentec, UF-RSMT-B0701) 10 µL/well	Go Taq qPCR Master Mix 2x (Promega, A600A) 10 µL/well
Primer forward/well	2,5 µL (2,8 nM)	2 µL (3 nM)
Primer reverse/well	2,5 µL (2,8 nM)	2 µL (3 nM)
Mix SYBR green + primers /well	15 µL	16 µL

Table 4 : Primers list for q-PCR

	Forward sequence	Reverse sequence
23kD	5'-GCCTACAAGAAAGTTTGCCTATCTG-3'	5'-TGAGCTGTTTCTTCTTCCGGTAGT -3'
IL-6	5'-CCTGAACCTTCCAAAGATGGC-3'	5'-CACCAGGCAAGTCTCCTCATT-3'
IL-8	5'-CTGGCCGTGGCTCTCTTG-3'	5'-GGGTGGAAAGGTTTGGAGTATG-3'
P16	5'-GCCCAACGCACCGAATAGT-3'	5'-CGCTGCCCATCATCATGAC-3'
P21	5'-CTGGAGACTCTCAGGGTCGAA-3'	5'-CCAGGACTGCAGGCTTCCT-3'
Lamin B1	5'-ACTGGCGAAGATGTGAAGGTTAT-3'	4'- CCCTGCTGGAAAAGTTC -3'
Integrin ß4	5'-CACCGCGTGCTAAGCACAT-3'	5'-TGTGGTCGAGTGTGAGTGTTCTG-3'
Keratin 10	5'-AATCAGATTCTCAACCTAACAAC-3'	5'-CTCATCCAGCACCCTACG-3'
Involucrin	5'-TGAAACAGCCAACTCCAC-3'	5'-TTCCTCTTGCTTTGATGGG-3'
Loricrin	5'-TCATGATGCTACCCGAGGTTTG-3'	5'-CAGAACTAGATGCAGCCGGAG-3'
RPLP0	5'-ATCAACGGGTACAAACGAGTC-3'	5'-CAGATGGATCAGCCAAGAAGG-3'
CTSD	5'-CCGAGGTGCTCAAGAACTAC-3'	5'-GTGTCGAAGACGACTGTGAA-3'
CAPN1	5'-TGAAGGAGTTGCGGACAATC-3'	5'-TTGCCATCACGATCCATGAG-3'
CCL17	5'-AGTACTTCAAGGGAGCCATTC-3'	5'-CTGGAGCAGTCCTCAGATGT-3'
CXCL1	5'-CGAAAAGATGCTGAACAGTGAC-3'	5'-ACATTAGGCACAATCCAGGTG-3'
CCL5	5'-AGCCTCTCCCACAGGTACCAT-3'	5'-GCGGGCAATGTAGGCAAA-3'
CCL2	5'-AAGTGTCCCAAAGAAGCTGT-3'	5'-TGGGTTGTGGAGTGAGTGTT-3'
IL-1β	5'-GCCCTAAACAGATGAAGTGCTC-3'	5'-GAGATTCGTAGCTGGATGCC-3'
CXCL10	5'-CCACGTGTTGAGATCATTGC-3'	5'-GCTCCCCTCTGGTTTTAAGG-3'

RHE flow cytometry
RHE were disaggregated following the " Trypsin (37°C-1h) -Triturated" protocol described above and cells in suspension were used for flow cytometry analysis (BD FACSVerse). Results were analyzed with BD FACSuite software.

RHE Histological Analysis
Histological hematoxylin and eosin staining of RHE are made following the protocol described by (Coquette and Poumay, 2009).

RNA extraction
RNA extraction is done with ReliaPrep™ RNA Tissue Miniprep System (Promega, Z6111) and following the manufacturer's instructions. For non-treated RHE, after submerging the polycarbonate filter into the lysis buffer, the filter is gently triturated and removed.

RNA Integrity analysis
RNA integrity analysis is done using Agilent 2100 Bioanalyzer system with Agilent RNA 6000 Nano kit (Agilent technologies, 5067-1511) and following manufacturer's instructions.

Reverse Transcription and quantitative PCR (RT-qPCR)
One µg of total RNA (0,5 µg for RHE) is used for reverse transcription (RT). RT is realized by using Promega kit (GoScript, Promega, A2791) following the manufacturer's instructions.
For qPCR, a mix is prepared with diluted SYBR green mix and primers (**Table 3**). Reactions are run on Viia7 instrument (Applied Biosystems). All primer sequences are available in **Table 4**. Relative abundance was determined with the $2^{-\Delta Ct}$ or $2^{-\Delta\Delta Ct}$ method normalized to the mRNA abundance of *23kD* or *RPL0* (Schmittgen and Livak, 2008).

Mass spectrometry
Samples preparation, mass spectrometry identification and database searching
These different steps were previously carried out by Emilie Bauwens, Catherine Demazy and Marc Dieu, and are described in the supplementary methods.

Protein identification
Scaffold (version Scaffold_4.10.0, Proteome Software Inc., Portland, OR) was used to validate MS/MS based peptide and protein identifications. Peptide identifications were accepted if they could be established at greater than 96.0% probability to achieve an FDR less than 1.0% by the Scaffold Local FDR algorithm. Protein identifications were accepted if they could be established at greater than 5.0% probability to achieve an FDR less than 1.0% and contained at least 2 identified peptides. Protein probabilities were assigned by the Protein Prophet algorithm (Nesvizhskii et al., 2003). Proteins that contained similar peptides and could not be differentiated based on MS/MS analysis alone were grouped to satisfy the principles of parsimony. Proteins sharing significant peptide evidence were grouped into clusters.
The proteins relative abondance were determined with spectral count and they were compared between UVB-exposed and unexposed NHEKs to determine the fold change.

Fold changes ≥ 2 or ≤0,5 with a p-value< 0,05 (assessed with a Benjamini- Hoechberg t-test) were considered as significant.

Results analysis

Gene ontology, pathway, and network analysis was performed using the GlueGO package, version 2.5.8, in Cytoscape (https://cytoscape.org/). Pathways enrichment were identified by using the following databases: GO Biological process, GO immune system process, GO molecular function, Reactome and KEGG Pathways, restricted to pathways with experimental evidence (EXP, IDA, IPI, IMP, IGI, IEP). The statistical cutoff for enriched pathways was Bonferroni-adjusted p-values <0.01. Connections between pathways were drawn for kappa scores >40%. Pathways obtained with ClueGo then compared with DAVID analysis (https://david.ncifcrf.gov).

RESULTS

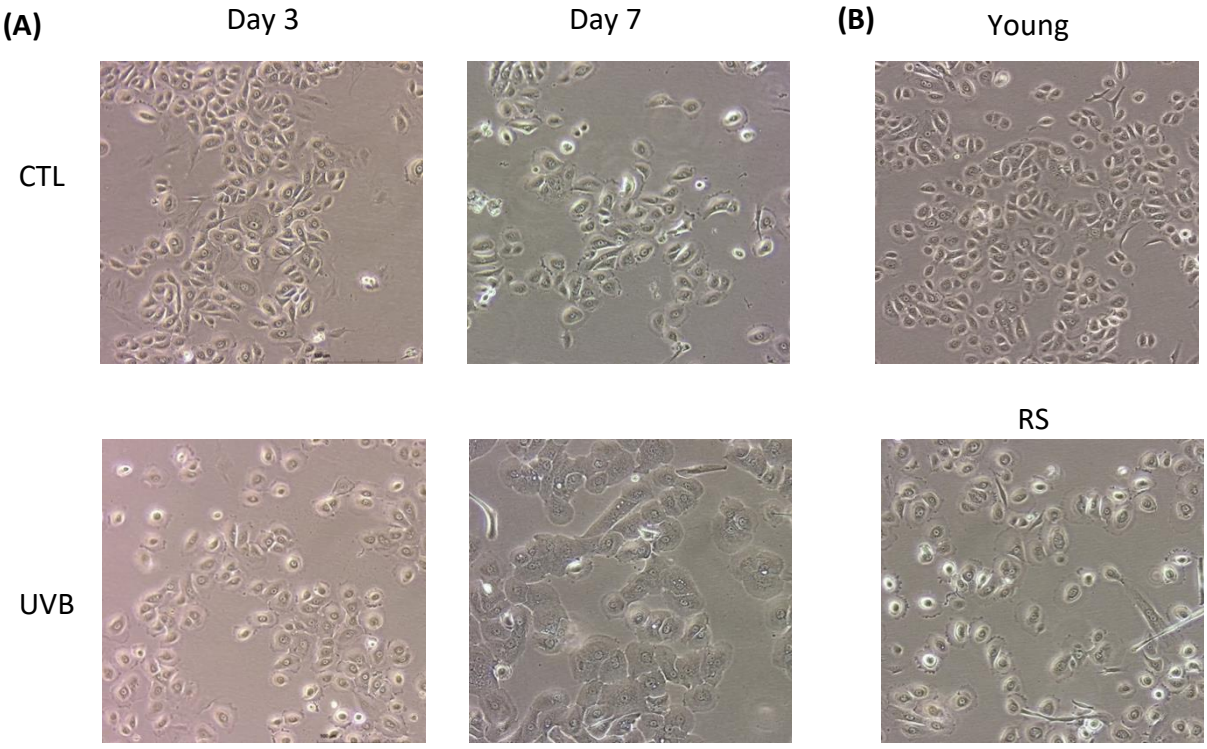

Figure 21: Morphology of NHEKs in UVB-induced senescence or in replicative senescence. NHEKs were studied at 3 or 7 days after three repeated UVB exposures (or not, CTL), and compared to young or replicative senescent (RS) NHEKs. **(A)** Representative cell morphology of NHEKs at 3 or 7 days after UVB exposures (or not, CTL). **(B)** Representative cell morphology of young NHEKs (passage 6) and replicative senescent (RS) NHEKs (passage 11). Cells were observed by phase contrast microscopy (100x).

The aim of this master thesis is to study the impact of senescent keratinocytes on skin cancer cells. For this purpose, the senescence of keratinocytes will be induced following repeated UVB exposures. The induction of senescence will first be verified by different senescence biomarkers. Then, we will test the effect of the conditioned medium (CM) harvested from senescent keratinocytes on the migration of skin cancer cells. We will then try to identify SASP factors potentially involved in skin cancer cell migration via RT-qPCR and secretome analysis. In order to study the interactions between senescent keratinocytes and melanoma cells in a more physiological cell culture model, we will then develop reconstructed human epidermis (RHE). First, we will evaluate if senescence can be induced in RHE following UVB exposures or incubation with CM from senescent keratinocytes. Then, we will develop RHE in which melanoma cells will be included.

1. Evaluation of the senescent phenotype in keratinocytes in UVB-induced senescence and in replicative senescence

The first part of our study was devoted to generate senescent keratinocytes and to harvest their conditioned medium. Before using the conditioned medium for migration assays, the induction of senescence in our conditions must be validated.

We used two different models of senescence in normal human epidermal keratinocytes (NHEKs): replicative-like senescence (RS) obtained after several passages (± 11-12) in culture and UVB-induced senescence following a protocol of repeated exposures to UVB previously developed by E. Bauwens (Bauwens *et al*., *in revision*). This model consists in three UVB exposures on a single day, at 675 mJ/cm^2. In comparison, NHEKs at early passage and unexposed NHEKs were used as respective controls. As there is no unique specific biomarker of senescence, several senescence biomarkers were analyzed in order to confirm the senescence induction.

1.1. Morphological changes and SA-βgal activity

Senescent cells present an enlarged morphology as well as an increase of their β–galactosidase activity, therefore detectable at pH 6.0 and referred as the senescence associated β-galactosidase (SA-βgal) (Hernandez-Segura et al., 2018).
At three and seven days after UVB exposures, and at passage 11 (RS), NHEKs displayed an enlarged and irregular morphology, compared to unexposed (CTL) and young NHEKs (**Figure 21 A and B**). The enlarged morphology of NHEKs at 3 days after UVB exposure is similar to the one of NHEKs in replicative-like senescence. The difference in morphology of NHEKs is much more marked at 7 days after the UVB exposures, with a very clear enlargement of the cells. On day 7, some unexposed NHEKs are larger than on day 3, this could be attributed to the fact that these cells continued to divide in culture, and that their population is therefore certainly weakly enriched in replicative-like senescent cells.

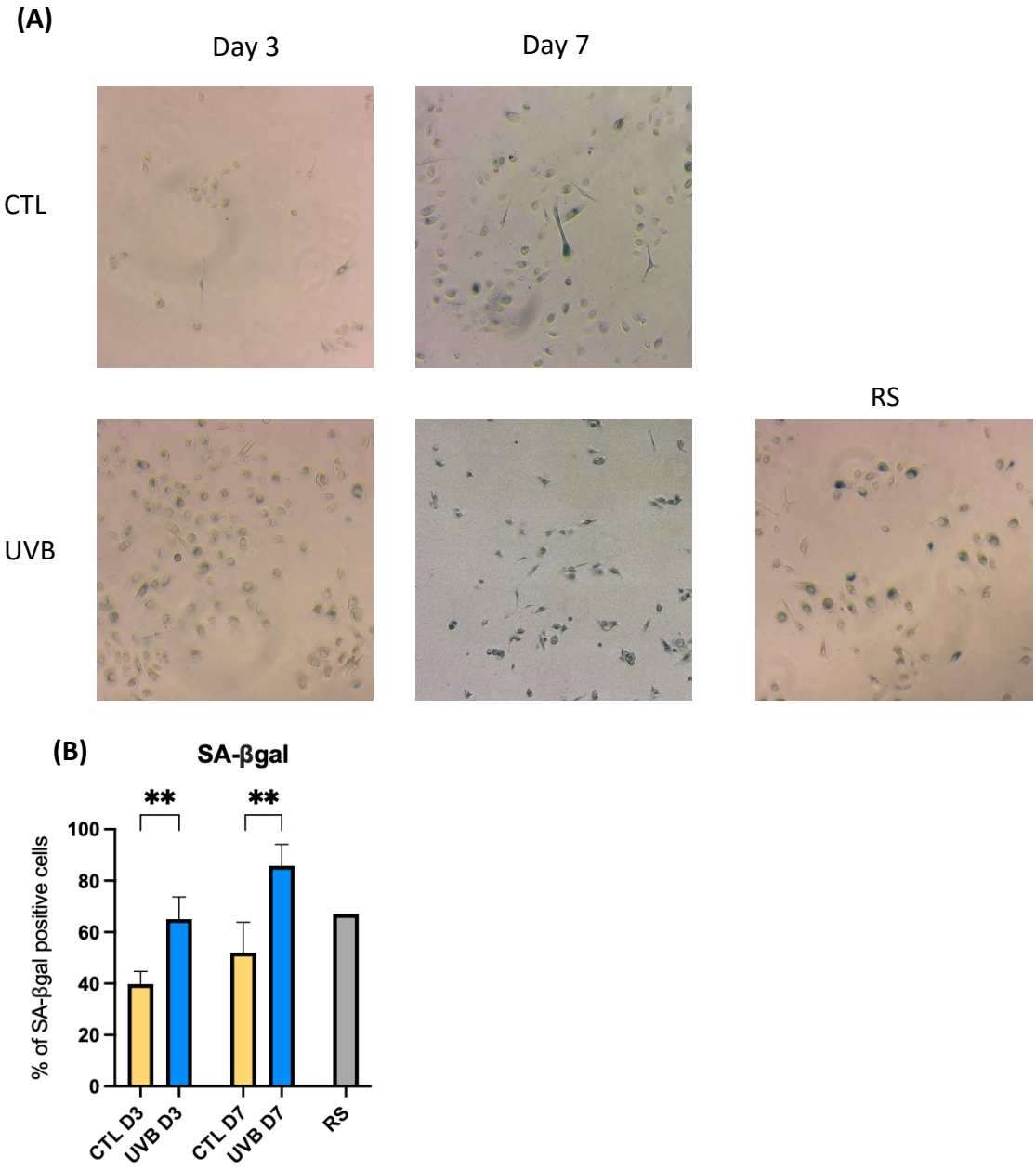

Figure 22: SA-βgal staining of NHEKs in UVB-induced senescence or in replicative senescence. NHEKs were studied at 3 or 7 days after three repeated UVB exposures (or not, CTL), and compared to replicative senescent (RS) NHEKs. **(A)** Representative pictures of NHEKs at 3 or 7 days after UVB exposure (or not, CTL) or RS (Passage 11), after SA-βgal staining. Cells were observed by phase contrast microscopy (100x). **(B)** Percentage of SA-βgal positive cells, determined by counting 400 cells/well, 3 wells per condition, N=4 for UVB and CTL (NHEKs from different donors), N= 1 for RS. Statistical significance is determined by unpaired t-test *(** = p <0 .01).*

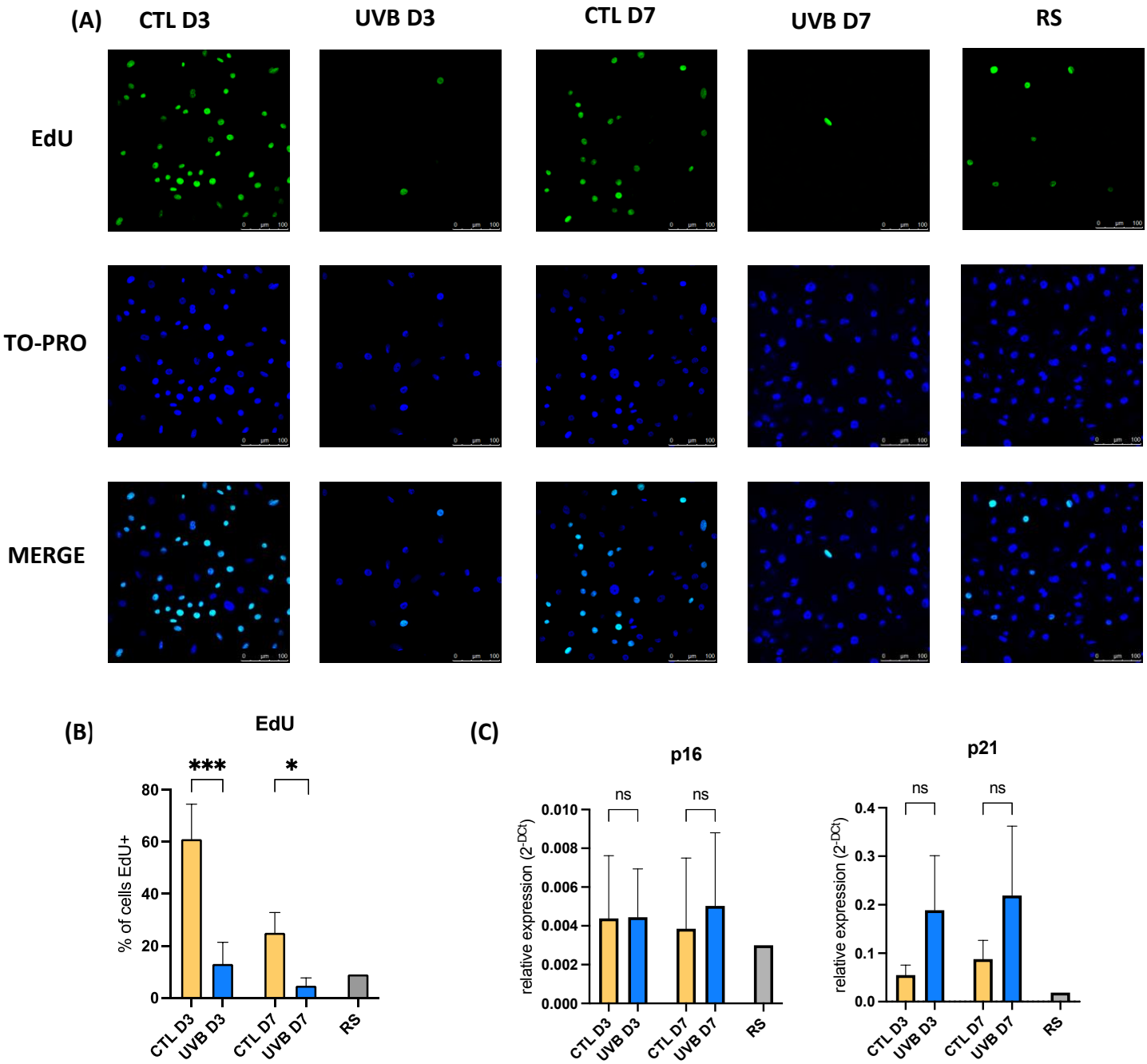

Figure 23: Evaluation of the proliferative potential of NHEKs in UVB-induced senescence or in replicative senescence. NHEKs were studied at 3 or 7 days after three repeated UVB exposures (or not, CTL), and compared to replicative senescent (RS) NHEKs. **(A)** Representative pictures of EdU staining (green); nuclei are stained with TO-PRO-3 (blue); scale bar = 100 µm. **(B)** Quantification of EdU positive cells, determined by counting at least 200 cells for each replicate. **(C)** Relative mRNA levels of *p21* and *p16*. Results are expressed as relative expression ($2^{-\Delta CT}$) of CTL, UVB and RS conditions reported to *23kD* (used as the housekeeping gene). Statistical significance is determined by unpaired t-test. *(ns = p >0 .05 ; * = p <0 .05 ; *** = p <0 .001)*. (N= 4 for UVB and CTL (NHEKs from different donors) ; N=1 for RS).

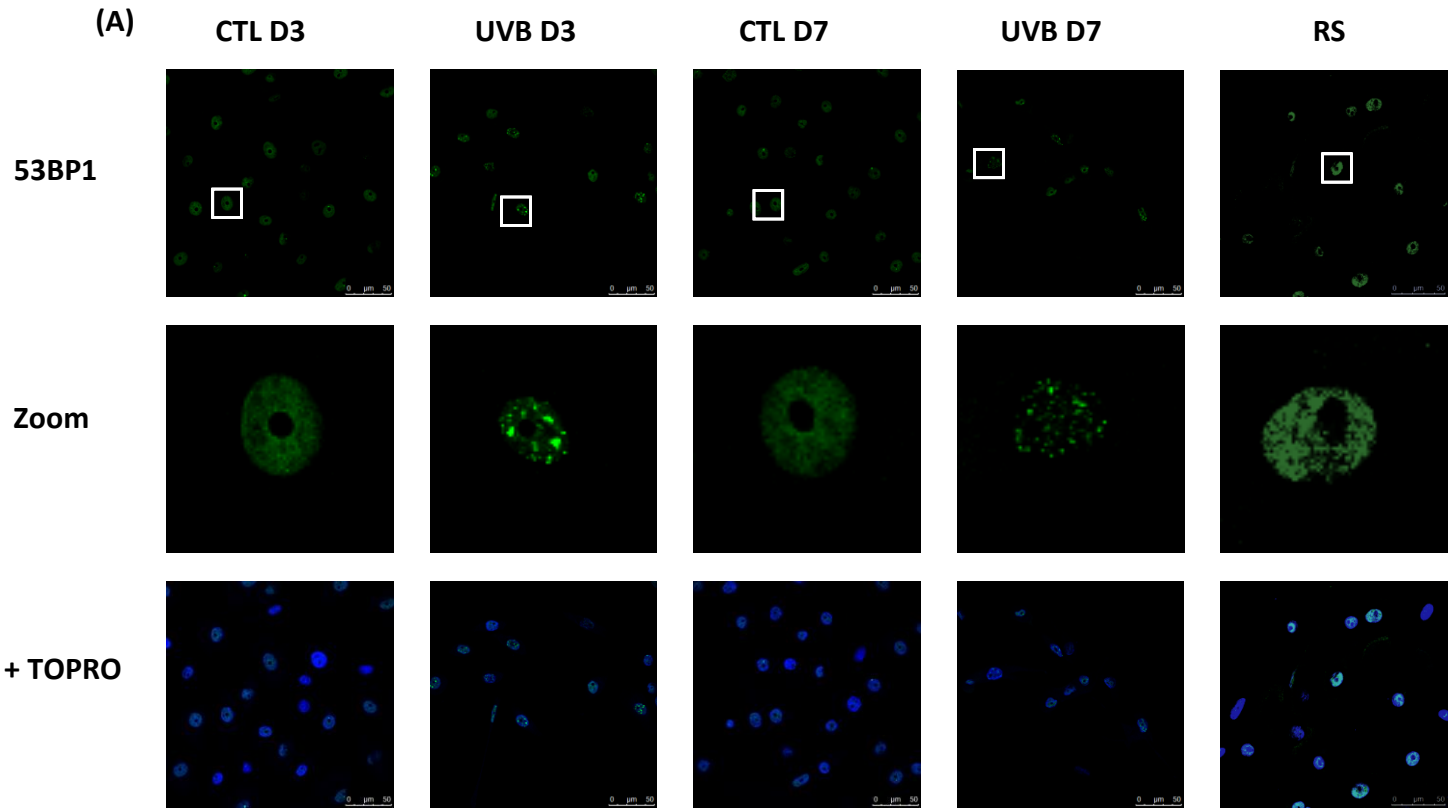

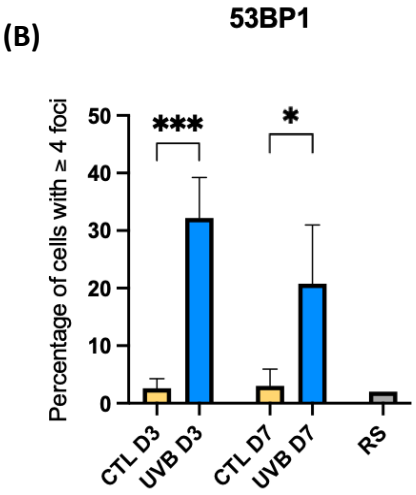

Figure 24 : 53BP1 DNA damage foci in NHEKs exposed to UVB or in replicative senescence. NHEKs were studied at 3 or 7 days after three repeated UVB exposures (or unexposed, CTL) and compared to replicative senescent (RS) NHEKs. **(A)** Representative pictures of 53BP1 immunostaining (green) and nuclei staining with TO-PRO-3 (blue) were observed with confocal microscopy; scale bar = 50 µm. **(B)** Quantification of the proportion of 53BP1 positive cells (with 4 or more foci), presented as mean ± SD (N=4 for CTL and UVB NHEKs from different donors, N=1 for RS), determined by counting at least 100 cells for each replicate. Statistical significance determined by unpaired t-test *(* = p <0 .05; *** = p <0 .001).*

The proportion of SA-βgal positive cells was then evaluated. After UVB exposures, the proportion of SA-βgal positive NHEKs increased from 40% in unexposed NHEKs, to 65% in UVB-exposed NHEKs at day 3 and from 56% in unexposed to 83% in UVB-exposed NHEKs at day 7 (**Figure 22 A and B**). Moreover, the proportion of SA-βgal positive NHEKs reached 67% in RS.
These results showed that an enlarged morphology and an increased proportion of SA-βgal positive cells are detected in UVB-exposed NHEKs on day 3 and are even more pronounced on day 7.

1.2. Cell cycle arrest

Another strong feature of senescent cells is their irreversible growth arrest. In order to determine the proliferative potential of NHEKs in the different conditions, the incorporation of 5-ethynyl-2'-deoxyuridine (EdU) (which is a thymidine analog) was evaluated. Cells exposed to UVB incorporated significantly less EdU than control cells on day 3 and 7 (13% versus 61% on day 3 and 5% versus 25% on day 7), showing a decreased proliferation in NHEKs after UVB exposures (**Figure 23 A and B**). However, an important decrease in EdU incorporation is also observed between controls on day 3 and 7, showing a decrease of proliferative potential between the third and the seventh day of culture, confirming the weak enrichment of senescent cells (**Figure 23 A and B**). Finally, only 9% of cells at passage 11 still incorporated EdU, confirming a decrease of proliferation in these "late" passage cells (**Figure 23 A and B**). This senescence-associated proliferation arrest is mainly dependent on the overexpression of CDKIs such as p16 and p21 (Campisi and d'Adda di Fagagna, 2007).
We then checked the gene expression level of these two CDKIs by RT- qPCR. We did not observe any change in p16 expression between NHEKs exposed to UVB and their controls. On the other hand, we observed a tendency for p21 to increase, although not significantly, suggesting that the growth arrest following UVB exposures could be mediated by p21 rather than by p16 (**Figure 23 C**). We did not observe any difference in the expression of these two CDKIs in RS cells, while the EdU assay did confirm that they were also in growth arrest (**Figure 23 B and C**).

1.3. Persistence of DNA damage

Unrepaired DNA damage and concomitant activation of the DDR pathway are often reported in senescence (Campisi and d'Adda di Fagagna, 2007). In order to highlight the presence of DNA damage, we checked the presence of p53-binding protein 1 (53BP1) foci, as 53BP1 is recruited at DNA double-strand breaks sites (Panier and Boulton, 2014). 53BP1 foci were stained by immunofluorescence and the cells containing more than four 53BP1 foci in their nucleus were counted as positive (**Figure 24 A and B**). The percentage of 53BP1 positive cells increased from 2% and 3% in controls to 32% and 21% after UVB exposures respectively on day 3 and day 7 (**Figure 24 B**). RS cells only present 2% of 53BP1 positive cells (**Figure 24 B**), as it was expected in this condition (Nassour et al., 2016).

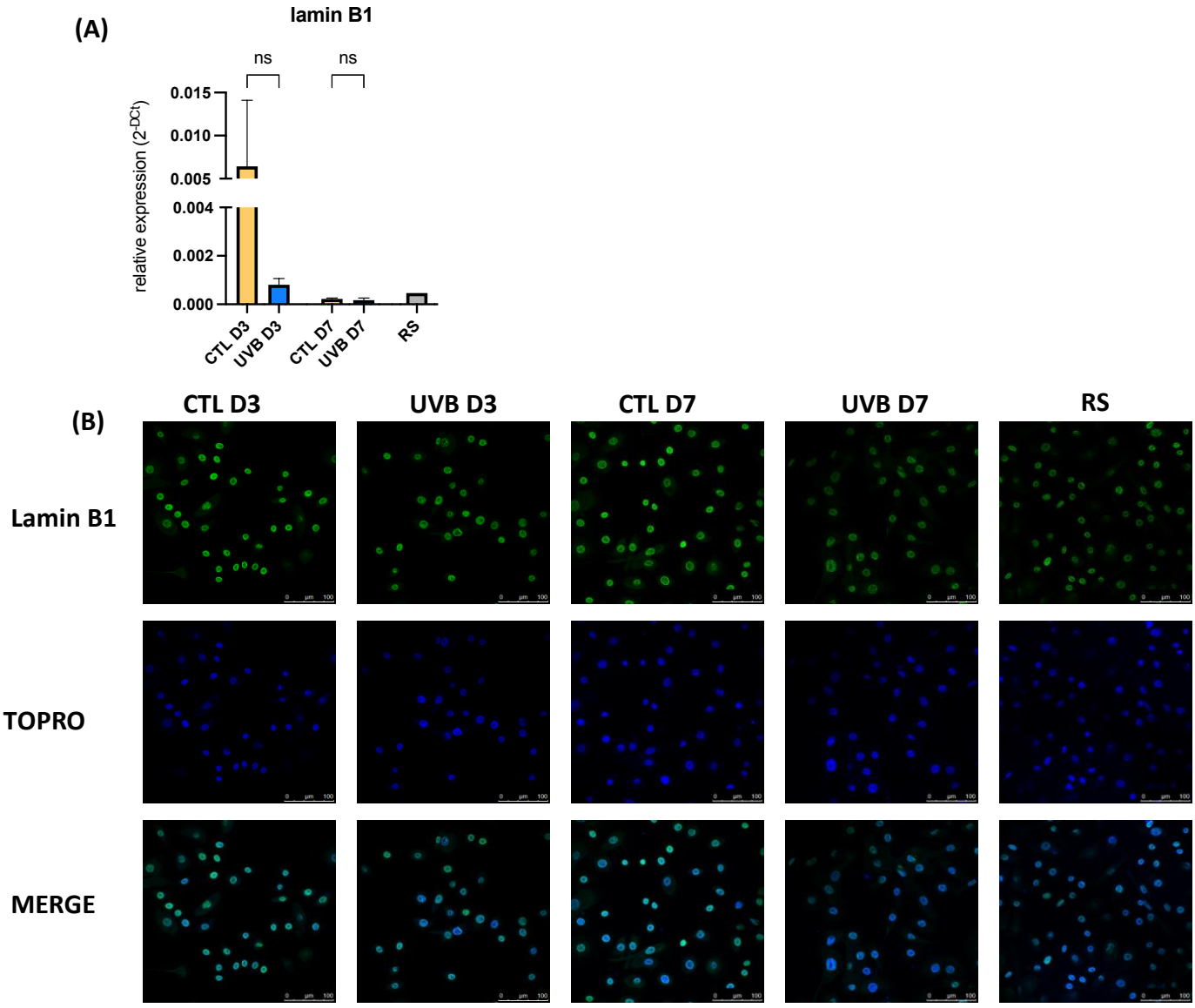

Figure 25 : Lamin B1 mRNA and protein expression in NHEKs exposed to UVB or in replicative senescence. NHEKs were studied at 3 or 7 days after three repeated UVB exposures (or not, CTL), and compared to replicative senescent (RS) NHEKs. **(A)** Relative mRNA levels of *lamin B1.* Results are expressed as relative expression ($2^{-\Delta CT}$) of CTL, UVB and RS conditions (*23kD* was used as housekeeping gene). Statistical significance determined by unpaired t-test *(ns = p >0 .05 ; * = p <0 .05 ; ** = p <0 .01)* (N=4 for UVB and CTL (NHEKs from different donors), N=1 for RS). **(B)** Representative pictures of lamin B1 immunostaining (green) and nuclei staining with TO-PRO-3 (blue) observed with confocal microscopy; scale bar = 100 µm.

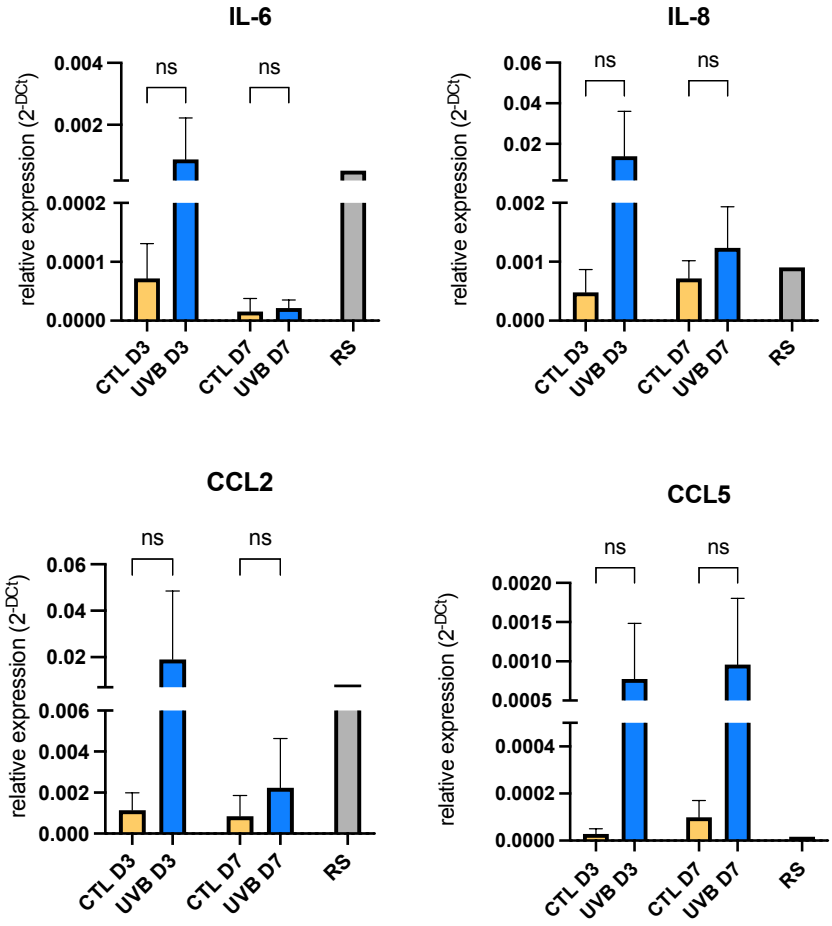

Figure 26 : Relative mRNA levels of SASP components. NHEKs were studied at 3 or 7 days after three repeated UVB exposures (or unexposed, CTL), and compared to replicative senescent (RS) NHEKs. Results are expressed as relative expression ($2^{-\Delta CT}$) of CTL, UVB and RS conditions (23kD was used as housekeeping gene) (N=4 for CTL and UVB conditions; N=1 for RS). Statistical significance is determined by unpaired t-test *(ns = p >0 .05).*

1.4. Decreased expression of lamin B1

Senescent cells are also characterized by a decreased expression of lamin B1, a constituent of the *nuclear lamina* that borders the inner surface of the nuclear envelope (Shimi et al., 2011). In order to study its expression, we first checked its mRNA level by RT-qPCR. *Lamin B1* mRNA levels showed a tendency to decrease after UVB exposures and in RS but also in CTL NHEKs on day 7, when compared to unexposed cells on day 3 (**Figure 25 A**). In addition, lamin B1 immunostaining showed a high intensity of fluorescence in the nucleus of unexposed NHEKs (on day 3 and 7), especially on the perimeter of the nucleus. In UVB-exposed NHEKs, we observed a slight decrease of lamin B1 intensity on day 3 whereas the signal is strongly reduced and more diffuse on day 7 as well as in NHEKs in replicative senescence (**Figure 25 B**). This corroborates with the decreased mRNA level in replicative senescence and UVB-exposed NHEKs on days 3 and 7. However, *lamin B1* mRNA level is strongly reduced in unexposed cells on day 7 whereas its labeling intensity is similar to unexposed cells on day 3.

1.5. Gene expression level of SASP factors

The last marker of senescence studied was the expression of SASP factors. SASP is mainly composed of pro-inflammatory cytokines, chemokines, proteases and growth factors and is mainly regulated at the transcriptional level (Lopes-Paciencia et al., 2019). We studied the gene expression level of several SASP factors: two pro-inflammatory cytokines (*IL6, IL8*) and two chemokines (*CCL2/MCP1* and *CCL5/RANTES*) (**Figure 26**). The gene expression of *CCL5* seems to be increased in UVB-exposed NHEKs on day 3 and day 7 but not in RS cells when compared with controls. *CCL2* and *IL8* also tend to be overexpressed in UVB-exposed NHEKs on day 3 and to a lesser extent on day 7. Additionally, *CCL2* tend to be overexpressed in RS cells while *IL8* expression is similar to the control cells. Finally, *IL6* is overexpressed in UVB-exposed NHEKs on day 3 and in RS.
These results confirm that UVB-exposed NHEKs tend to overexpress SASP factors and that their expression is changing over time as expression profiles are different on day 3 and day 7 following UVB exposures as shown with other senescence inducers (Childs et al., 2017). However, as the results obtained for the RS condition were only carried out on a single biological replicate, one must be prudent in their analysis.

To summarize, UVB-exposed NHEKs display several senescence biomarkers as an enlarged morphology, an increase of SA-βgal activity, a proliferation arrest, an onset of persistent DNA damage, a decreased expression of lamin B1 as well as an overexpression of several SASP factors. These data confirm that repeated UVB exposures induce NHEKs senescence.
Note, however, that some of these biomarkers are increased between day 3 and day 7 in unexposed NHEKs (CTL), which seems to be explained by a low enrichment of senescent cells over time. On the other hand, the RT- qPCR results seem to show trends but the variability between our biological replicates is important, this is not surprising as each replicate comes from a different donor. Anyway, these results confirm those obtained previously by Bauwens *et al.* (*in revision*) and validate the protocol.

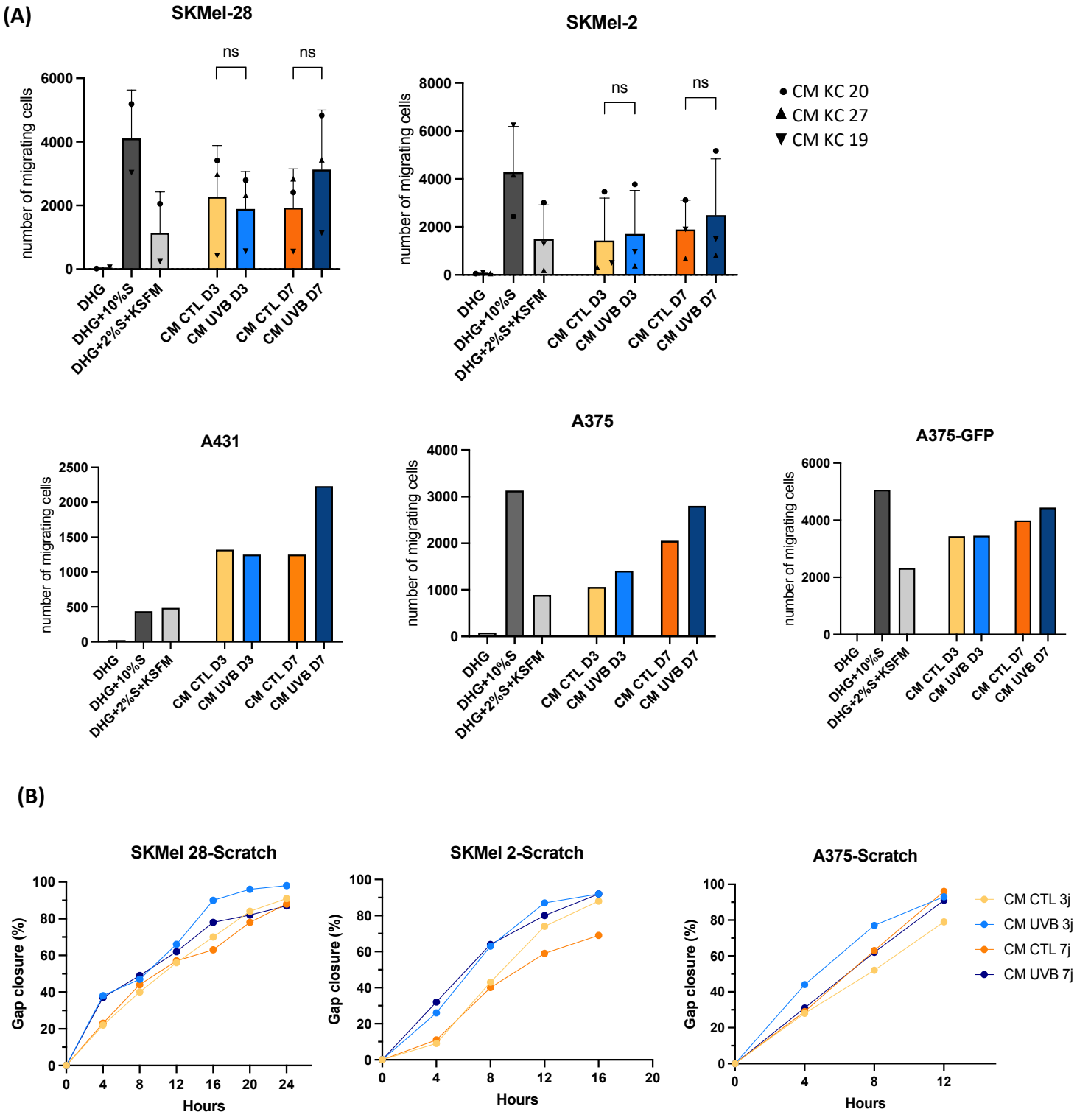

Figure 27 : Effect of keratinocytes conditioned medium (CM) on cancer cells migration. (A) Boyden chamber assay**.** Number of migrating cells (N= 3 for SKMel-28 and SKMel-2 (with CM harvested from NHEKs from 3 independent donors); N=1 for A375, A375-GFP and A431 (technical duplicates)). A375, A375-GFP, SK-Mel-2, SKMel-28 and A431 were seeded at a density of 15,000 cells on the top of Boyden chambers. CM from 65,000 UVB-exposed (UVB) or unexposed (CTL) NHEKs is then added in the lower part of the chamber. Boyden chambers were incubated with CM for 24 h. DHG is used as a negative control and DHG +10% serum as a positive control; DHG+2% serum + KSFM is used as the medium control. Pictures of the Boyden migration chambers are available on **Figure S1.** Statistical significance determined by paired t-test *(ns = p >0 .05).* **(B)** Scratch assays. Gap closure is monitored during 24h in presence of CM from 65,000 UVB-exposed (UVB) or unexposed (CTL) KC 27. Pictures of the scratch assays are available on **Figure S2.** (N=1)

2. Impact of senescent keratinocytes on the migration of melanoma and cSCC cell lines

As senescence was induced following repeated UVB exposures and validated by the onset of several biomarkers, we tested if the conditioned medium (CM) harvested from these cells could impact the migration of skin cancer cells, including melanoma and cSCC cells.

2.1. Impact of conditioned medium on cancer cells migration

The CM from UVB-exposed (CM UVB) and unexposed (CM CTL) NHEKs were harvested after 72 h in contact with the cells and the migration assays were done following the protocol of Malaquin *et al*. (2019). Cancer cells were seeded at a density of 15,000 cells/chamber, and directly incubated with harvested CM for 24 hours. Then, the number of migrating cells was counted following a staining of the cells at the bottom part of the chamber with crystal violet.
Different cancer cell lines were tested: A431 cells, isolated from a cSCC; A375 and SKMel-28 cells, originating from a primary melanoma; and SKMel-2 isolated from a metastatic melanoma. A375 cells expressing GFP (A375-GFP) were also tested as they will be used in reconstructed human epidermis (RHE) hereafter.
CM from NHEKs of 3 different donors (KC20, KC27 and KC19) were harvested and used to study their impact on SKMel-28 and SKMel-2 cells migration in Boyden chambers. Moreover, CM from NHEKs of one donor (KC20) was used to study A431, A375, and A375-GFP cells migration.
SKMel-28 migration tends to increase with CM collected at 7 days after UVB exposures, for all NHEKs donors. However, this effect is not observed with CM harvested at 3 days after UVB exposure (**Figure 27 A**). The same migration profile is observed with A431 cells (**Figure 27 A**) and confirms previous data (Bauwens *et al., in revision*). In contrast, the migration of SKMel-2 cells is not impacted by CM from senescent NHEKs (**Figure 27 A**). It seems that the CM harvested at 7 days in UVB-exposed NHEKs also has a slight pro-migratory effect in the A375 and A375-GFP cells but as this experiment was only performed with one replicate of CM, we have to be careful in the interpretation of these results (**Figure 27 A**).
These results, although to be confirmed by further biological replicates, are interesting and seem to indicate a pro-migratory effect of CM isolated at 7 days after repeated UVB exposures in NHEKs.

However, one of the limitations of this migration assay is that the impact on the migration is measured after a fixed time of 24 h. In order to verify if the migration kinetics varied with the different CM tested, we performed a scratch assay experiment associated with a camera allowing to follow the scratch closure over time.
Scratch assays were performed with CM from NHEKs of a single donor (KC27), and tested on three different melanoma cell lines (SK-Mel 28, SK-Mel-2 and A375). It appears that in all three melanoma cell lines tested, CM isolated at 3 days from UVB-exposed NHEKs shows a stronger effect on scratch closure than its respective control. This difference is present from 4h

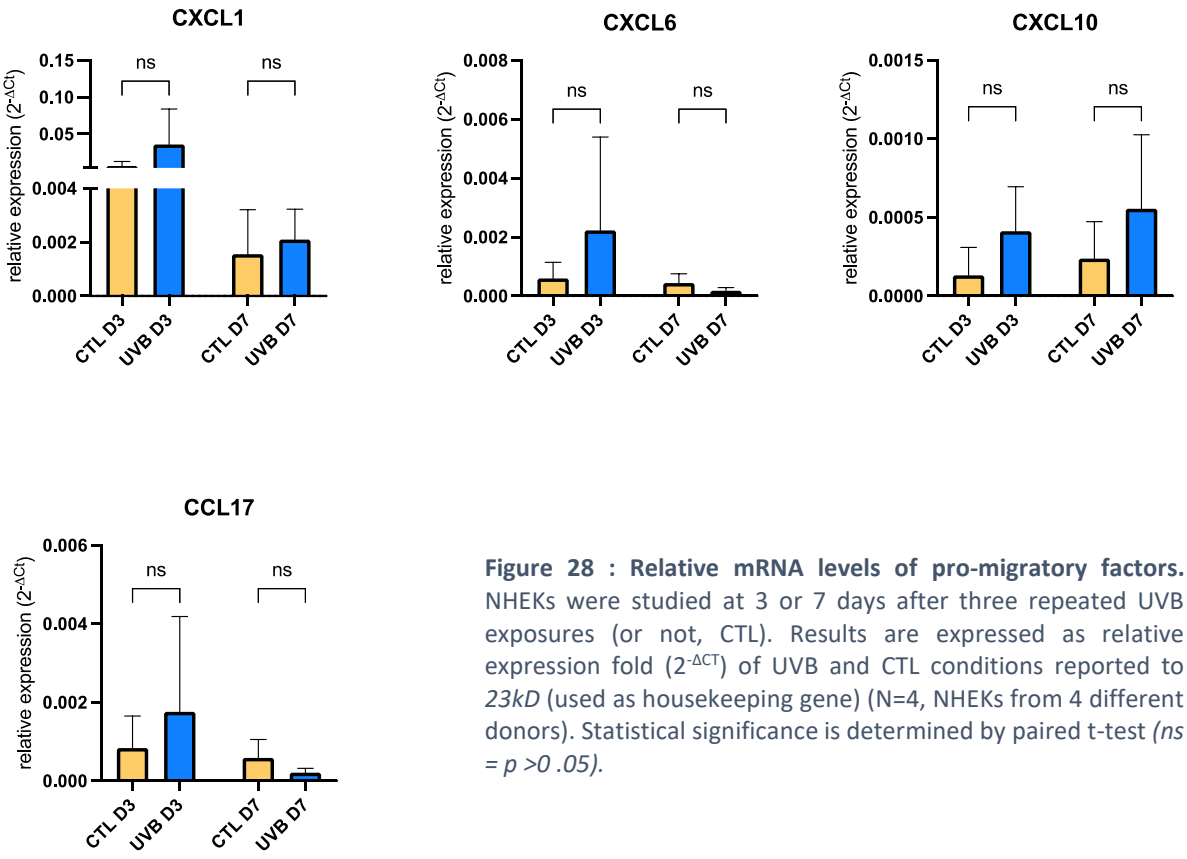

Figure 28 : Relative mRNA levels of pro-migratory factors. NHEKs were studied at 3 or 7 days after three repeated UVB exposures (or not, CTL). Results are expressed as relative expression fold ($2^{-\Delta CT}$) of UVB and CTL conditions reported to *23kD* (used as housekeeping gene) (N=4, NHEKs from 4 different donors). Statistical significance is determined by paired t-test *(ns = p >0 .05).*

of migration. We also detected a difference between the CM isolated at 7 days from UVB-exposed NHEKs and their respective control, but only with SK-Mel-2 cells (**Figure 27 B**). In contrast with Boyden chambers, scratch assays allow to study cell motility in 2D but not chemotaxis, which may explain why the results are different between these two types of experiments (Guy et al., 2017).
To conclude, the effect of CM from UVB-exposed NHEKs seems to be variable, sometimes depending on the NHEKs donor but also on the skin cancer cell line and on the experiment type. As these experiments are really far from what is happening in the organism, reconstructed human epidermis (RHE) will be used later to be closer to a physiological model.

2.2. Gene expression level of pro-migratory factors

To study whether this pro-migratory effect can be linked to the expression of proteins possibly secreted by senescent keratinocytes, we studied the expression of a series of cytokines and chemokines known to induce the migration of melanoma cells. As several chemokine receptors (as CCR4, CXCR2 or CXCR3) are known to be overexpressed in metastatic melanoma cells and to promote melanoma migration (Jacquelot et al., 2018), the expression of their ligands in UVB-exposed NHEKs was thus investigated by RT- qPCR. CXL1 and CXL6 are both CXCR2 ligands, CXL10 is a ligand of CXCR3 and CCL17 a ligand of CCR4 (Jacquelot et al., 2018). UVB-exposed NHEKs tend to overexpress *CXL1, CXCL6* and *CCL17* on day 3 after UVB exposure but not on day 7 (**Figure 28**). In addition, *CXCL10* expression is increased in UVB-exposed NHEKs on both day 3 and 7 compared to control NHEKs (**Figure 28**). However, these results are again very variable from one replicate (and therefore donor) to another. Moreover, they confirm the change in the composition of the SASP over time.

In order to get a more detailed overview of the secreted protein expression changes, we performed bioinformatics analysis of the secretome of NHEKs in UVB-induced senescence.

2.3. Characterization of the secretome of UVB-exposed NHEKs

We had the opportunity to analyze the secretome of NHEKs previously cultured by Emilie Bauwens, and harvested on day 3 and 7 after repeated UVB exposures, from 5 biological replicates. Sample preparation and mass spectrometry analysis of these samples were performed by Catherine Demazy and Marc Dieu, within the MaSun platform. The relative abundance of proteins was determined by spectral counts and was compared between UVB-exposed and unexposed NHEKs to determine the fold change using the Scaffold software. Proteins presenting an abundance fold change of at least 2-fold (UVB/CTL) with a p-value< 0.05 were considered as significantly increased in the secretome of UVB NHEKs while proteins presenting an abundance fold change under 0.5-fold (UVB/CTL) with a p-value< 0.05 were considered as significantly decreased in the secretome of UVB NHEKs.

(A)

Condition	**# protein clusters identified**	**# protein clusters with changed abundance** (UVB/CTL)
Day 3	3658	839 ↑ 196 ↓
Day 7	3947	369 ↑ 65 ↓

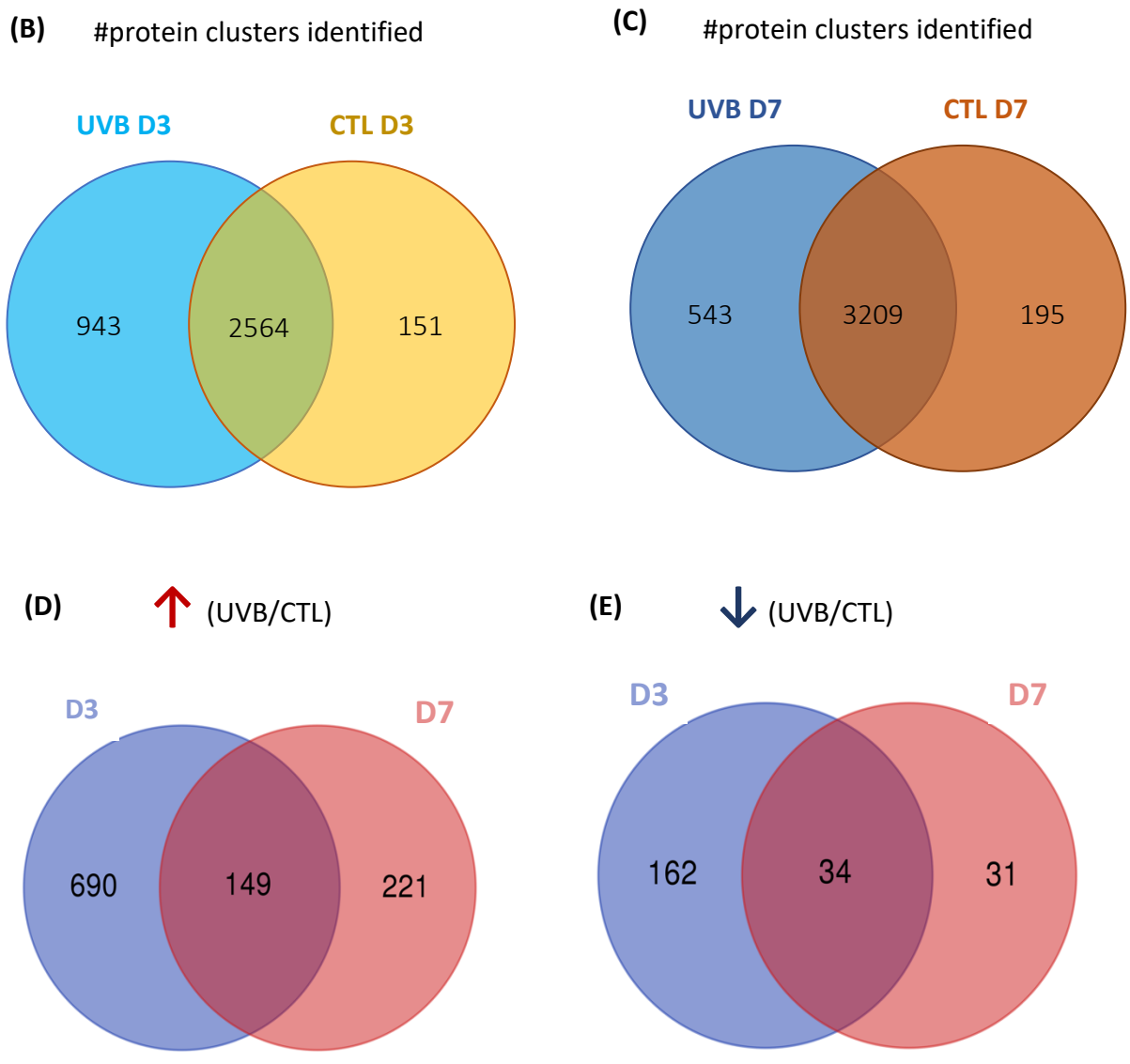

Figure 29 : SASP composition of NHEKs in UVB-SIPS is changing over time. Secretome from NHEKs in UVB-SIPS (UVB) was compared to unexposed (CTL) NHEKs (N=5 excepted for CTL on day 3, N=4 (biological replicates, NHEKs isolated from independent donors)). **(A)** Recapitulative table of the number of identified proteins and significantly increased or decreased in the secretome from NHEKs in UVB-SIPS compared to CTL. **(B)** Venn diagram comparing the number of protein clusters identified in the secretome of UVB- exposed and unexposed NHEKs at 3 days. **(C)** Venn diagram comparing the number of proteins clusters identified in the secretome of UVB- exposed and unexposed NHEKs at 7 days. **(D)** Venn diagram comparing protein clusters significantly increased in the secretome of NHEKs at 3 and 7 days after UVB exposures. **(E)** Venn diagram comparing protein clusters significantly decreased in the secretome of NHEKs at 3 and 7 days after UVB exposures. (↑ : fold change ≥ 2 ; ↓ : fold change $\leq 0,5$; p-value $\leq 0,05$).

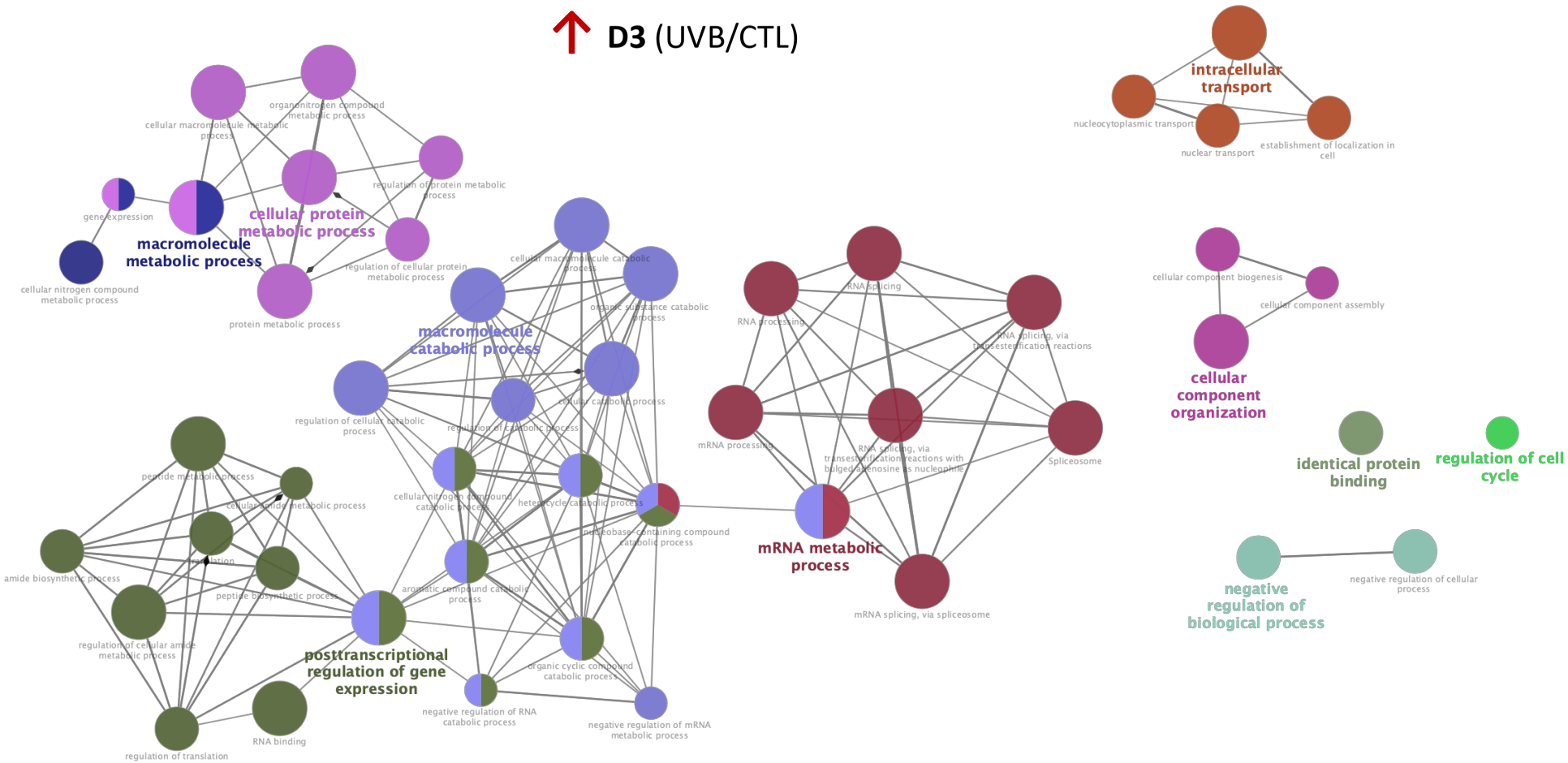

Figure 30 : Pathways linked with proteins significatively increased in secretome from UVB-SIPS NHEKs at 3 days after UVB exposures (when compared to CTL NHEKs secretome)

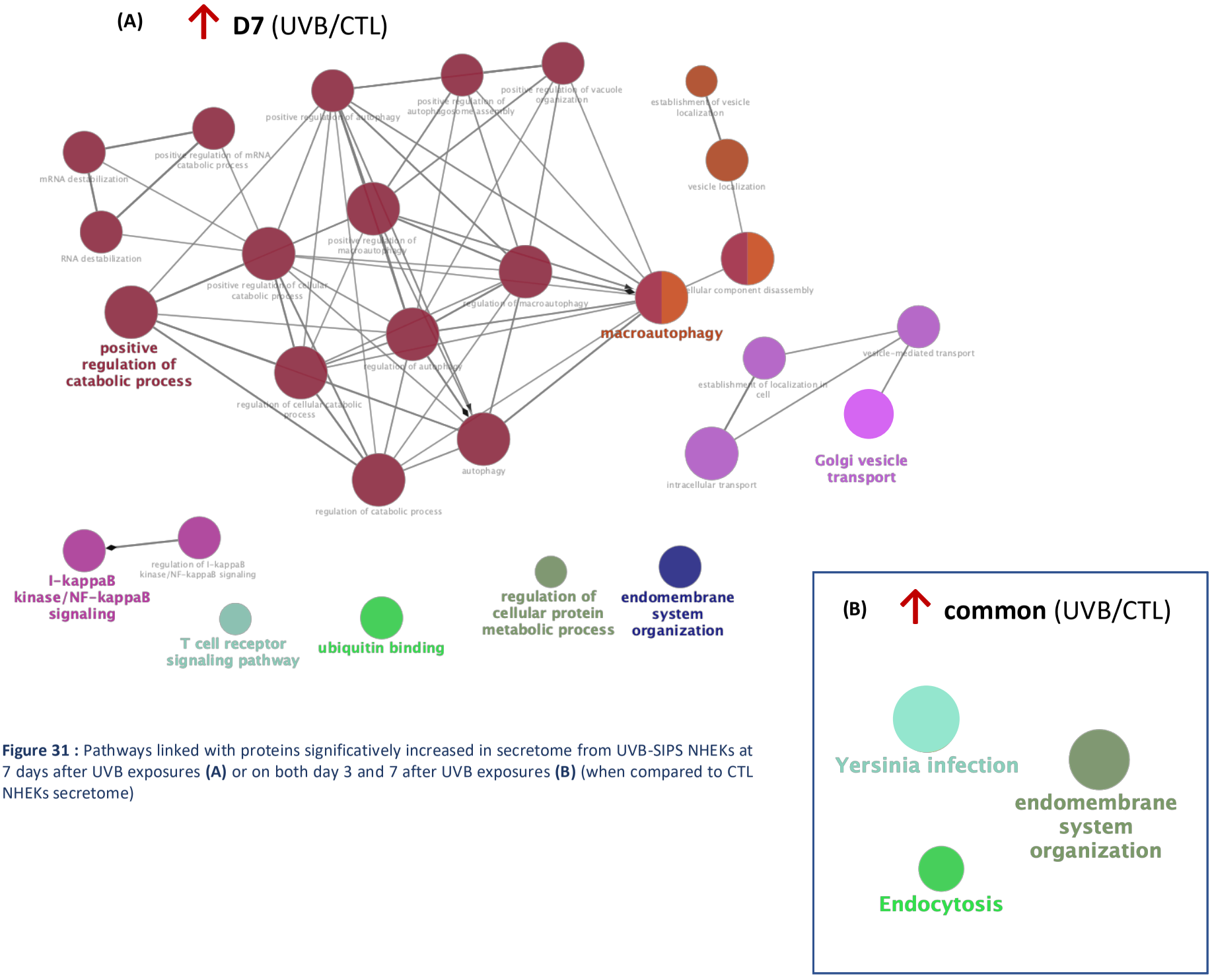

Figure 31 : Pathways linked with proteins significatively increased in secretome from UVB-SIPS NHEKs at 7 days after UVB exposures **(A)** or on both day 3 and 7 after UVB exposures **(B)** (when compared to CTL NHEKs secretome)

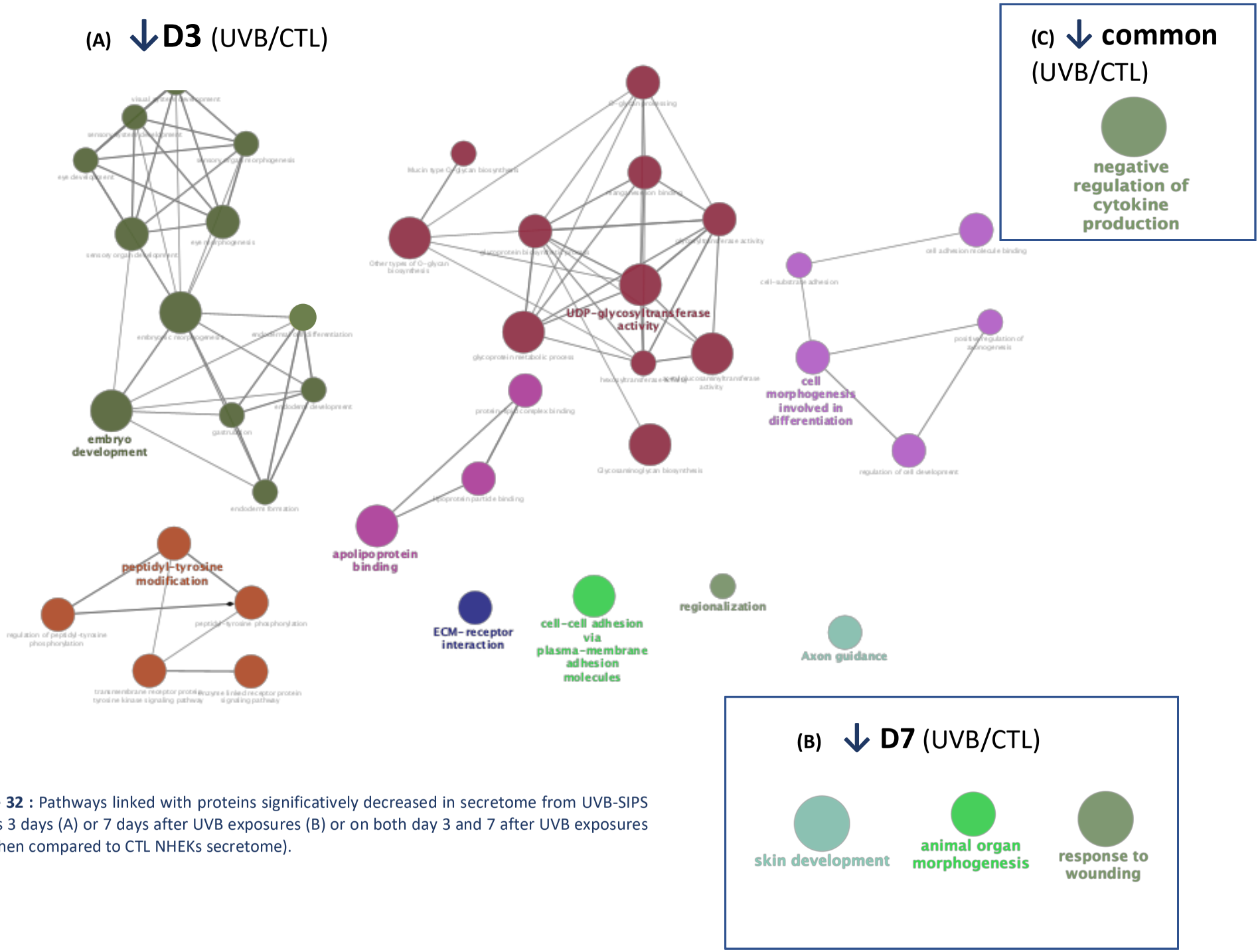

Figure 32 : Pathways linked with proteins significatively decreased in secretome from UVB-SIPS NHEKs 3 days (A) or 7 days after UVB exposures (B) or on both day 3 and 7 after UVB exposures (C) (when compared to CTL NHEKs secretome).

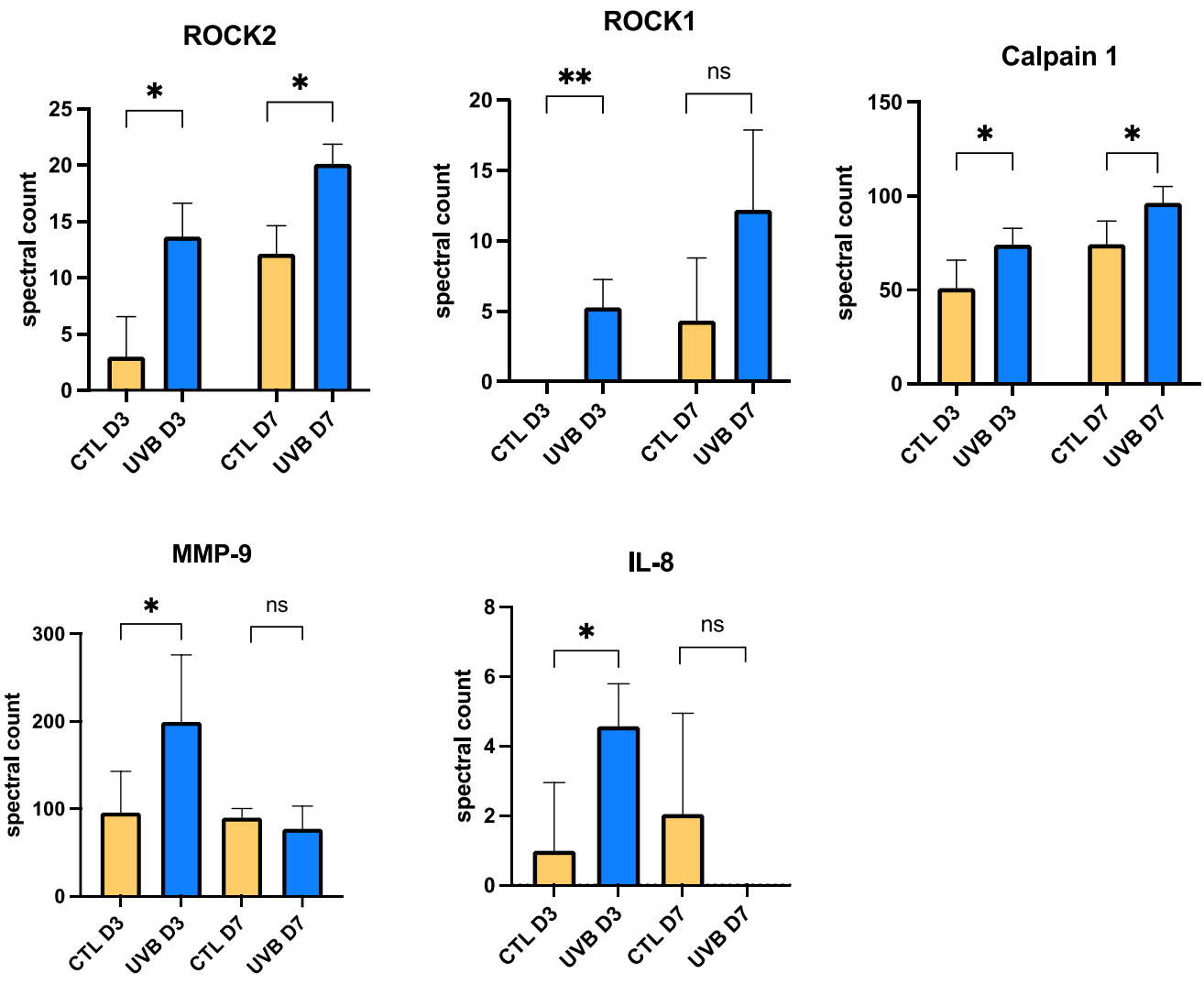

Figure 33 : Spectral counts of pro-tumorigenic proteins secreted by NHEKs. NHEKs were exposed to three repeated UVB exposures (or unexposed, CTL). At 3 or 7 days after the UVB exposures, their conditioned medium was collected and analysed by mass spectrometry. Statistical significance is determined by paired t-test *(ns = p >0 .05*; ** = p <0 .05; *** = p <0 .001).* (N=5 excepted for CTL on day 3, N=4).

Although the total number of identified proteins (CTL and UVB combined) is higher at 7 days, the number of proteins with different abundance is lower than at 3 days. At both times, the number of proteins with increased abundance is considerably higher than the proteins with decreased abundance in the secretome of UVB-exposed NHEKs (**Figure 29 A**).
Moreover, more proteins are identified in the secretome of UVB-exposed NHEKs than in the unexposed NHEKs secretome at both 3 and 7 days (**Figure 29 B and C**).
Even if some proteins with changed abundance are common between day 3 and day 7, the SASP composition is different on day 3 and day 7, confirming that the SASP evolves over time (**Figure 29 D and E**).

Pathway and network analysis of proteins showing an abundance change in the secretome with Cluego shows that proteins enriched on day 3 after UVB exposures are mainly involved in the metabolic processes of proteins and mRNA as well as the regulation of transcription. In addition, the UVB-exposed NHEKs secretome on day 3 is enriched in proteins implicated in the intracellular transport and in the cellular component organization. Interestingly, proteins related to the regulation of the cell cycle are also enriched in the SASP at day 3 (**Figure 30**).
The proteins that are enriched in the secretome on day 7 are mainly linked to the catabolic processes, the macroautophagy and the endomembrane system. Moreover, proteins from the NF-κB pathway, as NF-κB subunits or IKK inhibitory kinases are also enriched on day 7 in UVB-exposed NHEKs (**Figure 31 A**). Proteins involved in the infection response (like TNF receptor-associated proteins) and the endomembrane system are enriched in both secretomes on day 3 and 7 in UVB-exposed NHEKs (**Figure 31 B**).
Interestingly, on both days 3 and 7, the secretome of UVB-exposed NHEKs is depleted in proteins repressing the cytokine production (**Figure 32 C**). Moreover, proteins involved in the cell differentiation (like keratin 10) and the skin development are also decreased in the secretome of UVB-exposed NHEKs on day 3 and 7 respectively (**Figure 32 A and B**).
These data provide a general idea about the role of enriched or depleted proteins in the secretome of senescent NHEKs. However, many of the proteins found are essentially intracellular under normal conditions and do not necessarily exert their function in an extracellular context.

To focus on the potential pro-tumorigenic role of the SASP, several proteins known to be involved in tumorigenesis were studied. For example, ROCK1 and 2 could promote melanoma invasion (Díaz-Núñez et al., 2016). ROCK1 and 2 are significantly more abundant in the secretome of NHEKs exposed to UVB on day 3 and this increase in abondance is prolonged until day 7 for ROCK 2 (**Figure 33**).
In addition, the calpain 1 is a cysteine proteinase that can promote cancer cell migration and invasion by regulating the focal cell adhesions and promoting the extracellular matrix remodeling by MMP1 and MMP2 (Storr et al., 2011). Calpain 1 is already present in the secretome of unexposed NHEKs but its abundance is slightly but significantly increased in the secretome of UVB-exposed NHEKs (**Figure 33**).
IL-8 and MMP9, that are also known to promote melanoma invasion, are also increased in the secretome of UVB-exposed NHEKs on day 3 (Jobe et al., 2016; Tang et al., 2013). However,

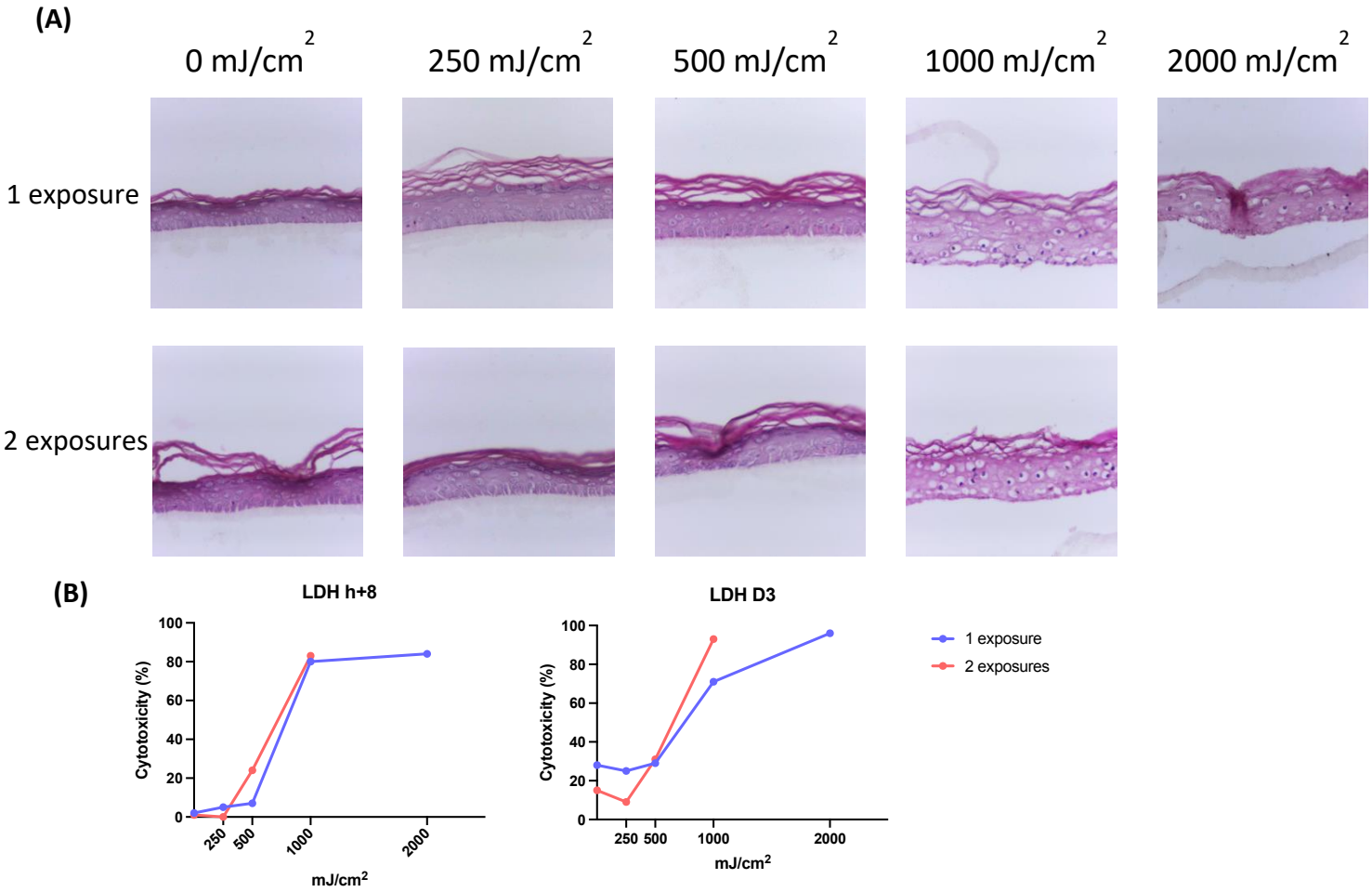

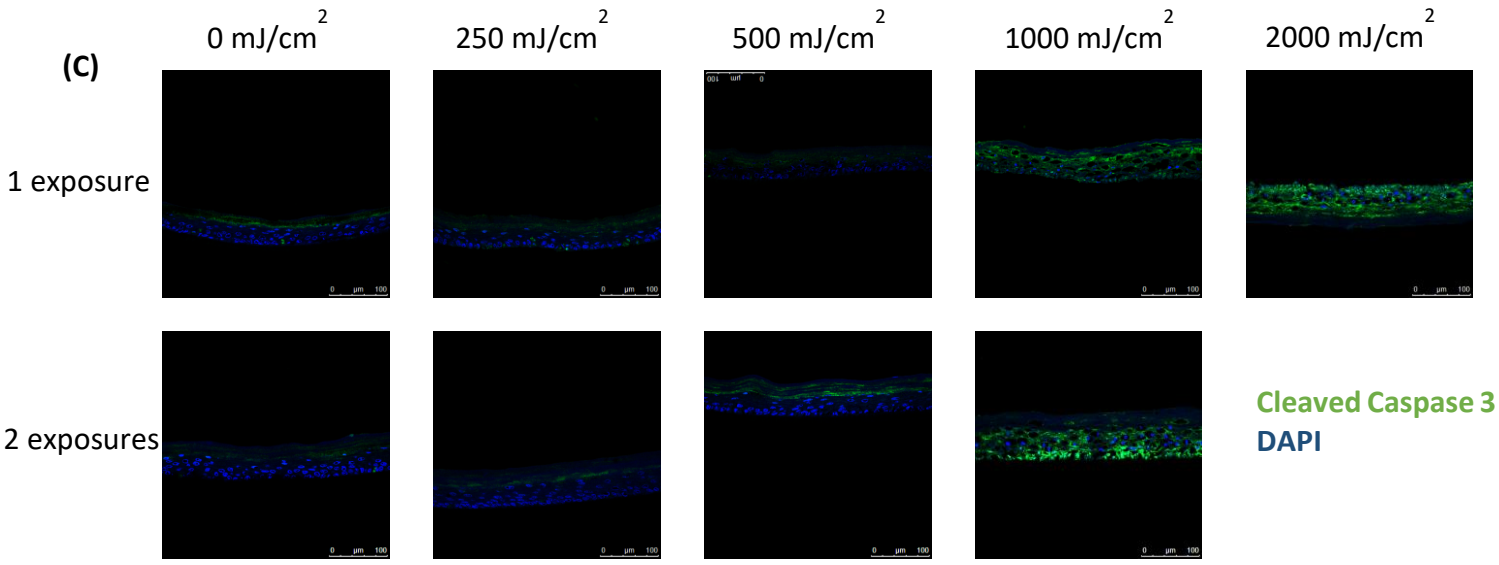

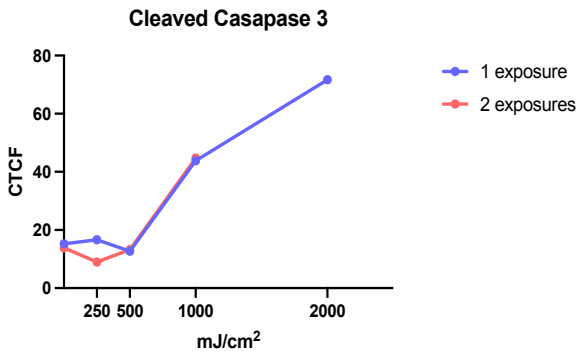

Figure 34: RHE mortality after UVB exposure(s). RHE were exposed to different UVB doses (0, 250, 500, 1000 or 2000 mJ/cm^2) once or twice (with 4h interval) in one day. **(A)** Histological sections are stained with haematoxylin and eosin (magnification: x200). **(B)** LDH activity is analysed at 8 h after the first UVB exposure and 3 days after exposure(s). **(C)** Representative pictures of cleaved caspase 3 immunostaining and quantification of the fluorescence (CTCF = Corrected Total Cell Fluorescence) (N= 2 technical replicates).

the increase in IL-8 and MMP9 abundance in the secretome is no longer observed at 7 days after UVB exposures (**Figure 33**).
These findings suggest that some secretome proteins could promote the cancer cells migration as it was partly suggested by previous experiments (Boyden chambers and scratch assays). To study if under more physiological conditions, senescent keratinocytes could have an impact on skin cancer cells, we decided to work on a reconstructed epidermis in order to have a model closer to what occurs *in vivo*.

3. Development of UVB-SIPS in reconstructed epidermis

After studying the senescent phenotype induced by repeated UVB exposures on NHEKs as well as the impact of their secretome on the migration of skin cancer cell lines in two-dimensional culture models, we wanted to develop culture models more representative of *in vivo* conditions. We have opted for the development of a reconstructed human epidermis (RHE) with HEKA1 keratinocytes isolated from adult skin biopsy. The first step was to develop a model of senescence induction in RHE. To do so, we exposed RHE to increasing doses of UVB to determine the best dose to induce senescence.

3.1. Evaluation of the UVB dose

In order to select the best UVB dose to induce senescence in RHE, we first need to determine the maximum UVB dose that does not provoke cell death. RHE were therefore exposed to increasing UVB doses (250, 500, 1000, 2000 mJ/cm^2) for one or two exposures in one day.
First, we checked RHE morphology via histological sections staining with hematoxylin and eosin. The morphology of RHE exposed to UVB at 250 mJ/cm^2 or 500 mJ/cm^2 exposure, even with 2 exposures, doesn't seem to be modified **(Figure 34 A).** However, when RHE are exposed to UVB at 1000 mJ/cm^2 or more, we observe the apparition of many rounded cells. These cells are probably apoptotic cells, also called sunburn cells, as described by V. Bertrand-Vallery (Bertrand-Vallery et al., 2010) **(Figure 34 A).**
In addition, to measure cell death associated with UVB exposures, we performed a LDH (lactate deshydrogenase) assay and an immunostaining of cleaved caspase 3 (associated to apoptosis). The results displayed an increased LDH release as well as an increased abundance of active caspase 3 staining when RHE were exposed to UVB at doses equal or greater than 1000 mJ/cm^2 UVB **(Figure 34 B and C)**.

3.2. Senescence induction in UVB-exposed RHE

In order to study whether the exposure to a subcytotoxic dose of UVB can induce senescence in RHE, we studied biomarkers of senescence following two repeated exposures at 500 mJ/ cm^2 of UVB.

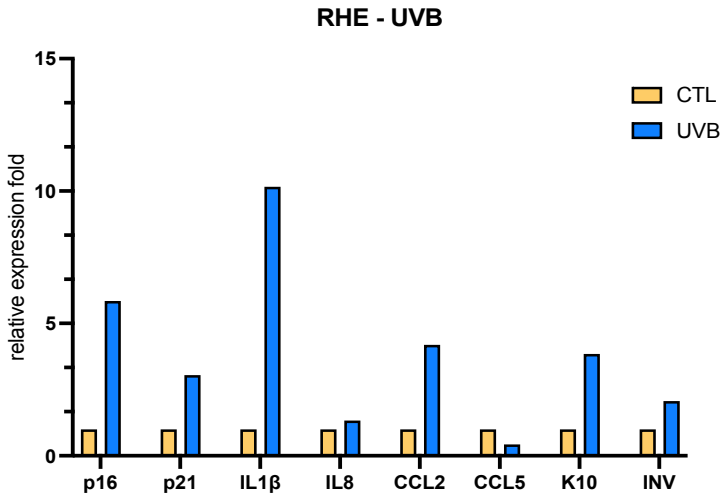

Figure 35: Relative mRNA level of senescence-associated genes after UVB exposures in RHE. RHE were exposed to two repeated exposures with UVB (500 mJ/cm^2) in one day or not (CTL). Senescence-associated genes (*p16, p21, IL-1β, IL-8, CCL2* and *CCL5*) as well as differentiation associated genes (*K10* and *INV*) are expressed as relative expression fold ($2^{-\Delta\Delta CT}$) of UVB compared to the control and *RPLP0* is used as housekeeping gene (N=1).

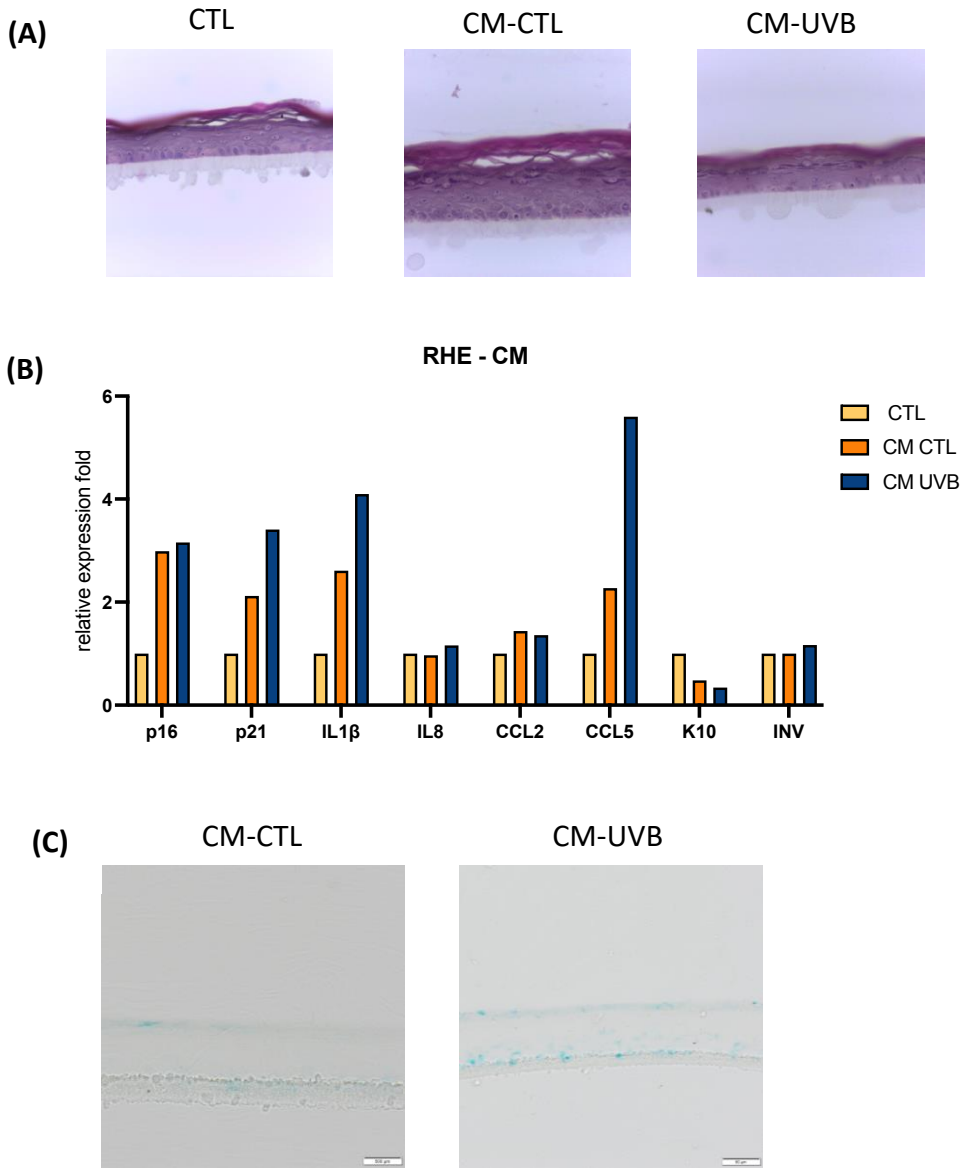

Figure 36: Effect of CM from UVB-SIPS NHEKs on RHE. RHE were exposed to conditioned medium from UVB exposed NHEKs (CM UVB) or unexposed (CM CTL) during 3 days and were compared to RHE incubated with Epilife medium (CTL). **(A)** Histological sections were stained with haematoxylin and eosin (magnification: x200). **(B)** Senescence associated genes (*p16, p21, IL-1β, IL-8, CCL2* and *CCL5*) as well as differentiation associated genes (*K10* and *INV*) are expressed as relative expression fold ($2^{-\Delta\Delta CT}$) of RHE in contact with CM UVB or CM CTL compared to CTL and *RPLP0* is used as housekeeping gene (N=1). **(C)** SA-βgal staining (scale bar=500 µm).

We first studied the expression of several genes associated with senescence by RT- qPCR. As shown in **Figure 35**, UVB exposures induce an increased gene expression of *p16* and *p21,* coding for the two CDKI involved in the cell cycle arrest, but also of *IL-1β* and *CCL2,* coding for two SASP factors. In addition, UVB exposures also induce the overexpression of *keratin 10* and *involucrin*, suggesting that UVB also promotes keratinocytes differentiation in RHE (**Figure 35**).
Then we wanted to complete this gene expression analysis with other biomarkers. In particular, we performed an immunostaining of RHE with Ki-67, a proliferation marker and with 53BP1 to detect DNA damage. Unfortunately, these labeling did not work and further technical adjustments are therefore necessary. In addition, we have made a SA-βgal staining but it did not work either (*data not shown*).
These results on senescence-associated genes expression are therefore encouraging, but need to be repeated and completed by the identification of other biomarkers of senescence.

3.3. Impact of CM from senescent NHEKs on RHE

One of the effect of the SASP is to induce senescence, as it was shown that CM of senescent melanocytes induces senescence in fibroblasts (Victorelli et al., 2019). We therefore studied if senescence in RHE can be induced by exposing them to the secretome of senescent NHEKs. To do so, the RHE medium was replaced with CM from UVB-exposed (CM UVB) or unexposed (CM CTL) NHEKs collected at 7 days after the UVB exposures, half completed with fresh Epilife medium, for 3 days.
First-of-all, the epidermis structure does not appear to be affected by the incubation with the different CM (**Figure 36 A**). However, following a 3-day incubation with CM harvested from UVB-exposed NHEKs, we observed an increased gene expression of *p21, IL-1β* and *CCL5* in RHE. Note that we also observed an increase in *p16* expression following incubation with CM from UVB-exposed NHEKs but also from controls NHEKs (**Figure 36 B**). Moreover, CM exposure does not seem to promote differentiation in RHE as *keratin 10* and *involucrin* mRNA levels are unchanged in RHE exposed to CM compared to RHE cultured with Epilife medium (CTL) (**Figure 36 B**).
SA-βGal staining was also performed and the number of SA-βGal positive cells tends to be more elevated in CM-UVB exposed RHE but this procedure did not allow to precisely quantify them and still requires improvements (**Figure 36 C**). In addition, other markers of senescence, such as 53BP1 and Ki-67 immunostainings, have been tested but unsuccessfully and require technical adjustments.
Again, the results obtained are interesting but need to be completed by further experiments and other biomarkers.

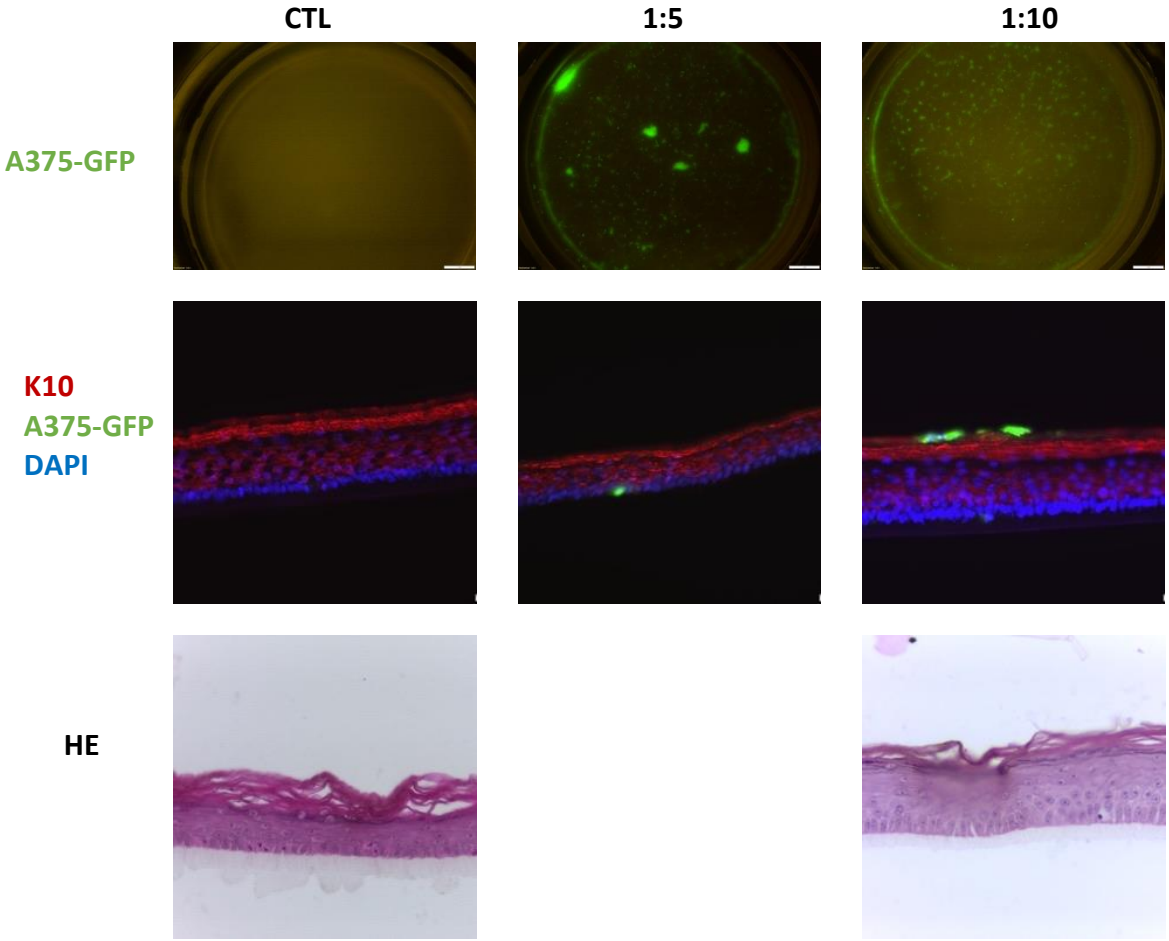

Figure 37: Development of RHE including A375-GFP melanoma cells. A375-GFP cells were incorporated in different proportions in RHE (A375-GFP/HEKA1 : 1:5 or 1:10 ; CTL= HEKA1 alone). After 11 days of reconstruction, pictures of the insert were taken. In addition, keratin 10 immunostaining (red) and nucleus staining with DAPI (blue) were achieved. Finally, histological sections were made with haematoxylin and eosin (magnification: x200) (N= 2 technical replicates).

4. Reconstructed epidermis including melanoma cells

To study the effect of senescent cells on melanoma cells in a more physiological model, we developed a new model of RHE in which melanoma cells are included. In order to differentiate the keratinocytes and the melanoma cells, we used A375 melanoma cells expressing GFP (A375-GFP) developed by the Prof. Poumay in collaboration with the lab of the Prof. Sekulic (Mayo Clinic, Scottsdale AZ).

4.1. Establishment of RHE including melanoma cells

Different ratios of A375-GFP/keratinocytes HEKA1 cells were seeded together (1:5 and 1:10) on a polycarbonate filter and then cultured until complete differentiation of RHE to determine the best proportion to form this RHE model. RHE only composed of HEKA1 were used as control. After 11 days of air-liquid interface, the RHE containing A375-GFP cells were analyzed. The overview of the filter shows a fluorescent signal in the two RHE containing A375-GFP cells, suggesting that A375-GFP cells are still present on day 11 of reconstruction. In the 1:5 ratio, some A375-GFP formed large clusters/cellular aggregates whereas with the 1:10 ratio many small clusters are observed (**Figure 37**).

Then we checked whether the reconstruction of RHE was correct despite the inclusion of melanoma cells. As scheduled, keratin 10 was detected in the suprabasal layers of the epidermis and allows to have an indication of the A375-GFP cells localization. For both A375-GFP/HEKA1 seeding ratios, the GFP positive cells were found either in the basal or in the cornified layer of the epidermis, suggesting that some of them succeeded in anchoring on the filter and that the others were gradually eliminated by desquamation (**Figure 37** and *data not shown*).

Histological sections were also achieved in order to evaluate the integrity of the RHE structure with the different ratio of A375-GFP/ HEKA1 cells. Seeding A375-GFP/ HEKA1 cells at 1:10 ratio did not seem to impact the RHE structure (**Figure 37)**. However, the RHE containing A375-GFP/ HEKA1 cells at 1:5 ratio disaggregated during the dehydration of the sample and was not usable.

To be certain to avoid destabilization of the epidermis structure, the 1:10 ratio was retained for the next experiments as it contains enough aggregates of A375-GFP cells.

4.2. RHE disaggregation

In order to be able to isolate the different cell types following the culture in RHE containing A375-GFP cells, for instance for subsequent flow cytometry analysis or single cell RNA seq analysis, a disaggregation protocol of the RHE must be established. We therefore focused on the development of an efficient protocol to disaggregate RHE to collect the maximum of living individual cells from RHE. For this purpose, the number of live cells recovered as well as the quantity and quality of the RNA that could be extracted from these cells was examined for each protocol. In addition, to determine which epidermal layers were disaggregated by the protocol,

Treatment	Cell count	Histological staining	RNA concentration	RIN	qPCR
D	✗	✓	✓	✓	✓
D+T-1h	✓	✗	✓	✓	✓
D+T-40'	✓	✓	✓	✓	✓
D+T-20'	✓	✓	✓	✓	✓
TT-37°C-1h	✓	✗	✓	✓	✓
TT-4°C-ON	✓	O	O	✓	✓
TF-37°C-1h	✓	✓	✓	✓	✓
TF-4°C-1h	✓	✓	✗	✗	✗
TF-4°C-ON	✓	✓	✓	✓	✓
TF-0°C-ON	✓	✓	✓	✓	✓
NT	✗	✓	✓	✓	✓

Table 5 : Summary of the analyses of RHEs disaggregation

RHEs were disaggregated by different treatments: Dispase (15 min) (**D**); Dispase (15 min) + Trypsin at 37°C during 1h (**D+T-1h**), 40 min (**D+T-40'**) or 20 min (**D+T-20'**) ; Trypsin at 37°C for 1h or at 4°C O/N followed by cell disaggregation by triturating (**TT-37°C-1h**, **TT-4°C-ON**); Trypsin at 37°C for 1h, 4°C for 1h, 4°C O/N or 0°C O/N followed by cell disaggregation by flushing (**TF-37°C-1h, TF-4°C-1h, TF-4°C-ON, TF-0°C-ON**); Non treated RHE (**NT**) were directly incubated in lysis buffer.

V : analysis performed; O : analysis not performed ; **X** : analysis not feasible. Cell counting could not be performed with treatments that do not allow cell separation (D and NT). A very efficient cell separation (D+T-1h and TT-37°C-1h) is not compatible for histological staining because the cornified layer alone disaggregates during histological treatment. When no cell is collected, as with TF-4°C-1h, no RNA could be extracted.

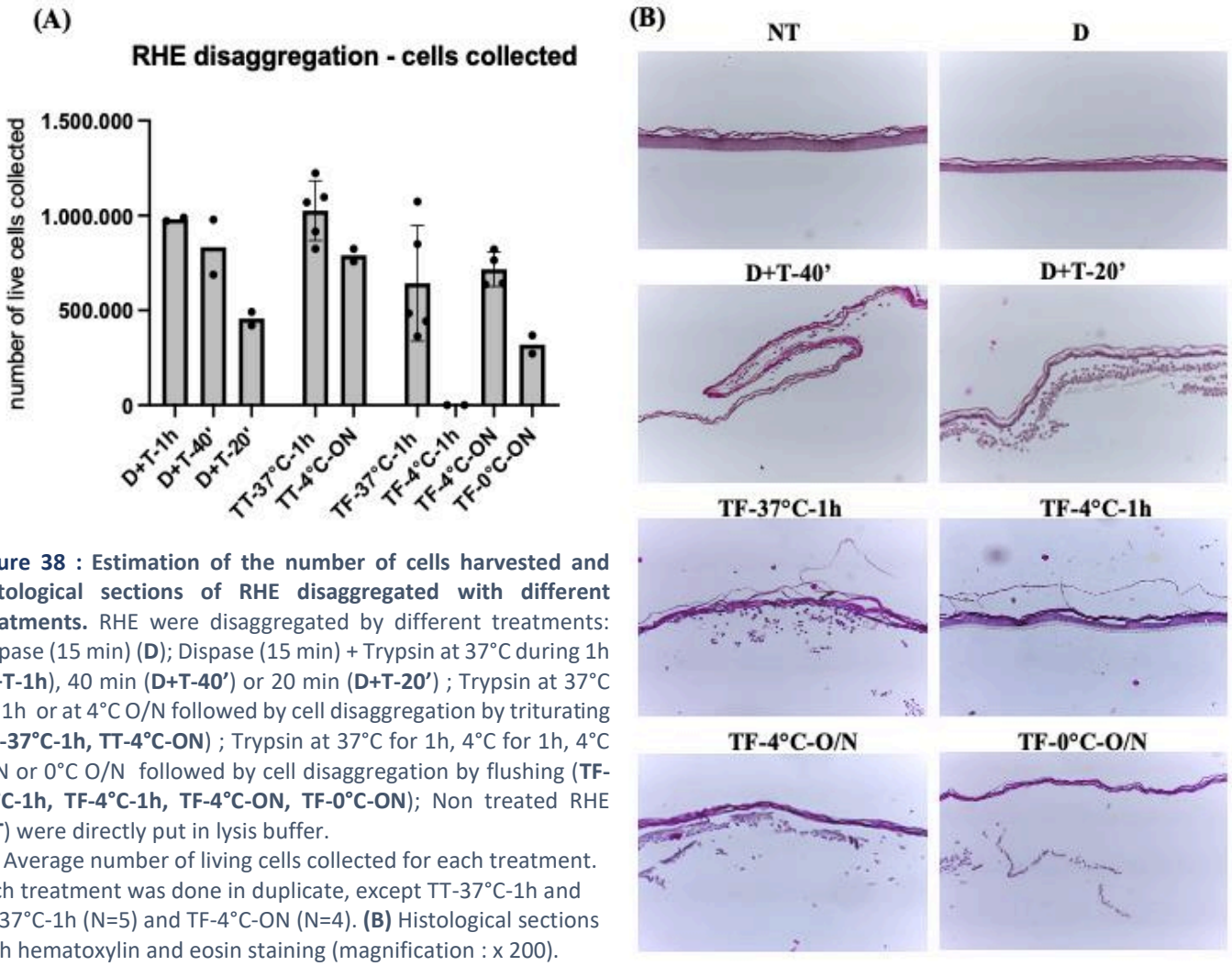

Figure 38 : Estimation of the number of cells harvested and histological sections of RHE disaggregated with different treatments. RHE were disaggregated by different treatments: Dispase (15 min) (**D**); Dispase (15 min) + Trypsin at 37°C during 1h (**D+T-1h**), 40 min (**D+T-40'**) or 20 min (**D+T-20'**) ; Trypsin at 37°C for 1h or at 4°C O/N followed by cell disaggregation by triturating (**TT-37°C-1h, TT-4°C-ON**) ; Trypsin at 37°C for 1h, 4°C for 1h, 4°C O/N or 0°C O/N followed by cell disaggregation by flushing (**TF-37°C-1h, TF-4°C-1h, TF-4°C-ON, TF-0°C-ON**); Non treated RHE (**NT**) were directly put in lysis buffer.
(A) Average number of living cells collected for each treatment. Each treatment was done in duplicate, except TT-37°C-1h and TF-37°C-1h (N=5) and TF-4°C-ON (N=4). **(B)** Histological sections with hematoxylin and eosin staining (magnification : x 200).

histological sections as well as analyses of gene expression of markers of the different epidermal layers were performed. RHE were treated with dispase during 15 min (D), dispase for 15 min followed by trypsin incubation at 37°C during 1h (D+T-1h), 40 min (D+T-40') or 20 min (D+T-20'), trypsin incubated 1h at 37°C or at 4°C O/N followed by cell disaggregation by triturating (TT-37°C-1h, TT-4°C-ON) or trypsin at 37°C for 1h, 4°C for 1h, 4°C O/N or 0°C O/N followed by cell disaggregation by flushing (TF-37°C-1h, TF-4°C-1h, TF-4°C-ON, TF-0°C-ON); Non treated RHE (NT) were directly incubated in lysis buffer (more detailed protocols are described in **Figure 4** and in **table 2,** Material and Methods section). A summary of the different analysis performed on RHE is done **table 5**.

Number of cells harvested

After disaggregation and filtration, the average of living cells collected is ± 1 million of cells with D+T-1h and TT-37°C-1h treatments, showing that dispase is not essential to recover a high number of cells (**Figure 38 A**). With D+T-40', TF-37°C-1h and TT/TF-4°C-ON, less cells were collected (between 70% and 83%). D+T-20' and TF-0°C-ON treatments allowed to collect less than 500,000 cells and finally, no cells were collected with TF-4°C-1h protocol.
Histological sections were fixed just after treatment (before trituration or flushing) and they confirmed that less cells were detached with D+T-20' than with D+T-40', indicating that trypsin incubation for 20 min at 37°C was not long enough to detach correctly RHE cells (**Figure 38 B**). On histological sections, treatment with Trypsin at 4°C or 0°C incubated overnight (TF-4°C-ON and TF-0°C-ON) did not allow to detach every cell from each other since cells are forming aggregates. Histological sections also confirm that trypsin incubated for 1h at 4°C (TF-4°C-1h) was insufficient to produce any effect on cell detachment as the RHE remains intact (**Figure 38 B**).
Taking together, these results indicate that the only treatment of RHE with trypsin could be sufficient to disaggregate RHE (with an incubation at 37°C for 1h or 40 min or incubation at 4°C ON). Moreover, trituration seems to be more effective than flushing at 37°C (TT-37°C-1h: ± 1.047.925 cells collected; TF-37°C-1h: ± 788.450 cells collected).

Quantity and quality of the RNA collected

After disaggregation, total RNA was isolated, and its concentration was dosed for each sample. Non-treated (NT) and dispase treated RHE (D) have the higher RNA concentrations (NT : 149.9 ng/µL ; D : 203.9 ng/µL) ; however, these methods do not allow the separation of cells from each other for their subsequent sorting and treatment (**Figure 39 A**).
RHE treatment with dispase + trypsin at 37°C for 1h (D+T-1h), 40 min (D+T-40') and 20 min (D+T-20') and with trypsin alone incubated 1h at 37°C (TT-37°C-1h and TF-37°C-1h) allow the recovery of a sufficient quantity of RNA (between 104 ng/µL and 92.6 ng/µL) to perform several RT-qPCR. RHE disaggregation using trypsin at 4°C or 0°C overnight (TF-4°C-ON and TF-0°C-ON) only allows the recovery of a low concentration of RNA (TF-0°C-ON: 46.7 ng/µL and TF-4°C-ON: 54.7 ng/µL). No RNA was collected with TF-4°C-1h as no cells could be recovered.

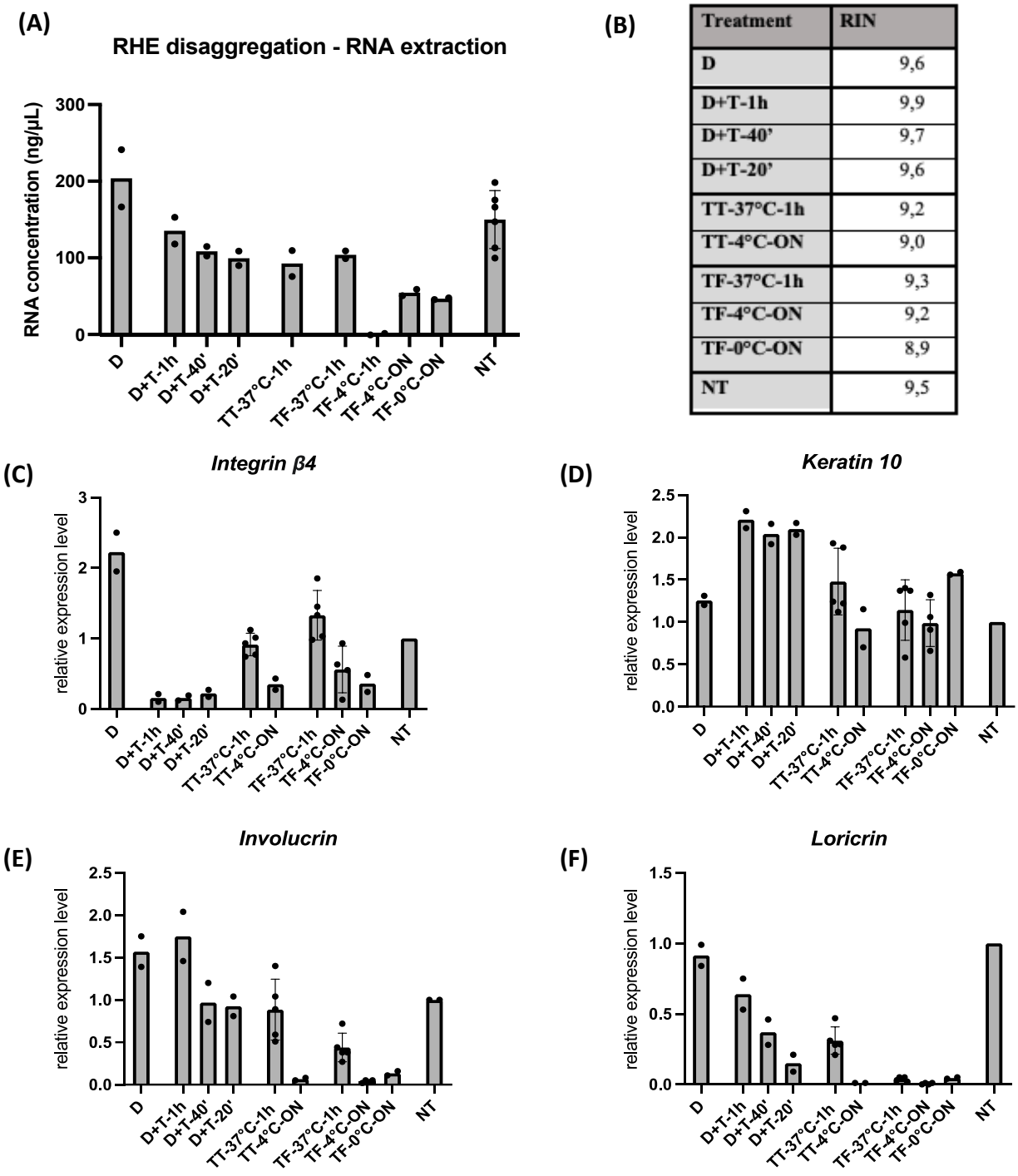

Treatment	RIN
D	9,6
D+T-1h	9,9
D+T-40'	9,7
D+T-20'	9,6
TT-37°C-1h	9,2
TT-4°C-ON	9,0
TF-37°C-1h	9,3
TF-4°C-ON	9,2
TF-0°C-ON	8,9
NT	9,5

Figure 39 : RNA concentration and quality, and relative mRNA levels of genes associated to keratinocytes' differentiation collected from RHE disaggregated by different treatments

RHEs were disaggregated by different treatments: Dispase (15 min) (**D**); Dispase (15 min) + Trypsin at 37°C during 1h (**D+T-1h**), 40min (**D+T-40'**) or 20min (**D+T-20'**) ; Trypsin at 37°C for 1h or at 4°C O/N followed by cell disaggregation by triturating (**TT-37°C-1h**, **TT-4°C-ON**); Trypsin at 37°C for 1h, 4°C for 1h, 4°C O/N or 0°C O/N followed by cell disaggregation by flushing (**TF-37°C-1h, TF-4°C-1h, TF-4°C-ON, TF-0°C-ON**); Non treated RHE (**NT**) were directly put in lysis buffer. **(A)** RNA concentrations after RNA extraction, determined with NanoDrop 2000 (ThermoFisher Scientific) **(B)** RNA integrity number (RIN) means between duplicates for each treatment estimated with Agilent Bioanalyzer. **(C)** *Integrin β4*, **(D)** *Keratin 10,* **(E)** *Involucrin* and **(F)** *Loricrin* relative mRNA levels. Results are expressed as relative expression fold (2^-ΔΔCT) of treated RHE compared to non-treated RHE (NT) and *RPLP0* was used as house-keeping gene. qPCR for each treatment was done in duplicate, except TT-37°C-1h and TF-37°C-1h which were done in 5 replicates and TF-4°C-ON in 4.

RNA integrity was also studied to check the quality of the collected RNA. RNA integrity number (RIN) is a number comprised between 1 (RNA totally degraded) and 10 (intact RNA). We can observe that the RIN obtained is higher or equal to 8.9 for every treatment, showing no major RNA degradation during RHE disaggregation treatment (**Figure 39 B**).

Study of the expression of several specific markers of NHEKs differentiation

To get some idea about which epidermal layer each treatment could detach, different markers of keratinocyte differentiation were studied by RT-qPCR. Here, integrin β4 is used to identify the cells from the basal layer, keratin 10 for the suprabasal layer, involucrin and loricrin for the cornified layer. However, involucrin is known to be also found in the upper part of the granular layer (Candi et al., 2005; Kadoya et al., 2016).
In RHE treated only with dispase, *integrin β4* is intriguingly overexpressed (2.22 x more than in NT RHE) while *keratin 10, involucrin* and *loricrin* expression levels are similar to non-treated RHE (figure 11 C, D, E and F), indicating a recovery of the cells originating from all the layers of the epidermis, which was predictable since dispase does not dissociate cells from each other.
Combined dispase + trypsin treatments showed strongly reduced expression of *integrin β4* compared to non-treated RHE, suggesting that these treatments are not really efficient to collect keratinocytes from the basal layer **(Figure 39 C)**. However, for the same treatments, we detect an overexpression of *keratin 10* (± 2 x compared to NT RHE), no change in the relative expression of *involucrin* (**Figure 39 D and E)** and a decreased expression of *loricrin* in comparison with non-treated (NT) RHE (**Figure 39 F**). These results demonstrate that the combined treatment of dispase + trypsin allows a good recovery of the suprabasal layers but is less efficient for basal and cornified layers.
Trypsin incubated at 37°C for 1h followed by trituration seems to be efficient to harvest cells from the basal to the upper granular layer as *integrin β4, keratin 10* and *involucrin* expression levels are similar to NT RHE (figure 11 C, D & E). Globally, the RHE that were flushed exhibited lower expression of upper layers marker (*involucrin* and *loricrin*). Moreover, Trypsin treatments at low temperature (0°C and 4°C) are only efficient to collect suprabasal cells (**Figure 39 C-F**).
Therefore, the condition TT-37°C-1h seems to be the more efficient to recover separated cells from the different layers.

4.3. Melanoma cells proportion in stressed RHE

As the protocol for RHE disaggregation is now established, RHE containing A375-GFP cells could be disaggregated and used for flow cytometry analysis in order to quantify the proportion of GFP positive cells in RHE to determine whether UVB exposure could impact it. To do so, RHE containing A375-GFP cells were exposed to two repeated exposures at 500 mJ/ cm^2 of UVB as described in paragraph 3.2. Control RHE were not exposed to UVB.

(A)

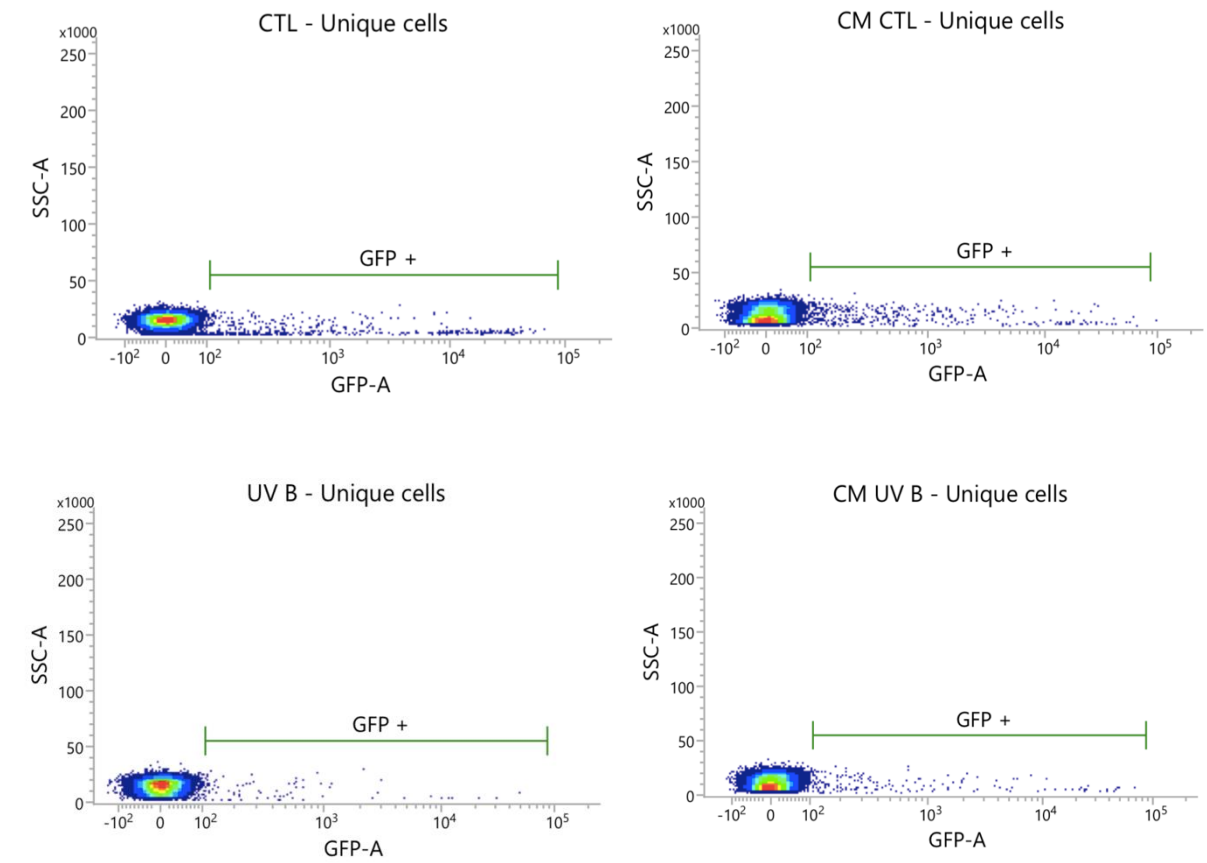

(B)

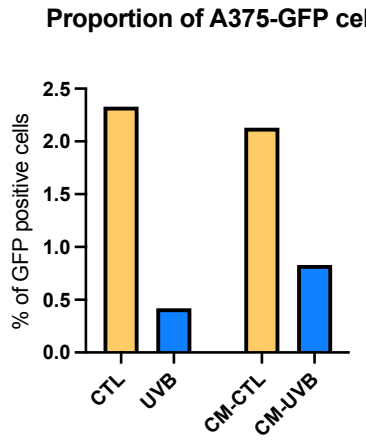

(C)

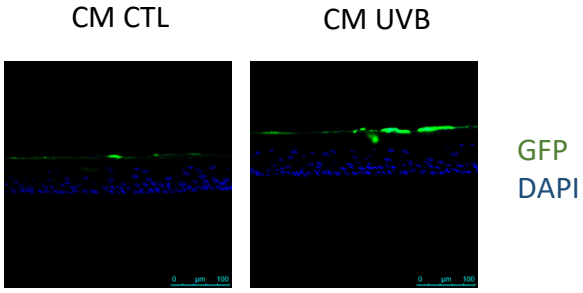

Figure 40 : Estimation of the proportion of A375-GFP cells in RHE including A375-GFP melanoma cells following UVB exposure. A375-GFP cells were incorporated in RHE (A375-GFP/HEKa1: 1/10). After 11 days of reconstruction, RHE were exposed to two exposures with UVB (500 mJ/cm^2) or incubated with conditioned medium from UVB exposed NHEKs (CM UVB) or unexposed ones (CM CTL). **(A)** At 3 days after exposure or incubation, RHE are disaggregated and analysed by flow cytometry. **(B)** Proportion of GFP positive cells in the epidermis collected cells (N=1). **(C)** Confocal imaging with nucleus staining (blue) (scale bar = 100 µm).

In addition, the effect of CM from senescent NHEKs on the proportion of GFP positive cells in RHE was also studied. To study this, RHE containing A375-GFP cells were incubated with CM from UVB-exposed NHEKs for 3 days, has presented in the paragraph 3.3.
To determine whether senescence has an impact on melanoma proliferation, A375-GFP proportion is monitored by flow cytometry in RHE exposed to UVB at 3 days after the UVB exposures or in RHE incubated 3 days with CM from UVB-exposed NHEKs.
Interestingly, the proportion of A375-GFP cells is only about 2% in RHE unexposed to UVB or exposed to CM from unexposed NHEKs (**Figure 40 A and B**). Moreover, in RHE exposed to UVB or to CM from UVB-exposed NHEKs the proportion of A375-GPF cells drops to +/- 0,5% of total cells, suggesting that senescence induction in the epidermis could reduce the number of melanoma cells (**Figure 40 A and B**). However, these results are only demonstrated in a single replicate and need to be reproduced.
To understand this very low A375-GFP cells proportion in RHE, they were observed by fluorescent microscopy. At 14 days after seeding, most of the observed A375-GFP cells were detected in the cornified layer (**Figure 40 C**). This phenomenon may explain the low proportion of GFP positive cells found in disaggregated epidermis analyzed by flow cytometry.

DISSCUTION AND PERSPECTIVES

Fibroblasts in replicative senescence were previously shown to promote cSCC cells migration through their secretion of chemerin (Farsam et al., 2016). Moreover, SASP from keratinocytes undergoing drug-induced premature senescence was shown to promote cSCC tumor growth (Alimirah et al., 2020). However, UV-induced premature senescence is poorly studied in keratinocytes and the effect of their secretome on skin cancers is also poorly explored. This master thesis therefore aims to study the impact of UV-induced premature senescent normal human epidermal keratinocytes (NHEKs) secretome on skin cancer cells migration.

Repeated UVB exposures are known to induce premature senescence in fibroblasts, and in keratinocytes (Debacq-Chainiaux et al., 2005; Lewis et al., 2008). The first step of this study was to confirm that senescence is well induced in NHEKs after three UVB exposures at 675 mJ/cm^2 in a single day as described by E. Bauwens during her PhD thesis (Bauwens *et al., in revision*). Indeed, UVB-exposed NHEKs display several senescence markers such as morphological enlargement, SA-βGal activity, a tendency of decreased *lamin B1* expression as well as cell proliferation arrest, characterized here by a decrease of EdU incorporation and a tendency to increased *p21* gene expression (Hernandez-Segura et al., 2018). These senescence markers are present at both 3 and 7 days after UVB exposures. However, some senescence hallmarks (low EdU incorporation, decrease of *lamin B1* gene expression) are also detected in unexposed NHEKs at day 7, probably reflecting an increase in the proportion of replicative senescent cells in culture. Indeed, unexposed NHEKs must be subcultured before day 7 and are therefore already in passage 8, whereas NHEKs at passage 11 already show strong characteristics of replicative senescence (enlarged morphology, SA-βGal activity, cell proliferation arrest). Generally, the replicative senescence is detected in NHEKs cultures between passage 10 and 15 (Nassour et al., 2016). However, as NHEKs need to be amplified before UVB exposures in order to have enough cells to perform the analysis, it is difficult to realize UVB exposure at a lower passage.

As expected, UVB-exposure is associated with persistent DNA damage characterized by the presence of persistent 53BP1 foci even at 7 days post exposures. Interestingly, 53BP1 foci are not detected in NHEKs in replicative senescence, as previously described by Nassour et al. (2016). Moreover, NHEKs in replicative senescence do not present an increase of *p21* mRNA level, which again corroborates with the work of Nassour and colleagues showing that the induction of replicative senescence in NHEKs is independent of the p53/p21 pathway (Nassour et al., 2016). These data indicate that 53BP1 recruitment and p53/p21 pathway activation in senescent NHEKs are events proper to UVB-SIPS.

Senescence is also accompanied by a SASP, notably composed of pro-inflammatory cytokines and chemokines and known to be regulated at the transcriptional level (Salminen et al., 2012). In our experiments, the mRNA level of some SASP components like *IL6, IL8, CCL2* and *CCL5* tends to be upregulated in UVB exposed NHEKs at 3 days after UVB exposures. However, only *CCL5* gene expression remains higher than in control NHEKs. E. Bauwens showed similar expression profiles for *IL6* and *IL8* expression that correlated with the level of secreted IL-6 and IL-8 in the conditioned medium from UVB-exposed NHEKs (Bauwens *et al., in revision*).

These results confirm the induction of senescence in UVB-exposed NHEKs and show that the SASP expression is changing over time.

The effect of the secretome of these UVB-exposed NHEKs on skin cancer cells migration was then investigated. Previous research by E. Bauwens demonstrates that SASP from UVB-induced senescent NHEKs at 7 days after UVB exposures promotes cSCC cells migration in scratch assays and Boyden chambers (Bauwens et al., *in revision*).Those results were confirmed in our study as CM (harvested as described in Malaquin et al., 2019 protocol) from UVB-exposed NHEKs at 7 days after exposures seems to promote cSCC cells migration in Boyden chambers. Moreover, CM from UVB-exposed NHEKs collected at 3 and at 7 days post exposures also seems to promote A375 cells migration in Boyden chambers. Interestingly A375-GFP cells migration is only slightly enhanced by CM from UVB-exposed NHEKs at 7 days. As the A375 and the A375-GFP cells are coming from two different labs, we suspect deviations in the cancer cell line that could explain these heterogeneous responses. To be sure that the GFP expression does not impact the migration of A375-GFP cells, it would be interesting to repeat the migration assay with the A375 which were used to produce the A375-GFP.

In addition, the CM harvested at 7 days after UVB exposures slightly promoted migration of SK-MEL-28 cells but has a variable effect on SK-MEL-2 cells migration, depending on the NHEKs donor in Boyden chambers. These results suggest that CM at 7 days after UVB exposures could have an effect on melanoma and cSCC cells migration in Boyden chambers, this effect is variable depending on the cancer cell lines and the NHEKs donors.

Moreover, the migration of SK-MEL-2, SK-MEL-28 and A375 cells was also studied with scratch assays. Surprisingly, with scratch assays, the CM from UVB-exposed NHEKs harvested on day 3 seems to have an effect on the three melanoma cell lines migration. However, on day 7, the CM from UVB-exposed NHEKs appears to only induce SK-MEL-2 cell migration. The results obtained by scratch assay do not therefore corroborate those obtained with Boyden chambers. This can be explained as scratch assays and Boyden chamber assays allow to study cell migration in two different ways: scratch assays evaluate 2D cell motility over time but not cell chemotaxis whereas Boyden chambers allow to study chemotaxis but only at a given time. Moreover, Boyden chambers are known to have a low reproducibility rate (Guy et al., 2017).
For A431 (cSCC), A375 and A375-GFP cell migration assays in Boyden chambers and for all melanoma cell lines in scratch assay, we only tested the CM from a single biological replicate. It will therefore be important to investigate this CM migratory effect with CM from NHEKs of different donors to determine whether this effect is donor-dependent and cell line dependent. In addition, cancer cells migration could also be investigated with NHEKs in replicative senescence to study if the pro-migratory effect is specific to SASP from UVB-SIPS NHEKs. CM effect should also be tested on normal keratinocytes migration to determine if UVB-exposed NHEKs CM only promotes cancer migration or cell migration in general.

To investigate the protein composition of the SASP in order to identify potential candidates that can play a pro-migratory effect on cSCC and melanoma, the secretome of UVB-exposed

NHEKs was analyzed by mass spectrometry. As expected, this analysis first confirmed that UVB-exposed NHEKs are secreting more proteins than unexposed NHEKs. Additionally, as described before in fibroblasts (Faget et al., 2019), the secretome composition of UVB-exposed NHEKs is changing over time, as the enriched secreted proteins are different at 3 and 7 days after UVB exposure. Moreover, the SASP of UVB-induced senescent NHEKs has some similarities with the SASP from x ray-induced senescent renal cortical epithelial cells studied by N. Basisty and his team (Basisty et al., 2020). Indeed, 40 proteins with enriched abundance were found in the secretome of both UVB-exposed NHEKs and x ray-induced senescent renal epithelial cells, showing that some SASP similarities could be observed in different cell types and with various senescence inducers.

The secretome analysis also allowed to find some proteins in the SASP that can enhance cancer cells migration. Indeed, ROCK activation is known to promote angiogenesis, and cancer proliferation and invasion (CHEN et al., 2014). ROCK1 and 2 are found in the SASP of UVB-exposed NHEKs at 3 days and could suggest a pro-tumorigenic effect of the SASP. However, as ROCK proteins promote cancer progression through the activation of intracellular pathways notably resulting in the activation by phosphorylation of myosin light chain and the inhibitory phosphorylation of cofilin, this effect may not be observable in the extracellular compartment (CHEN et al., 2014).

In addition, the secretion of calpain by NHEKs is also increased following UVB exposures. Calpain 1 is often overactivated in cancer cells and its inhibition can prevent cancer cells invasion and metastasis. Indeed, calpain 1 regulates the focal cell adhesion and can promote the extracellular matrix remodeling by MMP1 and MMP2 (Storr et al., 2011). Interestingly, calpain 1 is mostly an intracellular protein but it is also known to be secreted by lung carcinoma and melanoma cells (Hanouna et al., 2020; Xu and Deng, 2004). Furthermore, secreted calpain 1 maintains its protease activity in the extracellular medium, suggesting that it may directly promote cancer cells invasion by remodeling the extracellular matrix (Xu and Deng, 2004). Secreted calpain 1 also favors endothelial cells migration, therefore promoting the neo-angiogenesis (Hanouna et al., 2020).

MMP-9 abundance is also increased in the secretome from NHEKs at 3 days after UVB exposures. Unlike calpain-1, MMP-9 is normally localized in the extracellular matrix and degrades gelatin and collagen, inducing extracellular matrix remodeling that facilitates cancer cell invasion and metastasis (Mondal et al., 2020). In addition, MMP-9 inhibition prevents melanoma metastasis and limits tumor growth in mice (Tang et al., 2013).

We also detect a higher IL-8 abundance in the secretome of NHEKs at 3 days after UVB exposures, which correlates with the upregulated *IL8* gene expression observed at 3 days after UVB exposures. IL-8, also known as CXCL8, could promote angiogenesis as well as melanoma invasion and migration through its receptors (CXRC1 and 2) activation (Gabellini et al., 2009). However, mass spectrometry analysis does not allow the identification of proteins present in very small amounts. We probably did not detect most of the pro-migratory cytokines here, such as CXCL1, CXCL6, CXCL10 and CCL17 even if their mRNA levels tend to increase in UVB-

exposed NHEKs at 3 days after exposure. In order to detect their secretion, ELISA assays must be performed.

To summary, the SASP analysis allowed to find some proteins that can enhance melanoma cells migration in the secretome of UVB-exposed NHEKs. However, some of these proteins (IL-8 and MMP-9) seem to be enriched in the SASP only at 3 days after the UVB exposure and therefore can not explain the pro-migratory tendency effect with the CM harvested at 7 days after UVB exposure observed in Boyden chambers.

To determine if ROCK1/2, calpain-1, MMP-9 or IL-8 secretion can be responsible for skin cancer cells migration, Boyden chamber assays should be repeated with inhibitors of these proteins to see if the slight pro-migratory effect is lost without them. In addition, as these proteins have a direct or indirect effect on extracellular matrix remodeling, invasion assays using Boyden chambers coated with matrigel or spheroid invasion into a surrounding collagen matrix, as described by N.P Jobe and colleagues (Jobe et al., 2016), should be tested. However, we tested once SK-Mel-2 and A375 cell invasion in matrigel-coated Boyden chambers and there was no effect of CM from UVB-exposed NHEKs in melanoma cells invasion when compared to the CM from control NHEKs (*data not shown*). Since the composition of the matrigel was not provided by the manufacturer, it is possible that the composition of the "matrix" is not completely similar to the dermal extracellular matrix. However, this experiment must be replicated as they were only performed once.

Moreover, it is possible to study the invasion of cancer cells in organotypic tissue cultures to be as close as possible to *in vivo* conditions (Decaestecker et al., 2007). We have therefore started to develop senescence induction models in reconstructed human epidermis (RHE), with the aim of integrating melanoma cells into epidermis made of senescent keratinocytes and to study their interaction.

To induce senescence, RHE were exposed to a single or repeated UVB dose(s). The UVB doses above 1000 mJ/cm^2 seem to induce keratinocytes apoptosis while a 500 mJ/cm^2 UVB exposure repeated twice did not induce cell mortality. In addition, RHE exposed to two sublethal doses of UVB at 500 mJ/cm^2 present increased mRNA levels of several senescence biomarkers as *p16* and *p21* and some SASP components (*IL8, CCL2, CCL5*). However, this experiment was only done once and needs to be replicated. In addition, to confirm senescence induction, it will be necessary to evaluate other markers of senescence such as SA-βgal staining or proliferation arrest.

In addition to UVB exposure, we also tried to induce keratinocytes' senescence in RHEs by incubating them with CM of NHEKs exposed to UVB as CM from senescent cells can promote premature senescence in young cells (Victorelli et al., 2019). To do so, the CM from UVB exposed and unexposed NHEKs were mixed in the RHE medium (Epilife) in 1:1 ratio. CM from UVB-exposed NHEKs seems to promote the expression of some genes used as senescence biomarkers like *p21*, as well as an increase of SA-βgal activity. However, even the CM from unexposed NHEKs seems to promote the gene expression of senescence biomarkers, suggesting

that the contact with CM stressed the keratinocytes composing the RHE. This may be due to the lack of nutrients remaining in the CM because we only added half of the usual RHE medium for CM incubation. In addition, the collection of the CM was done with KSFM medium while the RHEs are grown in Epilife medium, so the change in medium composition may have also stressed them. To eliminate this possibility, RHE should be incubated for 3 days medium composed with half KSFM and half Epilife medium. If the increased expression of senescence-related genes persists in this condition, it could suggest that the change in media composition induces RHE stress. NHEKs should then be incubated with Epilife rather than KSFM to harvest their CM and thus avoid the bias induced by the change in culture medium.

We therefore have two approaches to induce keratinocyte senescence in RHE that require further investigation with new replicates and other senescence markers (e.g. Ki-67 markers to assess proliferation).

To determine whether senescent cells could impact melanoma cells in more physiological model, we developed a new RHE model including A375 cells that express GFP so that they could be easily distinguished from keratinocytes by fluorescence microscopy or flow cytometry. RHEs containing A375-GFP cells were exposed to UVB or CM from UVB-exposed NHEKs as a proof of concept. We therefore decided to quantify the proportion of GFP-positive cells at 3 days after UVB exposure or CM incubation.

First, to be able to separate all epidermal cells for flow cytometry, several disaggregation protocols were tested. We finally chose the trypsin treatment at 37°C for 1h with mechanical trituration, since this treatment seems to be very efficient to separate cells and to collect them from the different epidermal layers. After the disaggregation step, RHE containing A375-GFP cells were analyzed by flow cytometry and showed very low proportion of GFP-positive cells (under 2,5%) in contrast with their seeding at a 1:10 ratio for the epidermis reconstruction. In addition, a decreased proportion of GFP positive cells was observed after UVB exposure or incubation with CM from UVB-exposed NHEKs. Fluorescent microscopy observations showed that the majority of A375-GFP cells were present in the cornified layer on the day 14 of the reconstruction. Since trypsin treatment at 37°C for 1h with mechanical trituration does not allow to recover the cornified layer, this could explain why the proportion of GFP positive cells detected by flow cytometry is so low.

These results suggest that A375-GFP cells have difficulty anchoring to the polycarbonate filter, tend to climb into the layers of the RHE and are removed by desquamation. To improve their anchorage in the basal layer, we could add a dermal equivalent and thus make a skin equivalent model, as it was done by Arnette and his team to include melanocytes in skin equivalent (Arnette et al., 2018). Moreover, this model would allow to get even closer to what occurs *in vivo* and the invasion of melanoma cells through the dermis could be studied Indeed, as melanoma cells express GFP it would be easy to localize them and determine if they migrate into the dermis by tracking these cells by using lattice light-sheet microscopy for example. However, for developing senescence in a skin equivalent, it will be easier to induce senescence of keratinocytes in a monolayer culture and then to integrate them at different proportions into

the reconstructed epidermis as described by Yoshioka team (Yoshioka et al., 2021). This would also be a way to avoid exposing melanoma cells directly to UVB and thus observe migratory effects due to UV exposure of melanoma cells rather than to the secretome of senescent keratinocytes.

In addition, as the SASP from senescent keratinocytes may impact cancer cells, cancer cells could also impact their environment. Indeed, M. Toutfaire showed that cSCC cells co-cultured with fibroblasts cause fibroblasts senescence (Toutfaire et al., 2018). It will therefore be of great interest to be able to separate A375-GFP cells and keratinocytes after RHE disaggregation, for example by using magnetic antibodies specific to a melanoma antigen (e.g. S 100) and then using MACS technology (Myltenyi) to separate them from keratinocytes in a magnetic column. This will allow analyses to be performed on the two separate cell types and to study changes in gene and protein expression in the keratinocytes and melanoma cells to determine if the two cell types impact on each other.

To conclude, in this master thesis we confirmed that 3 repeated UVB exposures at 675 mJ/cm^2 in a single day were sufficient to induce NHEKs senescence. Moreover, the CM harvested from UVB-induced premature senescent NHEKs at 7 days after exposure tend to promote melanoma cell migration in Boyden chambers. This effect is modulated by the NHEKs donor and the melanoma cell line. Furthermore, CM harvested from UVB-induced premature senescent NHEKs at 3 days after exposure seems to enhance melanoma cells migration in scratch assays. To characterize the secretome of UVB-induced premature senescent NHEKs and to investigate the presence of pro-migratory proteins in it, the CM was analyzed by mass spectrometry at 3 and 7 days after UVB exposure. This revealed that the secretome composition is changing between day 3 and 7 and allowed to identify some pro-migratory proteins such as calpain 1 and MMP-9.

To study the interactions between senescent keratinocytes and melanoma, A375-GFP cells were integrated in RHE and several protocols were tried to induce senescence in keratinocytes within the RHE. We finally showed the UVB exposure as well as incubation with CM from UVB-induced premature senescent NHEKs may induce keratinocytes' senescence in RHE although we need further senescence biomarkers analysis to confirm it. In addition, UVB exposure and the incubation with CM from UVB-induced premature senescent NHEKs seems to induce a decrease of A375-GFP cells in RHE, that could be due to their desquamation.

This RHE experiments will need to be adjusted and repeated to draw conclusions from these experiments. Once fully developed, this model will allow to study the factors involved in the migration of melanoma cells in order to better understand the evolution of this cancer *in vivo* and perhaps to adapt the treatment of patients.

SUPPLEMENTARY DATA

Supplementary figures

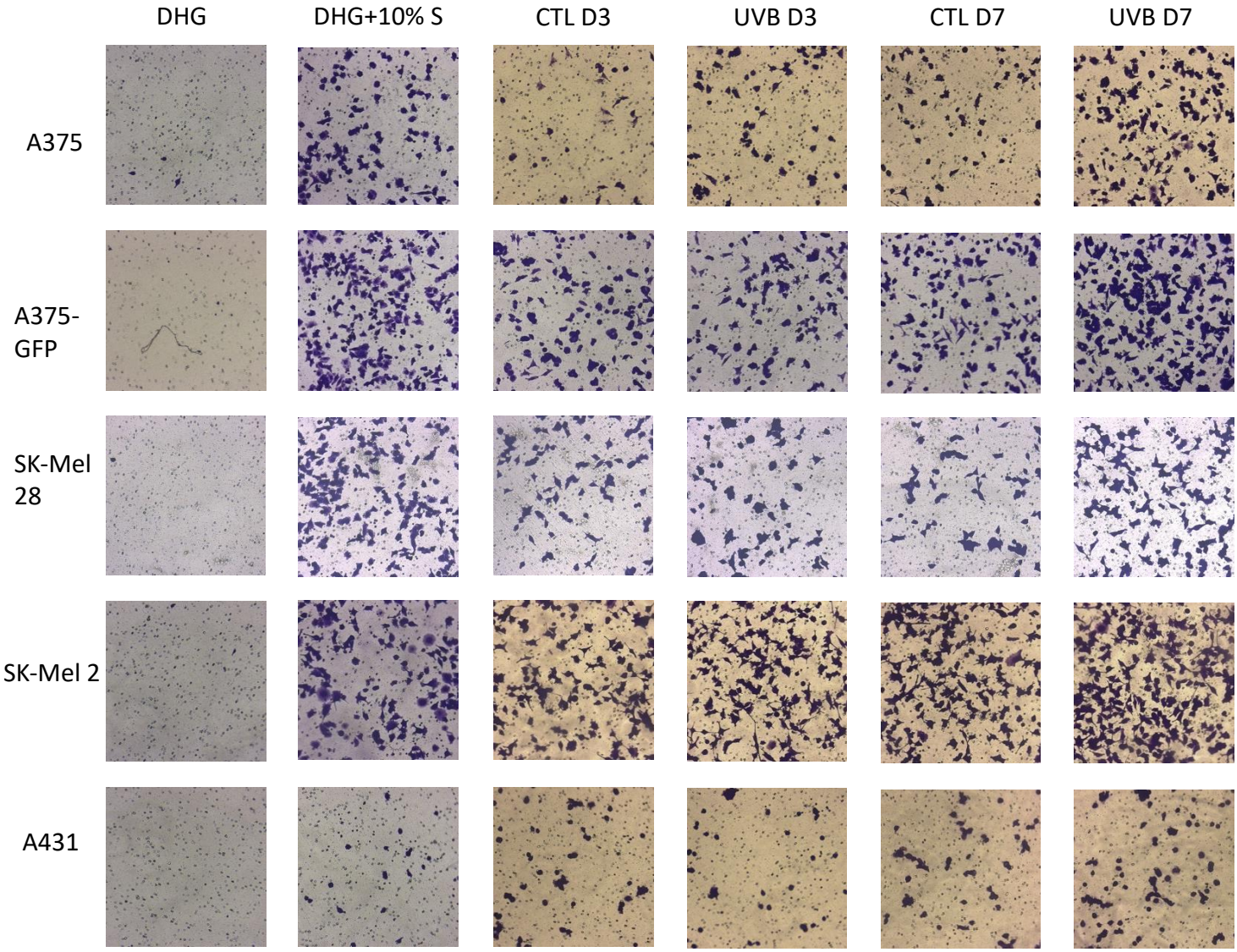

Figure S1 : Effect of keratinocytes conditioned medium (CM) on cancer cell migration in Boyden chambers. Representative microscopy pictures of stained migrated cells (200x). A375, SK-Mel-2, SK-Mel-28 and A431 cells were seeded at a density of 15,000 cells on the top of Boyden chambers. CM from 65,000 UVB-exposed (UVB) or non-exposed (CTL) keratinocytes is then added in the lower part of the chamber. Boyden chambers were incubated 24 h. DHG is used as a negative control and DHG +10% serum as a positive control.

SKMel-28 cells

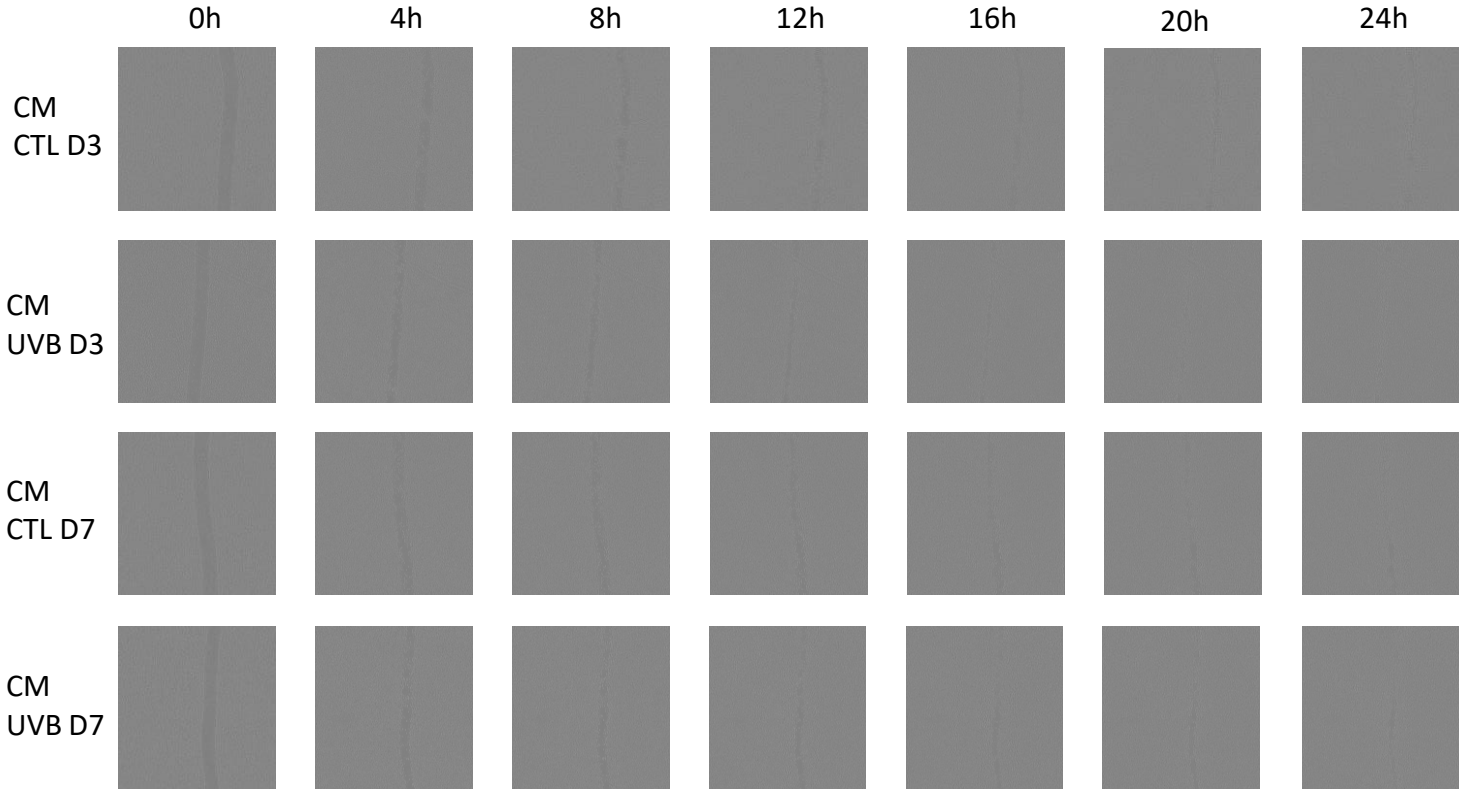

SKMel-2 cells

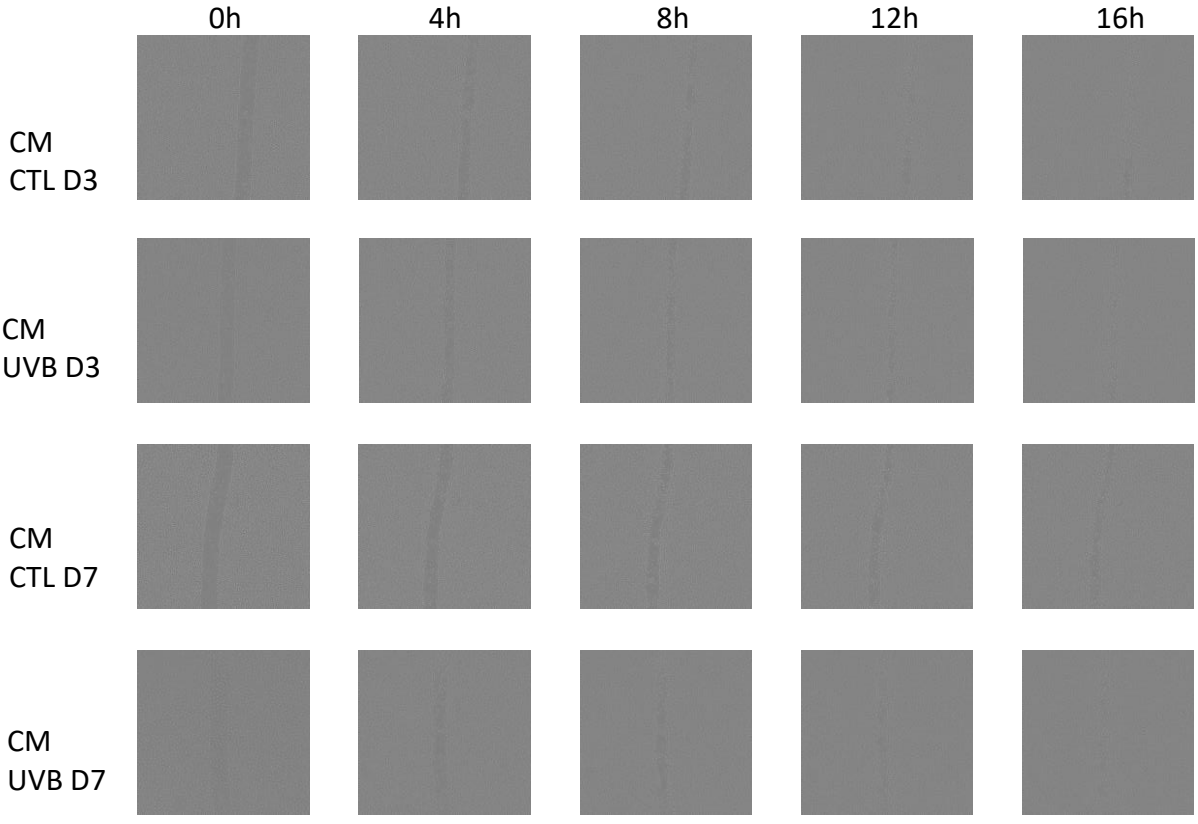

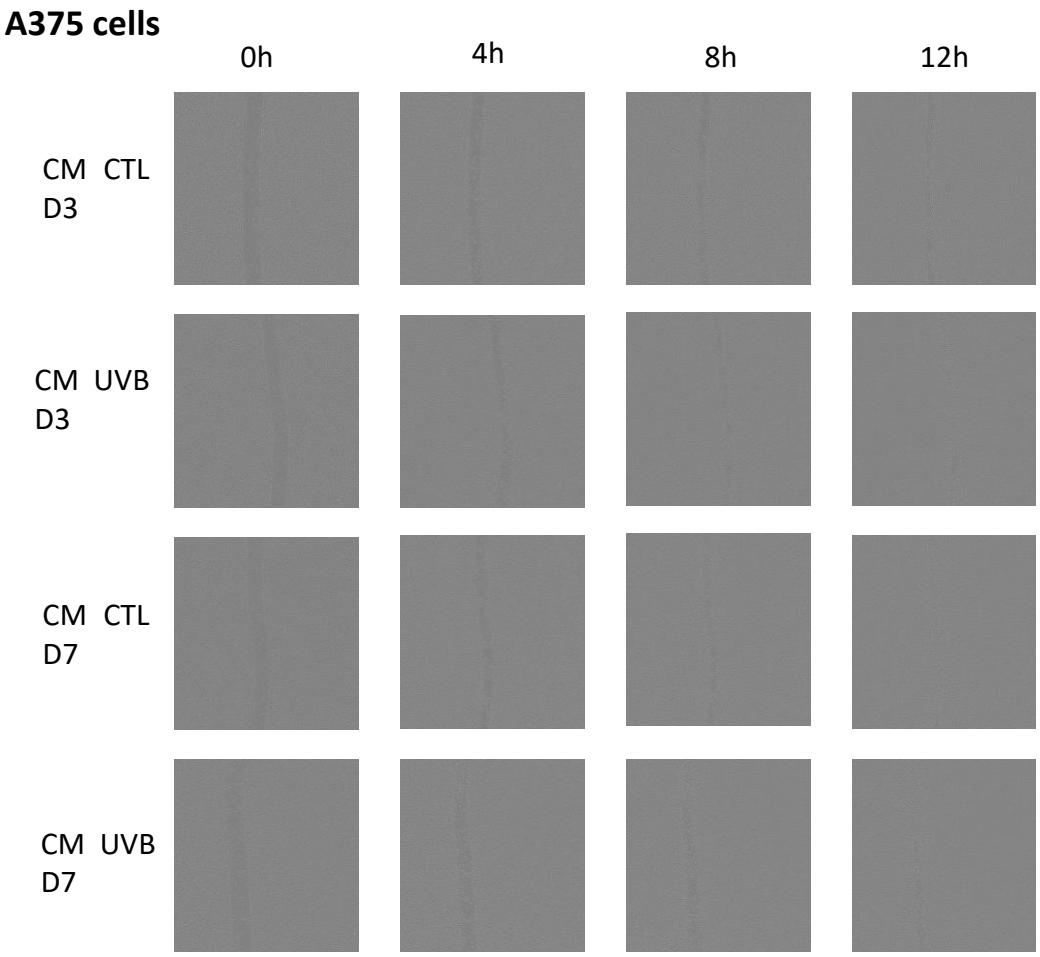

Figure S2 : Scratch assay. Confluent A375 SK-Mel-2, SK-Mel-28 cells were treated with mitomycin C to stop proliferation and a scratch was realized. Gap closure is monitored during 24h in presence of CM from 65,000 UVB-exposed (UVB) or unexposed (CTL) KC 27.

Supplementary methods

Samples preparation for mass spectrometry (made by E. Bauwens and C. Demazy)

Conditioned medium from 5 biological replicates were collected by E. Bauwens during her PhD thesis as described in **Figure 1**. For each condition, conditioned medium from 5 T75 was harvested. The CM was centrifuged for 10 minutes at 0.2 rcf and 4°C to remove cellular debris. The supernatant was then concentrated on 3 kDa amicon filter (Merck Millipore) (to obtain a at least 0.5 µg/µL of proteins). The protein concentration is determined by the Pierce 660 nm method according to the manufacturer's instructions.

The samples were then treated using Filter-aided sample preparation (FASP) using the following protocol: to first wash the filter, 100 µl of formic acid 1 % were placed in each filter (Millipore Microcon 30 MRCFOR030 Ultracel PL-30) before centrifugation at 20,800 rcf for 15 min. For each sample, 40 µg of protein adjusted in 150 µl of urea buffer 8M (urea 8 M in buffer Tris 0.1 M at pH 8,5) were placed individually in a column and centrifuged at 20,800 rcf for 15 minutes. The filtrate was discarded and the columns were washed three times by adding 200 µl of urea buffer followed by a centrifugation at 20,800 rcf for 15 minutes. For the reduction step, 100 µl of dithiothreitol (DTT) were added and mixed for 1 minute at 400 rpm with a thermomixer and were then incubated 15 min at 56°C. Samples were then centrifugated at 20,800 rcf for 15 min, the filtrate was discarded and the filter was washed by adding 100 µl of urea buffer before another centrifugation at 20,800 rcf for 15 min. An alkylation step was performed by adding 100 µl of iodoacetamide ((IAA), in urea buffer) in the column and mixing at 400 rpm for 1 minute before an incubation of 20 minutes in the dark and a centrifugation at 20,800 rcf for 10 minutes. To remove the excess of IAA, 100 µl of urea buffer were added and the samples were centrifugated at 20,800 rcf for 15 min. To quench the remaining IAA, 100 µl of DTT were placed on the column, mixed for 1 minute at 400 rpm and incubated for 15 minutes at 56°C before a centrifugation at 20,800 rcf for 10 minutes. To remove the excess of DTT, 100 µl of urea buffer were placed on the column and centrifuged at 20,800 rcf for 15 min. The filtrate was discarded and the column was washed three times by adding 100 µl of sodium bicarbonate buffer 50 mM ((ABC), in ultrapure water) followed by a centrifugation at 20,800 rcf for 10 minutes. The last 100 µl were kept at the bottom of the column to avoid any evaporation in the column. The digestion process was performed by adding 80 µl of mass spectrometry grade trypsin (1/50 in ABC buffer) in the column and mixed at 400 rpm for 1 minute before an incubation overnight at 37°C in a water saturated environment. The next day, the Microcon columns were placed on a LoBind tube of 1.5 ml and centrifuged at 20,800 rcf for 10 minutes. 40 µl of ABC buffer were placed on the column before centrifugation at 14,500 rpm for 10 minutes. Trifluoroacetic acid (TFA) 10 % in ultrapure water was added to the contain of the LoBind Tube to obtain 0.2 % TFA. The samples were dried in a SpeedVac and resuspended in 20 µl of an aqueous solution (2% acetonitrile and 0.1% formic acid) and they were transferred in an injection vial.

Mass spectrometry identification

The digestion was analyzed using nano-LC-ESI-MS/MS tims TOF Pro (Bruker, Billerica, MA, USA) coupled with an UHPLC nanoElute (Bruker).

Peptides were separated by nanoUHPLC (nanoElute, Bruker) on a 75 µm ID, 25 cm C18 column with integrated CaptiveSpray insert (Aurora, ionopticks, Melbourne) at a flow rate of 400 nl/min, at 50°C. LC mobile phases A was water with 0.1% formic acid (v/v) and B ACN with formic acid 0.1% (v/v). Samples were loaded directly on the analytical column at a constant pressure of 800 bar. The digest (1 µl) was injected, and the organic content of the mobile phase was increased linearly from 2% B to 15 % in 60 min, from 15 % B to 25% in 30 min, from 25% B to 37 % in 10 min and from 37% B to 95% in 5 min. Data acquisition on the tims TOF Pro was performed using Hystar 5.1 and tims Control 2.0. tims TOF Pro data were acquired using 160 ms TIMS accumulation time, mobility (1/K0) range from 0.7 to 1.4 Vs/cm . Mass-spectrometric analysis were carried out using the parallel accumulation serial fragmentation (PASEF) acquisition method(Meier et al., 2018). One MS spectra followed by six PASEF MSMS spectra per total cycle of 1.16 s. Two injections per sample were done. This whole analysis has been realized by Marc Dieu, within the MaSun platform (UNamur).

Database searching

Tandem mass spectra were extracted, charge state deconvoluted and deisotoped by Data analysis (Bruker) version 5.3. All MS/MS samples were analyzed using Mascot (Matrix Science, London, UK; version 2.7). Mascot was set up to search the Uniprot-HomoIsoform database (September 2019 version, 195195 entries) assuming the digestion enzyme trypsin. Mascot was searched with a fragment ion mass tolerance of 0.050 Da and a parent ion tolerance of 15 PPM. Carbamidomethyl of cysteine was specified in Mascot as fixed modifications. Oxidation of methionine and acetyl of the N-terminus were specified in Mascot as variable modifications.

REFERENCES

Aird, K.M., and Zhang, R. (2013). Detection of senescence-associated heterochromatin foci (SAHF). Methods Mol Biol *965*, 185–196.

Alimirah, F., Pulido, T., Valdovinos, A., Alptekin, S., Chang, E., Jones, E., Diaz, D.A., Flores, J., Velarde, M.C., Demaria, M., et al. (2020). Cellular senescence promotes skin carcinogenesis through p38MAPK and p44/p42 MAPK signaling. Cancer Res *80*, 3606–3619.

Apalla, Z., Nashan, D., Weller, R.B., and Castellsagué, X. (2017). Skin Cancer: Epidemiology, Disease Burden, Pathophysiology, Diagnosis, and Therapeutic Approaches. Dermatol Ther (Heidelb) *7*, 5–19.

Arnette, C.R., Koetsier, J.L., Broussard, J.A., Gerami, P., Johnson, J.L., and Green, K.J. (2018). Keratinocyte desmoglein 1 regulates the epidermal microenvironment and tanning response. BioRxiv 423269.

Ashkenazi, A., Fairbrother, W.J., Leverson, J.D., and Souers, A.J. (2017). From basic apoptosis discoveries to advanced selective BCL-2 family inhibitors. Nat Rev Drug Discov *16*, 273–284.

Baker, D.J., Wijshake, T., Tchkonia, T., LeBrasseur, N.K., Childs, B.G., van de Sluis, B., Kirkland, J.L., and van Deursen, J.M. (2011). Clearance of p16Ink4a-positive senescent cells delays ageing-associated disorders. Nature *479*, 232–236.

Basisty, N., Kale, A., Jeon, O.H., Kuehnemann, C., Payne, T., Rao, C., Holtz, A., Shah, S., Sharma, V., Ferrucci, L., et al. (2020). A proteomic atlas of senescence-associated secretomes for aging biomarker development. PLOS Biology *18*, e3000599.

Bauwens, E., Parée, T., Hannart, C., Wera, A.-C., Meurant, S., Kehlfi, A., Fattaccioli, A., Demazy, C., Fransolet, M., Bury, M., et al. (in revision). Senescence induced by UVB in keratinocytes impact amino acids balance.

Bennett, D.C., and Medrano, E.E. (2002). Molecular Regulation of Melanocyte Senescence. Pigment Cell Research *15*, 242–250.

Bertrand-Vallery, V., Belot, N., Dieu, M., Delaive, E., Ninane, N., Demazy, C., Raes, M., Salmon, M., Poumay, Y., Debacq-Chainiaux, F., et al. (2010). Proteomic Profiling of Human Keratinocytes Undergoing UVB-Induced Alternative Differentiation Reveals TRIpartite Motif Protein 29 as a Survival Factor. PLOS ONE *5*, e10462.

Blume-Peytavi, U., Kottner, J., Sterry, W., Hodin, M.W., Griffiths, T.W., Watson, R.E.B., Hay, R.J., and Griffiths, C.E.M. (2016). Age-Associated Skin Conditions and Diseases: Current Perspectives and Future Options. The Gerontologist *56*, S230–S242.

Bodnar, A.G., Ouellette, M., Frolkis, M., Holt, S.E., Chiu, C.-P., Morin, G.B., Harley, C.B., Shay, J.W., Lichtsteiner, S., and Wright, W.E. (1998). Extension of Life-Span by Introduction of Telomerase into Normal Human Cells. Science *279*, 349–352.

Bracken, A.P., Ciro, M., Cocito, A., and Helin, K. (2004). E2F target genes: unraveling the biology. Trends in Biochemical Sciences *29*, 409–417.

Burton, D.G.A., and Krizhanovsky, V. (2014). Physiological and pathological consequences of cellular senescence. Cell Mol Life Sci *71*, 4373–4386.

Cai, Y., Zhou, H., Zhu, Y., Sun, Q., Ji, Y., Xue, A., Wang, Y., Chen, W., Yu, X., Wang, L., et al. (2020). Elimination of senescent cells by β-galactosidase-targeted prodrug attenuates inflammation and restores physical function in aged mice. Cell Res *30*, 574–589.

Campisi, J. (2013). Aging, Cellular Senescence, and Cancer. Annu Rev Physiol *75*, 685–705.

Campisi, J., and d'Adda di Fagagna, F. (2007). Cellular senescence: when bad things happen to good cells. Nat. Rev. Mol. Cell Biol. *8*, 729–740.

Candi, E., Schmidt, R., and Melino, G. (2005). The cornified envelope: a model of cell death in the skin. Nat Rev Mol Cell Biol *6*, 328–340.

CHEN, W., MAO, K., LIU, Z., and DINH-XUAN, A.T. (2014). The role of the RhoA/Rho kinase pathway in angiogenesis and its potential value in prostate cancer (Review). Oncol Lett *8*, 1907–1911.

Childs, B.G., Gluscevic, M., Baker, D.J., Laberge, R.-M., Marquess, D., Dananberg, J., and van Deursen, J.M. (2017). Senescent cells: an emerging target for diseases of ageing | Nature Reviews Drug Discovery.

Cho, K.A., Ryu, S.J., Oh, Y.S., Park, J.H., Lee, J.W., Kim, H.-P., Kim, K.T., Jang, I.S., and Park, S.C. (2004). Morphological Adjustment of Senescent Cells by Modulating Caveolin-1 Status*. Journal of Biological Chemistry *279*, 42270–42278.

Coppé, J.-P., Patil, C.K., Rodier, F., Sun, Y., Muñoz, D.P., Goldstein, J., Nelson, P.S., Desprez, P.-Y., and Campisi, J. (2008). Senescence-associated secretory phenotypes reveal cell-nonautonomous functions of oncogenic RAS and the p53 tumor suppressor. PLoS Biol *6*, 2853–2868.

Coppé, J.-P., Desprez, P.-Y., Krtolica, A., and Campisi, J. (2010). The Senescence-Associated Secretory Phenotype: The Dark Side of Tumor Suppression. Annu Rev Pathol *5*, 99–118.

Coquette, A., and Poumay, Y. (2009). The Reconstructed Human Epidermis Models in Fundamental Research. Fundamentals of Tissue Engineering and Regenerative Medicine 967–976.

De Vuyst, E., Charlier, C., Giltaire, S., De Glas, V., de Rouvroit, C.L., and Poumay, Y. (2014). Reconstruction of Normal and Pathological Human Epidermis on Polycarbonate Filter. In Epidermal Cells: Methods and Protocols, K. Turksen, ed. (New York, NY: Springer), pp. 191–201.

Debacq-Chainiaux, F., Borlon, C., Pascal, T., Royer, V., Eliaers, F., Ninane, N., Carrard, G., Friguet, B., de Longueville, F., Boffe, S., et al. (2005). Repeated exposure of human skin fibroblasts to UVB at subcytotoxic level triggers premature senescence through the TGF-beta1 signaling pathway. J Cell Sci *118*, 743–758.

Decaestecker, C., Debeir, O., Van Ham, P., and Kiss, R. (2007). Can anti-migratory drugs be screened in vitro? A review of 2D and 3D assays for the quantitative analysis of cell migration. Medicinal Research Reviews *27*, 149–176.

Demaria, M., Ohtani, N., Youssef, S.A., Rodier, F., Toussaint, W., Mitchell, J.R., Laberge, R.-M., Vijg, J., Van Steeg, H., Dollé, M.E.T., et al. (2014). An essential role for senescent cells in

optimal wound healing through secretion of PDGF-AA. Dev Cell *31*, 722–733.

Di Micco, R., Krizhanovsky, V., Baker, D., and d'Adda di Fagagna, F. (2021). Cellular senescence in ageing: from mechanisms to therapeutic opportunities. Nat Rev Mol Cell Biol *22*, 75–95.

Díaz-Núñez, M., Díez-Torre, A., De Wever, O., Andrade, R., Arluzea, J., Silió, M., and Aréchaga, J. (2016). Histone deacetylase inhibitors induce invasion of human melanoma cells in vitro via differential regulation of N-cadherin expression and RhoA activity. BMC Cancer *16*, 667.

Dimri, G.P., Lee, X., Basile, G., Acosta, M., Scott, G., Roskelley, C., Medrano, E.E., Linskens, M., Rubelj, I., and Pereira-Smith, O. (1995). A biomarker that identifies senescent human cells in culture and in aging skin in vivo. Proc Natl Acad Sci U S A *92*, 9363–9367.

Dongre, A., and Weinberg, R.A. (2019). New insights into the mechanisms of epithelial–mesenchymal transition and implications for cancer. Nat Rev Mol Cell Biol *20*, 69–84.

Dreesen, O., Chojnowski, A., Ong, P., Zhao, T., Common, J., Lunny, D., Lane, E., Lee, S., Vardy, L., Stewart, C., et al. (2013). Lamin B1 fluctuations have differential effects on cellular proliferation and senescence. The Journal of Cell Biology *200*, 605–617.

Druelle, C., Drullion, C., Deslé, J., Martin, N., Saas, L., Cormenier, J., Malaquin, N., Huot, L., Slomianny, C., Bouali, F., et al. (2016). ATF6α regulates morphological changes associated with senescence in human fibroblasts. Oncotarget *7*, 67699–67715.

d'Adda di Fagagna, F. (2008). Living on a break: cellular senescence as a DNA-damage response. Nat Rev Cancer *8*, 512–522.

Faget, D.V., Ren, Q., and Stewart, S.A. (2019). Unmasking senescence: context-dependent effects of SASP in cancer. Nature Reviews Cancer *19*, 439–453.

Farsam, V., Basu, A., Gatzka, M., Treiber, N., Schneider, L.A., Mulaw, M.A., Lucas, T., Kochanek, S., Dummer, R., Levesque, M.P., et al. (2016). Senescent fibroblast-derived Chemerin promotes squamous cell carcinoma migration. Oncotarget *7*, 83554–83569.

Freund, A., Laberge, R.-M., Demaria, M., and Campisi, J. (2012). Lamin B1 loss is a senescence-associated biomarker. MBoC *23*, 2066–2075.

Fumagalli, M., Rossiello, F., Clerici, M., Barozzi, S., Cittaro, D., Kaplunov, J.M., Bucci, G., Dobreva, M., Matti, V., Beausejour, C.M., et al. (2012). Telomeric DNA damage is irreparable and causes persistent DNA-damage-response activation. Nat Cell Biol *14*, 355–365.

Gabellini, C., Trisciuoglio, D., Desideri, M., Candiloro, A., Ragazzoni, Y., Orlandi, A., Zupi, G., and Del Bufalo, D. (2009). Functional activity of CXCL8 receptors, CXCR1 and CXCR2, on human malignant melanoma progression. European Journal of Cancer *45*, 2618–2627.

Gilchrest, B.A., and Krutmann, J. (2006). Skin Aging (Springer Science & Business Media).

Gonzaga, E.R. (2009). Role of UV Light in Photodamage, Skin Aging, and Skin Cancer. AM J Clin Dermatol *10*, 19–24.

González-Gualda, E., Baker, A.G., Fruk, L., and Muñoz-Espín, D. (2021). A guide to assessing cellular senescence in vitro and in vivo. The FEBS Journal *288*, 56–80.

Gosselin, K., Martien, S., Pourtier, A., Vercamer, C., Ostoich, P., Morat, L., Sabatier, L., Duprez, L., Roodenbeke, C.T. de, Gilson, E., et al. (2009). Senescence-Associated Oxidative DNA Damage Promotes the Generation of Neoplastic Cells. Cancer Res *69*, 7917–7925.

Graham, H.K., Eckersley, A., Ozols, M., Mellody, K.T., and Sherratt, M.J. (2019). Human Skin: Composition, Structure and Visualisation Methods. In Skin Biophysics, From Experimental Characterisation to Advanced Modelling, pp. 1–18.

Guy, J.-B., Espenel, S., Vallard, A., Battiston-Montagne, P., Wozny, A.-S., Ardail, D., Alphonse, G., Rancoule, C., Rodriguez-Lafrasse, C., and Magne, N. (2017). Evaluation of the Cell Invasion and Migration Process: A Comparison of the Video Microscope-based Scratch Wound Assay and the Boyden Chamber Assay. J Vis Exp 56337.

Hanouna, G., Tang, E., Perez, J., Vandermeersch, S., Haymann, J.-P., Baud, L., and Letavernier, E. (2020). Preventing Calpain Externalization by Reducing ABCA1 Activity with Probenecid Limits Melanoma Angiogenesis and Development. Journal of Investigative Dermatology *140*, 445–454.

Hayflick, L., and Moorhead, P.S. (1961). The serial cultivation of human diploid cell strains. Exp Cell Res.

Hennies, H.C., and Poumay, Y. (2021). Skin Disease Models In Vitro and Inflammatory Mechanisms: Predictability for Drug Development. Handb Exp Pharmacol *265*, 187–218.

Hernandez-Segura, A., Nehme, J., and Demaria, M. (2018). Hallmarks of Cellular Senescence. Trends Cell Biol *28*, 436–453.

Herranz, N., and Gil, J. (2018). Mechanisms and functions of cellular senescence (American Society for Clinical Investigation).

Herranz, N., Gallage, S., Mellone, M., Wuestefeld, T., Klotz, S., Hanley, C.J., Raguz, S., Acosta, J.C., Innes, A.J., Banito, A., et al. (2015). mTOR regulates MAPKAPK2 translation to control the senescence-associated secretory phenotype. Nat Cell Biol *17*, 1205–1217.

Hewitt, G., Jurk, D., Marques, F.D.M., Correia-Melo, C., Hardy, T., Gackowska, A., Anderson, R., Taschuk, M., Mann, J., and Passos, J.F. (2012). Telomeres are favoured targets of a persistent DNA damage response in ageing and stress-induced senescence. Nat Commun *3*, 708.

Jacquelot, N., Duong, C.P.M., Belz, G.T., and Zitvogel, L. (2018). Targeting Chemokines and Chemokine Receptors in Melanoma and Other Cancers. Frontiers in Immunology *9*, 2480.

Jobe, N.P., Rösel, D., Dvořánková, B., Kodet, O., Lacina, L., Mateu, R., Smetana, K., and Brábek, J. (2016). Simultaneous blocking of IL-6 and IL-8 is sufficient to fully inhibit CAF-induced human melanoma cell invasiveness. Histochem Cell Biol *146*, 205–217.

Kadoya, K., Amano, S., Nishiyama, T., Inomata, S., Tsunenaga, M., Kumagai, N., and Matsuzaki, K. (2016). Changes in the expression of epidermal differentiation markers at sites where cultured epithelial autografts were transplanted onto wounds from burn scar excision.

International Wound Journal *13*, 412–417.

Kang, C., Xu, Q., Martin, T.D., Li, M.Z., Demaria, M., Aron, L., Lu, T., Yankner, B.A., Campisi, J., and Elledge, S.J. (2015). The DNA damage response induces inflammation and senescence by inhibiting autophagy of GATA4. Science *349*, aaa5612.

Kaur, A., Webster, M.R., Marchbank, K., Behera, R., Ndoye, A., Kugel, C.H., Dang, V.M., Appleton, J., O'Connell, M.P., Cheng, P., et al. (2016). sFRP2 in the aged microenvironment drives melanoma metastasis and therapy resistance. Nature *532*, 250–254.

Krunic, D., Moshir, S., Greulich-Bode, K.M., Figueroa, R., Cerezo, A., Stammer, H., Stark, H.-J., Gray, S.G., Nielsen, K.V., Hartschuh, W., et al. (2009). Tissue context-activated telomerase in human epidermis correlates with little age-dependent telomere loss. Biochimica et Biophysica Acta (BBA) - Molecular Basis of Disease *1792*, 297–308.

Krutmann, J., Bouloc, A., Sore, G., Bernard, B.A., and Passeron, T. (2017). The skin aging exposome. Journal of Dermatological Science *85*, 152–161.

Kurz, D.J., Decary, S., Hong, Y., and Erusalimsky, J.D. (2000). Senescence-associated (beta)-galactosidase reflects an increase in lysosomal mass during replicative ageing of human endothelial cells. J Cell Sci *113 (Pt 20)*, 3613–3622.

Lee, B.Y., Han, J.A., Im, J.S., Morrone, A., Johung, K., Goodwin, E.C., Kleijer, W.J., DiMaio, D., and Hwang, E.S. (2006). Senescence-associated beta-galactosidase is lysosomal beta-galactosidase. Aging Cell *5*, 187–195.

Leiter, U., Eigentler, T., and Garbe, C. (2014). Epidemiology of Skin Cancer. In Sunlight, Vitamin D and Skin Cancer, J. Reichrath, ed. (New York, NY: Springer), pp. 120–140.

Lewis, D.A., Yi, Q., Travers, J.B., and Spandau, D.F. (2008). UVB-induced Senescence in Human Keratinocytes Requires a Functional Insulin-like Growth Factor-1 Receptor and p53. Mol Biol Cell *19*, 1346–1353.

Liu-Smith, F., Jia, J., and Zheng, Y. (2017). UV-Induced Molecular Signaling Differences in Melanoma and Non-melanoma Skin Cancer. In Ultraviolet Light in Human Health, Diseases and Environment, S.I. Ahmad, ed. (Cham: Springer International Publishing), pp. 27–40.

Lopes-Paciencia, S., Saint-Germain, E., Rowell, M.-C., Ruiz, A.F., Kalegari, P., and Ferbeyre, G. (2019). The senescence-associated secretory phenotype and its regulation. Cytokine *117*, 15–22.

López-Otín, C., Blasco, M.A., Partridge, L., Serrano, M., and Kroemer, G. (2013). The Hallmarks of Aging. Cell *153*, 1194–1217.

Malaquin, N., Martinez, A., and Rodier, F. (2016). Keeping the senescence secretome under control: Molecular reins on the senescence-associated secretory phenotype. Experimental Gerontology *82*, 39–49.

Malaquin, N., Tu, V., and Rodier, F. (2019). Assessing Functional Roles of the Senescence-Associated Secretory Phenotype (SASP). In Cellular Senescence, M. Demaria, ed. (New York, NY: Springer New York), pp. 45–55.

Matthews, N.H., Li, W.-Q., Qureshi, A.A., Weinstock, M.A., and Cho, E. (2017). Epidemiology of Melanoma. In Cutaneous Melanoma: Etiology and Therapy, W.H. Ward, and J.M. Farma, eds. (Brisbane (AU): Codon Publications), p.

Maya-Mendoza, A., Ostrakova, J., Kosar, M., Hall, A., Duskova, P., Mistrik, M., Merchut-Maya, J.M., Hodny, Z., Bartkova, J., Christensen, C., et al. (2015). Myc and Ras oncogenes engage different energy metabolism programs and evoke distinct patterns of oxidative and DNA replication stress. Mol Oncol *9*, 601–616.

Miller, A.J., and Mihm, M.C. (2006). Melanoma. N Engl J Med *355*, 51–65.

Mondal, S., Adhikari, N., Banerjee, S., Amin, S.A., and Jha, T. (2020). Matrix metalloproteinase-9 (MMP-9) and its inhibitors in cancer: A minireview. European Journal of Medicinal Chemistry *194*, 112260.

Muzic, J.G., Schmitt, A.R., Wright, A.C., Alniemi, D.T., Zubair, A.S., Olazagasti Lourido, J.M., Sosa Seda, I.M., Weaver, A.L., and Baum, C.L. (2017). Incidence and Trends of Basal Cell Carcinoma and Cutaneous Squamous Cell Carcinoma: A Population-Based Study in Olmsted County, Minnesota, 2000 to 2010. Mayo Clin Proc *92*, 890–898.

Nassour, J., Martien, S., Martin, N., Deruy, E., Tomellini, E., Malaquin, N., Bouali, F., Sabatier, L., Wernert, N., Pinte, S., et al. (2016). Defective DNA single-strand break repair is responsible for senescence and neoplastic escape of epithelial cells. Nat Commun *7*, 10399.

Nesvizhskii, A.I., Keller, A., Kolker, E., and Aebersold, R. (2003). A statistical model for identifying proteins by tandem mass spectrometry. Anal Chem *75*, 4646–4658.

Orioli, D., and Dellambra, E. (2018). Epigenetic Regulation of Skin Cells in Natural Aging and Premature Aging Diseases. Cells *7*, 268.

Ovadya, Y., Landsberger, T., Leins, H., Vadai, E., Gal, H., Biran, A., Yosef, R., Sagiv, A., Agrawal, A., Shapira, A., et al. (2018). Impaired immune surveillance accelerates accumulation of senescent cells and aging. Nat Commun *9*, 5435.

Panier, S., and Boulton, S.J. (2014). Double-strand break repair: 53BP1 comes into focus. Nature Reviews Molecular Cell Biology *15*, 7–18.

Pfeifer, G.P. (2020). Mechanisms of UV-induced mutations and skin cancer. GENOME INSTAB. DIS. *1*, 99–113.

Rodier, F., Coppé, J.-P., Patil, C.K., Hoeijmakers, W.A.M., Muñoz, D.P., Raza, S.R., Freund, A., Campeau, E., Davalos, A.R., and Campisi, J. (2009). Persistent DNA damage signalling triggers senescence-associated inflammatory cytokine secretion. Nat Cell Biol *11*, 973–979.

Salminen, A., Kauppinen, A., and Kaarniranta, K. (2012). Emerging role of NF-κB signaling in the induction of senescence-associated secretory phenotype (SASP). Cellular Signalling *24*, 835–845.

Schadendorf, D., van Akkooi, A.C.J., Berking, C., Griewank, K.G., Gutzmer, R., Hauschild, A., Stang, A., Roesch, A., and Ugurel, S. (2018). Melanoma. Lancet *392*, 971–984.

Schmittgen, T.D., and Livak, K.J. (2008). Analyzing real-time PCR data by the comparative

C(T) method. Nat Protoc *3*, 1101–1108.

Schuch, A.P., Garcia, C.C.M., Makita, K., and Menck, C.F.M. (2013). DNA damage as a biological sensor for environmental sunlight. Photochem. Photobiol. Sci. *12*, 1259–1272.

Shimi, T., Butin-Israeli, V., Adam, S.A., Hamanaka, R.B., Goldman, A.E., Lucas, C.A., Shumaker, D.K., Kosak, S.T., Chandel, N.S., and Goldman, R.D. (2011). The role of nuclear lamin B1 in cell proliferation and senescence. Genes Dev *25*, 2579–2593.

Singh, B., Malhotra, H., Kumar, D., Mujtaba, S., and Upadhyay, A. (2019). Understanding Cellular and Molecular Events of Skin Aging and Cancer: An Integrative Perspective. pp. 11–28.

Storr, S.J., Carragher, N.O., Frame, M.C., Parr, T., and Martin, S.G. (2011). The calpain system and cancer. Nature Reviews Cancer *11*, 364–374.

Tan, C.Y.R., Tan, C.L., Chin, T., Morenc, M., Ho, C.Y., Rovito, H.A., Quek, L.S., Soon, A.L., Lim, J.S.Y., Dreesen, O., et al. (2021). Nicotinamide Prevents UVB- and Oxidative Stress-Induced Photoaging in Human Primary Keratinocytes. J Invest Dermatol *0*.

Tang, J., Fewings, E., Chang, D., Zeng, H., Liu, S., Jorapur, A., Belote, R.L., McNeal, A.S., Tan, T.M., Yeh, I., et al. (2020). The genomic landscapes of individual melanocytes from human skin. Nature *586*, 600–605.

Tang, Z.-Y., Liu, Y., Liu, L.-X., Ding, X.-Y., Zhang, H., and Fang, L.-Q. (2013). RNAi-mediated MMP-9 silencing inhibits mouse melanoma cell invasion and migration in vitro and in vivo. Cell Biology International *37*, 849–854.

Tigges, J., Krutmann, J., Fritsche, E., Haendeler, J., Schaal, H., Fischer, J.W., Kalfalah, F., Reinke, H., Reifenberger, G., Stühler, K., et al. (2014). The hallmarks of fibroblast ageing. Mechanisms of Ageing and Development *138*, 26–44.

Todorova, K., and Mandinova, A. (2020). Novel approaches for managing aged skin and nonmelanoma skin cancer. Advanced Drug Delivery Reviews *153*, 18–27.

Toussaint, O., Medrano, E.E., and von Zglinicki, T. (2000). Cellular and molecular mechanisms of stress-induced premature senescence (SIPS) of human diploid fibroblasts and melanocytes. Experimental Gerontology *35*, 927–945.

Toutfaire, M., Bauwens, E., and Debacq-Chainiaux, F. (2017). The impact of cellular senescence in skin ageing: A notion of mosaic and therapeutic strategies. Biochem Pharmacol *142*, 1–12.

Toutfaire, M., Dumortier, E., Fattaccioli, A., Van Steenbrugge, M., Proby, C.M., and Debacq-Chainiaux, F. (2018). Unraveling the interplay between senescent dermal fibroblasts and cutaneous squamous cell carcinoma cell lines at different stages of tumorigenesis. The International Journal of Biochemistry & Cell Biology *98*, 113–126.

Valerio, H.P., Ravagnani, F.G., Ronsein, G.E., and Di Mascio, P. (2021). A single dose of Ultraviolet-A induces proteome remodeling and senescence in primary human keratinocytes. Sci Rep *11*, 23355.

Victorelli, S., Lagnado, A., Halim, J., Moore, W., Talbot, D., Barrett, K., Chapman, J., Birch, J., Ogrodnik, M., Meves, A., et al. (2019). Senescent human melanocytes drive skin ageing via paracrine telomere dysfunction. The EMBO Journal *38*, e101982.

Wang, A.S., and Dreesen, O. (2018). Biomarkers of Cellular Senescence and Skin Aging. Front. Genet. *9*.

Weinmüllner, R., Zbiral, B., Becirovic, A., Stelzer, E., Nagelreiter, F., Schosserer, M., Lämmermann, I., Liendl, L., Lang, M., Terlecki, L., et al. (2020). Organotypic human skin culture models constructed with senescent fibroblasts show hallmarks of skin aging. Npj Aging and Mechanisms of Disease *6*.

WHO (2021). percentage of total population aged 60 years or over.

Xu, L., and Deng, X. (2004). Tobacco-specific Nitrosamine 4-(Methylnitrosamino)-1-(3-pyridyl)-1-butanone Induces Phosphorylation of μ- and m-Calpain in Association with Increased Secretion, Cell Migration, and Invasion *. Journal of Biological Chemistry *279*, 53683–53690.

Yi, Y., Xie, H., Xiao, X., Wang, B., Du, R., Liu, Y., Li, Z., Wang, J., Sun, L., Deng, Z., et al. (2018). Ultraviolet A irradiation induces senescence in human dermal fibroblasts by down-regulating DNMT1 via ZEB1. Aging (Albany NY) *10*, 212–228.

Yosef, R., Pilpel, N., Tokarsky-Amiel, R., Biran, A., Ovadya, Y., Cohen, S., Vadai, E., Dassa, L., Shahar, E., Condiotti, R., et al. (2016). Directed elimination of senescent cells by inhibition of BCL-W and BCL-XL. Nat Commun *7*, 11190.

Yoshioka, H., Yamada, T., Hasegawa, S., Miyachi, K., Ishii, Y., Hasebe, Y., Inoue, Y., Tanaka, H., Iwata, Y., Arima, M., et al. (2021). Senescent cell removal via JAG1-NOTCH1 signalling in the epidermis. Exp Dermatol *30*, 1268–1278.

Zaidi, Z., and Lanigan, S.W. (2010). Skin: Structure and Function. In Dermatology in Clinical Practice, S.W. Lanigan, and Z. Zaidi, eds. (London: Springer), pp. 1–15.

Zhang, S., and Duan, E. (2018). Fighting against Skin Aging. Cell Transplant *27*, 729–738.